STATISTICAL MECHANICS OF TWO-DIMENSIONAL MATERIALS; FROM BIOLOGICAL MEMBRANES TO GRAPHENE

A Dissertation

Presented to

the Faculty of the Department of Mechanical Engineering

University of Houston

In Partial Fulfillment

of the Requirements for the Degree

Doctor of Philosophy

in Mechanical Engineering

by

Fatemeh Ahmadpoor

December 2016

STATISTICAL MECHANICS OF TWO-DIMENSIONAL MATERIALS; FROM BIOLOGICAL MEMBRANES TO GRAPHENE

Fatemeh Ahmadpoor

Approved:

Chair of Committee
Pradeep Sharma, Professor,
Department of Mechanical Engineering

Committee Members:

Ashutosh Agrawal, Assistant Professor,
Department of Mechanical Engineering

Yi-Chao Chen, Professor,
Department of Mechanical Engineering

Gemunu Gunaratne, Professor,
Department of Physics

Yashashree Kulkarni, Associate Professor,
Department of Mechanical Engineering

Suresh K. Khator, Associate Dean,
Cullen College of Engineering

Pradeep Sharma, Department Chair,
Department of Mechanical Engineering

Acknowledgements

I would like to thank my advisor Professor Pradeep Sharma for being a tremendous mentor to me and encouraged my research and supported me to grow as a research scientist. I gratefully appreciate his patience, motivation, immerse knowledge and priceless advice on research, life and career.

Many results of this dissertation are accomplished with the help of fellow lab-mates and collaborators whose sincere supports and helpful discussions are very much appreciated:

- I would like to acknowledge my fellow lab-mates: Xin Yan, Nikhil Walani, Xiaobao Li and Qian Deng from whom I learned a lot about atomistic simulations, differential geometry, thermodynamics and continuum electromechanics.
- Thanks to Professor Gemunu Gunaratne for the invaluable lectures and fruitful discussions on statistical mechanics.
- Thanks to Professor Liping Liu for the great advice and guidance and many helpful discussions on continuum electromechanics of 2D materials.

Thanks to my committee members, Prof. Yasharshree Kulkarni, Prof. Yi-Chao Chen, Prof. Ashutosh Agrawal and Prof. Gemunu Gunaratne for reviewing my dissertation and valuable suggestions and comments.

A special thank to my parents for their selfless supports, guidance and sacrifices. They are indeed happier than anybody for my achievement. I cannot express how much I am grateful to them for giving me the courage, confidence and opportunity to find my own way.

Huge thanks, love and appreciation go to my loving, supportive, encouraging and patient husband, Mehdi, who made the most special moments of my life.

STATISTICAL MECHANICS OF TWO-DIMENSIONAL MATERIALS; FROM BIOLOGICAL MEMBRANES TO GRAPHENE

An Abstract

of a

Dissertation

Presented to

the Faculty of the Department of Mechanical Engineering

University of Houston

In Partial Fulfillment

of the Requirements for the Degree

Doctor of Philosophy

in Mechanical Engineering

by

Fatemeh Ahmadpoor

December 2016

Abstract

2D materials are fascinating for numerous reasons. Their geometrical and mechanical characteristics along with other associated physical properties have opened up fascinating new application avenues ranging from electronics, energy harvesting, biological systems among others. Due to the 2D nature of these materials, they are known for their unusual flexibility and the ability to sustain large curvature deformations. Further, they undergo noticeable thermal fluctuations at room temperature. In the following, we highlight both the characteristics and implications of thermal fluctuations in 2D materials and discuss the following problems in biological physics and material science :

(i) The minimum electric field that can be detected by a biological membrane: Using a nonlinear continuum electromechanical model, and methods of statistical mechanics, we developed a variational approximation to analytically obtain the benchmark results for model fluid membranes as well as physically reasonable estimates of the minimum electric field that can be detected by a biological membrane.

(ii) Thermal fluctuations of vesicles and nonlinear curvature elasticity— Implications for sized-dependent renormalized bending rigidity and vesicle size distribution: In this work, we discuss the statistical mechanics of closed membranes (vesicles) incorporating both constitutive and geometrical nonlinearities. Our closed-form results may also be used to determine nonlinear curvature elasticity properties from either experimentally measured fluctuation spectra or microscopic calculations such as molecular dynamics.

(iii) Fluctuations and effective bending stiffness of solid membranes within nonlinear elasticity: The study of thermal fluctuations of graphene is rendered rather complicated due to the necessity of accounting for geometric deformation nonlinearity in its deformation. Coupling of stretching and flexural modes leads to a highly anharmonic elastic Hamiltonian. In this study, using a variational perturbation method, we present a "mechanics-oriented" novel treatment of the thermal fluctuations of graphene, fully accounting for deformation nonlinearities, and evaluate their effect on the effective bending stiffness.

(iv) The quest for the determination of the Gaussian modulus—exploiting membrane edge fluctuations: In this work, recognizing that the Gaussian modulus plays a non-trivial role in the fluctuations of a membrane edge, we derive closed-form expressions for edge fluctuations. Combined with atomistic simulations, we use the developed approach to extract Gaussian modulus of graphene.

Table of Contents

List of Figures

List of Tables

Chapter 1

Introduction

1.1 2D materials as elastic sheets

2D materials may be mechanically described as elastic sheets that are resistant to areal change (in-plane deformations), but are quite flexible and can therefore bend easily. Solid 2D membranes[1] include materials such as graphene, Boron Nitride, MOS_2 among many others. Fluid membranes, such as lipid bilayer membranes, are relatively easier to describe mathematically as they are isotropic[2] and often only bending elastic energy has to be accounted for and in-plane stretching, even if incorporated, may be regarded as uncoupled with bending deformation[3]. Specifically, the well-known Helfrich-Canham [1, 2] theoretical framework parametrizes the bending energy cost of a tensionless patch of a fluid membrane by a quadratic function of the curvature

$$F_b = \int \frac{1}{2}\kappa_b(H - H_0)^2 + \kappa_G(K - K_0). \tag{1.1.1}$$

Here κ_b and $\bar{\kappa}$ are the bending moduli that, respectively, correspond to the energy change due to changes in the mean (H) and Gaussian (K) curvatures. The corresponding sponta-

[1] The word "membrane" has a different connotation in the area of solid mechanics than in physics. In solid mechanics, plates, shells and membranes are carefully distinguished. In the physics literature, essentially any 2D elastic sheet is referred to as a membrane and we have adopted this practice here.

[2] Fluid membranes are usually isotropic within the plane. Among solid membranes, graphene exhibits in-plane isotropy while most other solid 2D materials are anisotropic.

[3] We will revisit the complexity surrounding the modeling of solid membranes later in the work.

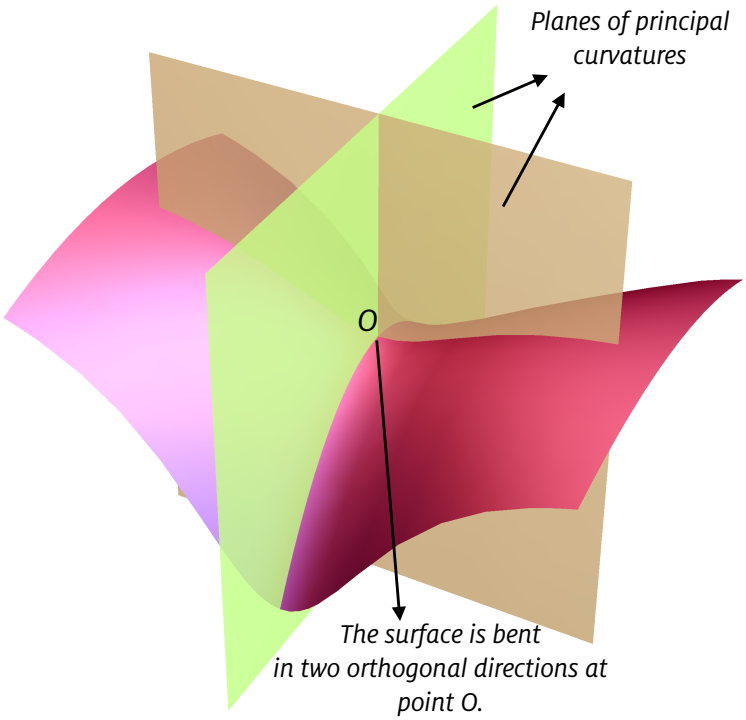

Figure 1.1.1: This figure depicts the principal directions on a surface at a given point O.

neous curvatures are denoted by H_o and K_o.

The *directional* curvature of a surface can be described as gradient of the normal vector, along a given direction. There are always two orthogonal directions that the corresponding curvatures are extremals and are referred to as principal curvatures, denoted by c_1 and c_2 (Figure 1.1.1 [4]). The mean and Gaussian curvatures are then defined as: $H = c_1 + c_2$, $K = c_1 c_2$ [3].

The spontaneous curvature models the situation where the minimizer of energy (in the absence of an external stimuli) corresponds to a preferred curvature. This is quite common for asymmetric membranes, where the molecular structure varies asymmetrically along the thickness.

[4]The directions of the normal planes where the curvature takes its extremum (maximum and minimum) values are called principal directions. The corresponding curvatures are principal curvatures, for which their summation gives the mean curvature and their product yields the Gaussian curvature at the given point O.

There are many ways to parametrize a surface, depending on its geometry. Perhaps, the one used most often in the literature is the so-called Monge representation [3], and is convenient for surfaces with a flat equilibrium(ground) state. In this representation, the surface is characterized by a height function $h(\mathbf{x})$, with $\mathbf{x}$ being the position of each point on the surface. The mean and Gaussian curvatures can then be expressed in terms of $h(\mathbf{x})$[3]

$$\begin{aligned} H &= \nabla \cdot \left(\frac{\nabla h(\mathbf{x})}{\sqrt{1 + |\nabla h(\mathbf{x})|^2}} \right) \\ K &= \frac{\det(\nabla \nabla h(\mathbf{x}))}{(1 + |\nabla h(\mathbf{x})|^2)^2}. \end{aligned} \tag{1.1.2}$$

The above expressions are the general nonlinear forms of the mean and Gaussian curvatures. If the deformations are "small" enough, upon linearization, Equation (1.1.2) reduces to

$$H = \nabla^2 h(\mathbf{x}), \qquad K = \frac{\partial^2 h}{\partial x^2} \frac{\partial^2 h}{\partial y^2} - \left(\frac{\partial^2 h}{\partial x \partial y} \right)^2. \tag{1.1.3}$$

1.2 Statistical Mechanics of 2D Materials

Equation (1.1.1) has been extensively used to described the mechanics of fluid and biological membranes. Typical bending modulus (κ_b) of most lipid-bilayers is between 5 and $25 k_B T$—-small enough compared to the thermal energy scale that membranes undulate or fluctuate noticeably at physiological temperatures [4, 5, 6, 7, 8]. Bending rigidity of 2D crystalline graphene has also been measured by atomistic and quantum simulations [9, 10, 11]. Reported values for graphene bending rigidity at zero Kelvin, range from (1.2-1.6 eV) [9, 10, 11]—just a few times larger than the bending rigidity of biological membranes (at room temperature)[5]. Thus, the energy cost for bending deformations of these materials is typically very low.

Consider a toy model of an elastic sheet—shown in Figure 2. At zero Kelvin, the sheet will adopt the configuration corresponding to minimum bending energy. If spontaneous

[5]Graphene's larger apparent bending stiffness originates from the nonlinear coupling of in-plane stretching deformation and out-of-plane bending.

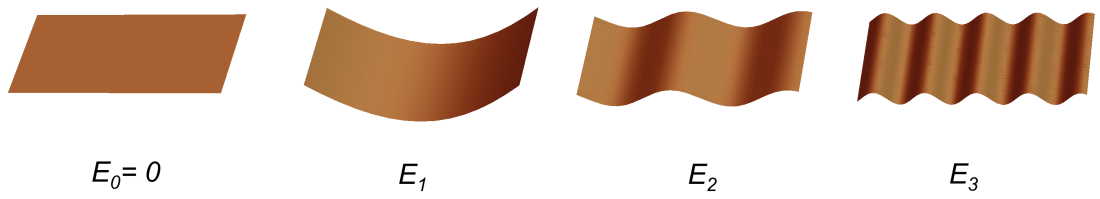

Figure 1.2.1: An elastic sheet at finite temperature undergoes out-of-plane undulations.

curvature is absent then an infinite elastic sheet will simply minimize its energy by adopting a perfectly flat configuration. At a non-zero temperature, however, there is a *finite* probability that even a non-zero bending-energy-state can occur—some illustrative samples are given in Figure 1.2.1[6]. The probability of occurrence of any of these deformation modes is dictated by the Boltzmann factor [8]:

$$p_i \propto \exp(-E_i/k_BT), \tag{1.2.1}$$

where p_i is the probability of occurrence of state i, E_i is its associated elastic energy cost and k_BT is the thermal energy scale.The notion expressed in Equation (1.2.1) can be elaborated further. The probability distribution can be normalized to 1 with a normalizing factor $1/Z$, where Z is known as the partition function and is obtained by summing over all possible states[7]

$$Z = \sum_i \exp(-E_i/k_BT). \tag{1.2.2}$$

Further, the ensemble average of any physical quantity X can be obtained using the probability distribution

$$\langle X \rangle = \sum_i X_i \rho_i = \frac{1}{Z} \sum_i X_i \exp(-E_i/k_BT). \tag{1.2.3}$$

For deformation modes that correspond to extensive curvature changes, the energetic cost can be fairly high and the probability of its occurrence (accordingly) very low but nevertheless, all states are, in principle, *possible*. At any given time, if a 2D membrane is

[6]All deformation modes are *possible* with a probability that is proportional to the Boltzmann factor ($\propto \exp(-E_i/k_BT)$). Deformations with higher energy cost are less probable and the equilibrium state that minimizes the energy, is the most probable state.

[7]Since we have used a *field theory* as a starting point, the number of possible deformation states or deformation modes are infinite

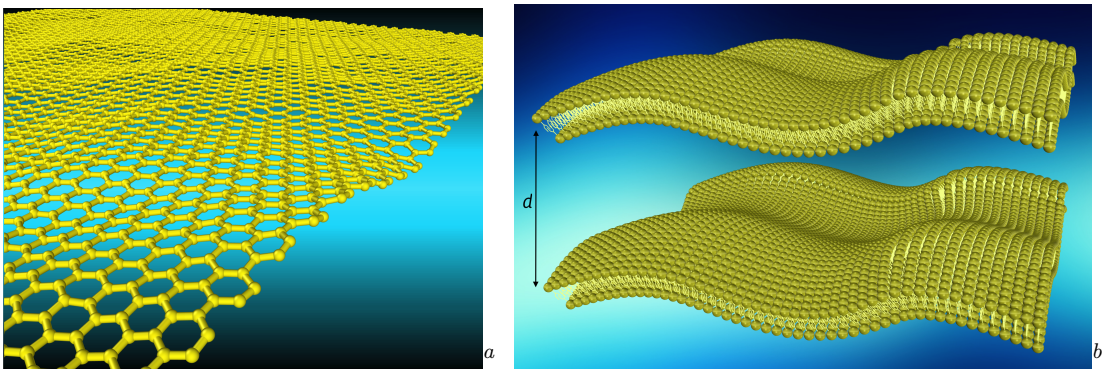

(a) (b)

Figure 1.2.2: (a)Snapshot of graphene sheet in a molecular dynamics simulation. (b)Entropic pressure between two fluctuation membranes

[a]Graphene as a solid membrane, has shear resistance, that results in coupling between in and out-of-plane deformations. This leads to a nonlinear contribution from the in-plane stretching energy that suppresses the height field fluctuations, compared to the simple harmonic result in Equation (1.3.6)

[b]While a single membrane fluctuates freely, its undulations are impeded when it is close to another surface or, for example, another fluctuating membrane. This "hindrance" results in the decrease of the total system entropy and thus increases the overall free energy of the system. The increase in free energy depends on the inter-membrane distance and can be interpreted as a repulsive force that acts to push the membranes apart.

observed at a finite temperature, there is a finite probability that one of the infinite set of modes will be observed (as opposed to just the flat state at zero Kelvin). Accordingly, 2D sheets always appear to be fluctuating in a random manner around the ground (equilibrium-minimized) state. Even though the average of the height field $\langle h \rangle$ is zero, the fluctuations, $\langle h^2 \rangle$ around the flat state are nonzero and depend on the membrane size, temperature as well as the mechanical properties of the sheet. The relatively low bending modulus of many 2D materials ensures that fluctuations are noticeable at room temperature.

1.3 Thermal Fluctuations

In the case of a large, nearly flat membrane, occupying a domain of $\{\mathbf{x} \in \mathbb{S} |\ \mathbb{S} = [0, L]^2\}$, with periodic boundary condition in all directions, the out-of-plane displacement field $h(\mathbf{x})$,

can be expanded in Fourier series as[8]

$$h(\mathbf{x}) = \sum_{\mathbf{q}\in\mathbb{K}} \overline{h}(\mathbf{q}) \exp(\imath \mathbf{q}\cdot\mathbf{x}). \tag{1.3.1}$$

The Fourier transform of the height function then is

$$\overline{h}(q) = \frac{1}{L^2}\int_{\mathbb{S}} h(\mathbf{x})\mathbf{e}^{-\imath\mathbf{q}\cdot\mathbf{x}} d\mathbf{x}. \tag{1.3.2}$$

Assuming linearized elasticity, described in (1.1.3), the energy formulation in (6.1.1) can be expanded in Fourier space as follows[9]

$$F_b = L^2 \sum_{\mathbf{q}\in\mathbb{K}} \frac{1}{2}\kappa_b |\mathbf{q}|^4 |\overline{h}(\mathbf{q})|^2. \tag{1.3.3}$$

We remark that the contribution from the Gaussian curvature vanishes for a system with no boundaries [3]. The mean square of the amplitude in each mode $\langle |h_{\mathbf{q}}|^2\rangle$ can be then evaluated from (1.2.3)[10]. More frequently, the phase averages are computed by taking recourse to the so-called equipartition theorem [8, 12], that states that the thermal energy

[8] $q := |\mathbf{q}| \in [q_{\min}, q_{\max}]$, i.e.

$$\mathbb{K} = \left\{\mathbf{q} : \mathbf{q} = \frac{2\pi}{L}(\nu_x, \nu_y), \nu_x, \nu_y \in \mathbb{Z}, |\mathbf{q}| \in [q_{\min}, q_{\max}]\right\}$$

[9] Note that we have used the orthogonality property of the Fourier transformation that decouples the modes in a quadratic energy formulation

$$\begin{aligned}\int (\nabla^2 h)^2 d\mathbf{x} &= \sum_{\mathbf{q},\mathbf{q}'} |\mathbf{q}|^2 |\mathbf{q}'|^2 \overline{h}(\mathbf{q})\overline{h}(\mathbf{q}') \int \mathrm{e}^{\imath(\mathbf{q}+\mathbf{q}')\cdot\mathbf{x}} d\mathbf{x} \\ &= L^2 \sum_{\mathbf{q}} |\mathbf{q}|^4 \overline{h}(\mathbf{q})\overline{h}(-\mathbf{q})\delta(\mathbf{q}, -\mathbf{q}').\end{aligned}$$

Also, note that $\overline{h}(-\mathbf{q}) = \overline{h}^*(\mathbf{q})$ are conjugates and hence we can set $\overline{h}(\mathbf{q})\overline{h}(-\mathbf{q}) = |\overline{h}(\mathbf{q})|^2$

[10] The partition function is calculated as

$$\begin{aligned}Z &= \int_{-\infty}^{\infty} \mathrm{e}^{-\frac{L^2}{2k_B T}\sum_{\mathbf{q}\in\mathbb{K}} \kappa_b |\mathbf{q}|^4 |\overline{h}(\mathbf{q})|^2} \prod_{\mathbf{q}\in\mathbb{K}} dh_{\mathbf{q}} \\ &= \prod_{\mathbf{q}\in\mathbb{K}} \sqrt{\frac{2\pi k_B T}{L^2 \kappa_b q^4}},\end{aligned} \tag{1.3.4}$$

where $\mathbb{K} := \{\mathbf{q} = 2\pi(\nu_x, \nu_y)/L : \nu_x, \nu_y \in \mathbb{Z}, |\mathbf{q}| \geqslant 2\pi/L\}$. Then the average of the square of the amplitude in

is equally shared among all the modes of deformations[11]. Accordingly, the average of the energy in each mode is

$$\left\langle \frac{L^2}{2}\kappa_b|\mathbf{q}|^4|\overline{h}(\mathbf{q})|^2 \right\rangle := \frac{1}{2}k_BT. \tag{1.3.5}$$

Consequently, the mean-square average of the fluctuations of each mode may be obtained as

$$\langle|\overline{h}(\mathbf{q})|^2\rangle = \frac{k_BT}{L^2\kappa_b|\mathbf{q}|^4}. \tag{1.3.6}$$

Equation (1.3.6), implies that for smaller $\mathbf{q}$, the amplitude is larger and dominant. Further, for a periodic geometry, the fluctuations at all points are identical, i.e. $\langle h(\mathbf{x}_1)^2\rangle = \langle h(\mathbf{x}_2)^2\rangle$ and is represented by a *spatial* average as: [12]

$$\begin{aligned}\langle h^2\rangle &= \frac{1}{L^2}\int \langle h(\mathbf{x})^2\rangle d\mathbf{x} \\ &\propto \frac{k_BT}{\kappa_b}L^2.\end{aligned} \tag{1.3.8}$$

Equation (1.3.8) is a critical result with many applications. For example, the thermal fluctuation spectra may be measured by experimental methods or computed using atomistic simulations and the above formula can then be used to estimate the bending rigidity of membranes [13, 14, 15, 16]. This result has been also extended to other contexts providing

each mode is obtained as

$$\begin{aligned}\langle|\overline{h}_{\mathbf{q}}|^2\rangle &= \frac{1}{Z}\int_{-\infty}^{\infty}|h_{\mathbf{q}}|^2 \mathrm{e}^{-\frac{L^2}{2k_BT}\sum_{\mathbf{q}\in\mathbb{K}}\kappa_b|\mathbf{q}|^4|\overline{h}(\mathbf{q})|^2}\prod_{\mathbf{q}\in\mathbb{K}}dh_{\mathbf{q}} \\ &= \frac{k_BT}{L^2\kappa_b|\mathbf{q}|^4}.\end{aligned}$$

[11] This is however, valid only when the energy is a quadratic function of uncoupled degrees of freedom.

[12] Also, since the two-point correlation function is translationally and rotationally invariant, it only depends on the distance between the two points, $r = |\mathbf{r}| = |\mathbf{x} - \mathbf{x}'|$, rather than their positions $(\mathbf{x}, \mathbf{x}')$

$$\begin{aligned}\langle h(\mathbf{x})h(\mathbf{x}')\rangle &= \sum_{\mathbf{q},\mathbf{q}'\in\mathbb{K}}\langle\bar{h}_{\mathbf{q}}\bar{h}_{\mathbf{q}'}\mathrm{e}^{\imath(\mathbf{q}\cdot\mathbf{x}+\mathbf{q}'\cdot\mathbf{x}')}\rangle \\ &= \frac{k_BT}{L^2\kappa_b}\sum_{\mathbf{q}\in\mathbb{K}}\frac{\mathrm{e}^{\imath\mathbf{q}\cdot\mathbf{r}}}{|\mathbf{q}|^4},\end{aligned} \tag{1.3.7}$$

which is clearly independent of the position of the two points. We remark that in case of *finite* membranes, where pertinent boundary conditions must be accounted for, these simple results are no longer valid.

a facile route to extract useful information about membranes e.g. the incorporation of electromechanical coupling [17], tilt of lipids [18, 19], presence of heterogeneities [20, 21, 22], proximity to substrates or other vesicles [23, 24] among others.

1.4 Implications of Thermal Fluctuations in Biology and Material Science

Thermal fluctuations appear to have several fascinating implications in material science and biology. In the context of 2D *crystalline* materials, of which graphene is a good example, its morphology is strongly dictated by thermal fluctuations at room temperature. Graphene can be experimentally made in different geometries such as rectangular sheet and ribbons. However, it is found that at finite temperature, graphene sheet cannot exist in perfectly *flat* state and there is always intrinsic rippling on the surface of a graphene sheet[25]. This has been explained theoretically by nonlinear elasticity theory of crystalline membranes, where the in- and out-of-plane deformations are coupled and at finite temperature result in permanent ripples in graphene sheet. Further, graphene nano-ribbons exhibit self-folding and warping at finite temperature. In this case, the edge effects along with thermal fluctuations, render the ribbon geometry to be unstable. Consequently, with small twisting stimuli, the ribbon can be transformed into a nano-tube—a more stable configuration without any edge [26]. Accordingly, the morphology of graphene is highly affected by temperature, and the temperature dependence of the graphene morphology can be used as a method in experiments for graphene-based structures [27].

Many physiological processes are involved with thermal fluctuations such as exo and endo-cytosis, membrane fusion, pore formation, cell adhesion, binding-unbinding transitions, self assembly and vesicle size distributions among many others. These aforementioned biophysical phenomena are governed by a complex interplay between the various attractive and repulsive forces that mediate between biological membranes. A key role is played by a repulsive force termed "steric hindrance", or simply entropic pressure, the origins of which lie in the thermally excited fluctuations of membranes. As mentioned ear-

lier, biological membranes are quite flexible and fluctuate noticeably at room temperature. While a single membrane fluctuates freely, its undulations are impeded when it is close to another surface or another fluctuating membrane. This hindrance decreases the entropy and the ensuing overall increase of the free-energy of the membrane system, which depends on the intermembrane distance, leads to a repulsive force that tends to push the membranes apart. Stated differently, a finite external pressure is required to maintain the mean distance between the interacting membranes. Accordingly, the study of thermal fluctuations and entropic effects has been one of the cornerstones of biophysical research on membranes [28, 29, 30, 31, 32, 33, 34].

A more recent topic of growing interest is the entropic interaction of ultra-thin 2D nano-materials such as graphene with cellular membranes and its study has implications for several biomedical applications such as biosensors [35], tissue scaffolds [36, 37], carriers for drug delivery [38, 39] and gene therapy [40]. The graphene sheet undergoes thermal motion in the vicinity of the cellular membrane. Rather than adhering to cellular membrane, graphene sheet is observed to penetrate the bilayer, through one of its sharp corner [41]. We speculate that this type of interaction (which does not change the total elastic energy) is primarily controlled by entropic effects arising from thermal undulations of both the membrane and the graphene sheet. Generally speaking, adhesion and cellular uptake of nano-materials, depending on their shapes and sizes, can be strongly affected by thermal fluctuations [42].

1.5 Dissertation overview

There exists a rich and extensive literature on thermal fluctuations of 2D materials. In the majority of these works the Helfrich's classical quadratic energy function is used within linearized elasticity and periodic boundary condition. Specifically, geometric and constitutive nonlinearities as well as non-vanishing boundary conditions are not usually accounted for.

In this dissertation, nonlinearities and effects of boundary conditions are explored for 2D materials including biological membranes and graphene. Several implications of nonlinearities are addressed, including thermal noise limit of cellular membranes, fluctuations and effective bending stiffness of small biological vesicles and fluctuations of graphene as a nonlinear solid membrane. Further, fluctuations of a free edge as a non-vanishing boundary condition is exploited to estimate the Gaussian modulus and edge properties of graphene monolayers.

Chapter 2

Thermal Fluctuations and the Minimum Electrical Field that can be Detected by a Biological Membrane

Thermal electrical noise in living cells is considered to be the minimum threshold for several biological response mechanisms that pertain to electric fields. Existing models that purport to explain and interpret this phenomena yield perplexing results. The simplest model, in which the biomembrane is considered to be a linear dielectric, yields an equilibrium noise level that is several orders of magnitude larger than what is observed experimentally. An alternative approach of estimating the thermal noise as the Nyquist noise of a resistor within a finite frequency bandwidth, yields little physical insight. In this work, we argue that the nonlinear dielectric behavior must be accounted for. Using a statistical mechanics approach, we analyze the thermal fluctuations of a fully coupled electromechanical biomembrane. We develop a variational approximation to analytically obtain the benchmark results for model fluid membranes as well as physically reasonable estimates of the minimum electrical field threshold that can be detected by cells. Qualitatively, at least, our

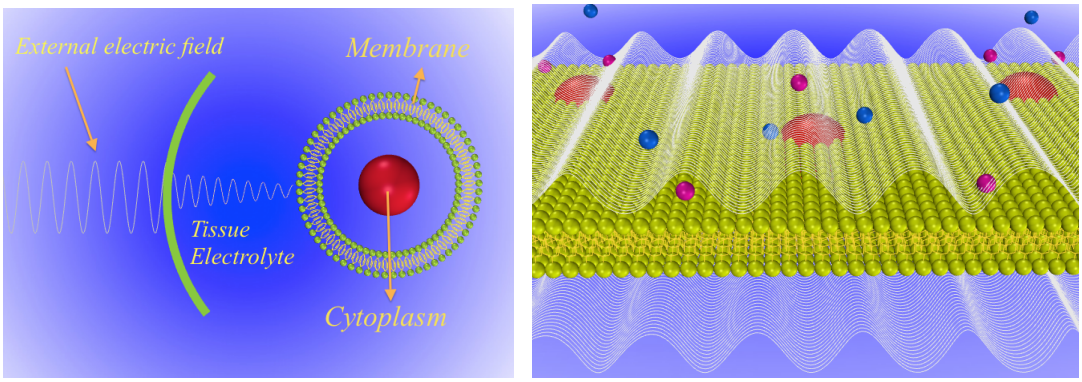

(a) (b)

[a]

Figure 2.1.1: (a): An external electrical field weakened by the tissue, (b): Thermally fluctuating electric field on the surface of the membrane, in equilibrium.

[a](a): An external electrical field is weakened by the tissue, reducing to about 10^{-6} times the original value by the time it impinges on the cell membranes
(b): Thermally fluctuating electric field on the surface of the membrane, in equilibrium. Only electrical fields larger than the thermal noise threshold of the membrane are expected to be detected and therefore induce electromechanical conformational changes.

model is capable of predicting all known experimental results. The predictions of our model also suggest that further experimental work is warranted to clarify the inconsistencies in the literature.

2.1 Introduction

Over the last several decades, the response of biological systems to external electromagnetic fields has attracted much attention and controversy. Several important biological processes in cell, such as electroporation, [43, 44, 45], activation of ion gated channels, [46, 47] among many others, are directly related to the interaction of cells with an imposed electric field. The source of the electric field could be ionic concentration gradients in the local environment of the cell or simply an external stimuli. While the former is of interest due to the fundamental quest to understand transduction mechanisms and signaling in cells, the latter—disruption of biological processes by very weak extremely low frequency fields (ELF) from external sources of electricity—has also been an active topic of discussion [48, 49, 50, 51, 52, 53]. It is generally supposed that below a certain threshold–i.e. the thermal-electrical noise, the cell cannot detect an electrical field. As it is schematically

shown in Figure 2.1.1, most (typical) external ELF field levels, are severely diminished at the cell level. Whether the electrical field sources are external or internal, the question of the limit of electrical field detection by cells is of fundamental interest.

The limit for electrical field detection is that the field should exceed, *at least*, the noise generated by thermal fluctuations in the cells. Although widely studied theoretically e.g. [54, 55, 56, 57], experimental results have been somewhat scarce [58, 59, 60].

In a frequently quoted, and relatively simple, model to estimate the noise threshold [61, 62, 63], the cell-membrane is considered to be a resistor-capacitor system with corresponding values of membrane resistivity and dielectric permittivity respectively. In the so-called Johnson-Nyquist noise of a RC circuit, the time averaged noise voltage at low frequencies can be obtained as

$$\overline{V}_{k_BT} = \sqrt{4Rk_BT\triangle\nu}, \tag{2.1.1}$$

where k_B is the Boltzmann constant (Joule/Kelvin), T is the temperature (Kelvin) and $\triangle\nu$ accounts for the frequency bandwidth (Hz). Using this model, [64] estimated the thermal noise of a spherical cell with radius $r \approx 10^{-5}m$ and $R \approx 4\times10^6\ \Omega$, to be $\overline{V}_{k_BT} \approx 2.6\times10^{-6}$V for a frequency bandwidth of about $100Hz$. [64] recognized that the wisdom of considering the entire cell with its attendant complexities is dubious. A meaningful and more relevant estimate of the noise threshold is likely if the membrane noise limit is examined rather than that of the entire cell. From this point of view, he estimated the noise for a small piece of membrane with area $d^2 \approx 2.5\times10^{-17}m^2$, within a frequency band of 100Hz, to be $\overline{V}_{k_BT} \approx 0.02$V. Here d is the typical thickness of the membrane ($\sim 5nm$).

We may also consider a (yet another) alternative approach. Consider the membrane of size $\mathbb{S} = (0, L)^2$ as a linear dielectric surface in equilibrium with a thermal bath. Thermal fluctuations will lead to a spatially fluctuating and non-uniform polarization field: we identify $P(\mathbf{x})$ as the out-of-plane dipole areal density at point $\mathbf{x}$. Then, for a membrane with permittivity ϵ, the electrostatic contribution to the total Hamiltonian can be written as

$$H = \int_{\mathbb{S}} \tfrac{1}{2} a P(\mathbf{x})^2 d\mathbf{x}, \tag{2.1.2}$$

where $a = 1/(\epsilon - \epsilon_0)d$. Discretizing the above Hamiltonian in the real space, in which each degree of freedom ($\mathbf{x}_i$) has an area of A_0–that fluctuates independently; we obtain

$$H = \sum_{\mathbf{x}_i} \frac{1}{2} a P(\mathbf{x}_i)^2 A_0. \tag{2.1.3}$$

The equipartition theorem immediately yields an estimate of the polarization fluctuation: $\langle P^2 \rangle = \frac{k_B T}{a A_0}$. Assuming that A_0 has the same order of magnitude as d^2, the thermal noise of the voltage across the membrane is $\overline{V}_{k_B T} = \sqrt{k_B T / \epsilon_0 d}$. This gives us a value as large as 0.3V at room temperature. Although this approach is based on fundamental statistical mechanics, the result is physically unreasonable and the ambiguity in deciding the patch of membrane that fluctuates independently (i.e. A_0) offers little insight.

Most other models also predict noise thresholds that are similar in magnitude to the ones described in the preceding paragraphs. In sharp contrast, for some large mammalian cells, experiments [58, 59, 60] suggest values that are almost 1000 times smaller than all the theoretical models!

Elucidation of the puzzling discrepancies as outlined in the preceding paragraphs is the key objective of this work. In Section 2.2, we present our central physical ideas and formulate the corresponding Hamiltonian that accounts for nonlinear dielectric behavior and coupled electromechanical behavior of fluid membranes. The statistical mechanics of the nonlinear estimation of the noise threshold in model fluid membranes is outlined in Sections 2.3 and 2.4. Experiments indicate that the limit of noise-detection is frequency dependent. We discuss the modification of our results, that account for finite frequency bandwidth, in Section 2.5. In Section 2.6, we speculate on the relevance of the model fluid membrane results for real biological membranes, and finally discuss and compare our results with experiments in Section 2.7.

2.2 Central Ideas and Formulation

The dielectric behavior of biological membranes (whether model or real) is nonlinear. The assumption of linearity i.e., the notion that the polarization is linearly proportional to the electric field $\mathbf{P} \propto \mathbf{E}$ implies that a membrane is capable of being polarized to unrealistically high values at high fields. This is of course physically incorrect. Aside from the obvious fact pertaining to the limits imposed by dielectric breakdown, it is expected that beyond a certain field, a limit will be reached where all the relevant microscopic dipoles in the membrane have been aligned. Corresponding to this, the polarization will saturate—in other words, there is an upper limit to which the membranes are capable of being polarized (hence forth referred to as the saturation polarization). The most compelling evidence of this, at least among recent works, is provided by the experiments and modeling of [47] —and indeed, their estimate of the saturation polarization (on the specific membrane that they studied) is not only far below the dielectric breakdown limit but also below that of the polarization corresponding to the resting voltage.

This concept is schematically illustrated in Figure 2.2.1(a) where we compare the linear dielectric behavior to the dipole saturating trend in which the change in the polarization field becomes negligible once it approaches P_S. In other words, the membrane cannot be polarized to arbitrarily large values by an imposed electrical field and is restricted to a finite range. There is close analogy of this problem to the confinement of *mechanical* fluctuations between confined hard walls—-here the amplitude of the thermal-mechanical fluctuations is restricted by the hard walls. This analogy is depicted in Figure 2.2.1(b) in which the membrane's polarization cannot exceed the yellow bounds. The problem of thermal-mechanical fluctuations of a confined membrane has been discussed by a number of works [65], [66] including a few recent ones: [33] and [67]. Since the strict finite range is difficult to treat analytically (and may not be physical anyway) we mimic the saturation phenomena with a smooth nonlinear function shown in blue in Figure 2.2.1(a).

Now consider a membrane of $\mathbb{S} = (0, L)^2$ and thickness $d \ll L$. The membrane is described by the state variables $(P, h) : \mathbb{S} \to \mathbb{R}$, where P is the out-of-plane polarization

area density and h is the out-of-plane displacement of the mid-plane of the membrane. For simplicity (and almost completely justifiable in most situations), we have neglected the in-plane components of the polarization. Let $\frac{1}{2}K_h$ be the mean curvature of mid-plane and within a linearized elastic approximation,

$$K_h(\mathbf{x}) = \nabla^2 h(\mathbf{x}). \tag{2.2.1}$$

Although the effect of electromechanical coupling will later be found to be negligible, for the sake of completeness, here we take it into account and postulate that the total Hamiltonian of the membrane can be written as

$$H[P,h] = \int_{\mathbb{S}} \frac{1}{2}\kappa_b K_h^2 + \frac{1}{2}a|P|^2 + fPK_h + g(P)ds, \tag{2.2.2}$$

where κ_b and f are the bending modulus and the flexoelectric coefficient of the membrane respectively, and the non-quadratic function $g(P)$ is designed to increasingly penalize the fluctuations of the polarization field as it gets close to a saturation value. The simplest form of $g(P)$ is a higher order polynomial of polarization—such that its contribution to the electrostatic energy is negligible at fields that correspond to well below the saturation point, P_s. We remark that the analogy to non-linear elastic-plastic behavior is evident. From this point of view, we propose $g(P)$ as below

$$g(P) = aP^2(\varepsilon_4\frac{P^2}{P_s^2} + \varepsilon_6\frac{P^4}{P_s^4} + \varepsilon_8\frac{P^6}{P_s^6} + \cdots), \tag{2.2.3}$$

were ε_i are phenomenological scalar constants that represent the nonlinear behavior. In the absence of flexoelectric coupling (i.e., $f = 0$), the out-of-plane electric field is given by

$$\begin{aligned} E &= \frac{\partial}{\partial P}(\frac{1}{2}aP^2 + g(P)) \\ &= aP(1 + 4\varepsilon_4\frac{P^2}{P_s^2} + 6\varepsilon_6\frac{P^4}{P_s^4} + 8\varepsilon_8\frac{P^6}{P_s^6} + \cdots). \end{aligned} \tag{2.2.4}$$

The function in equation (2.2.4) can mathematically represent the nonlinear behavior,

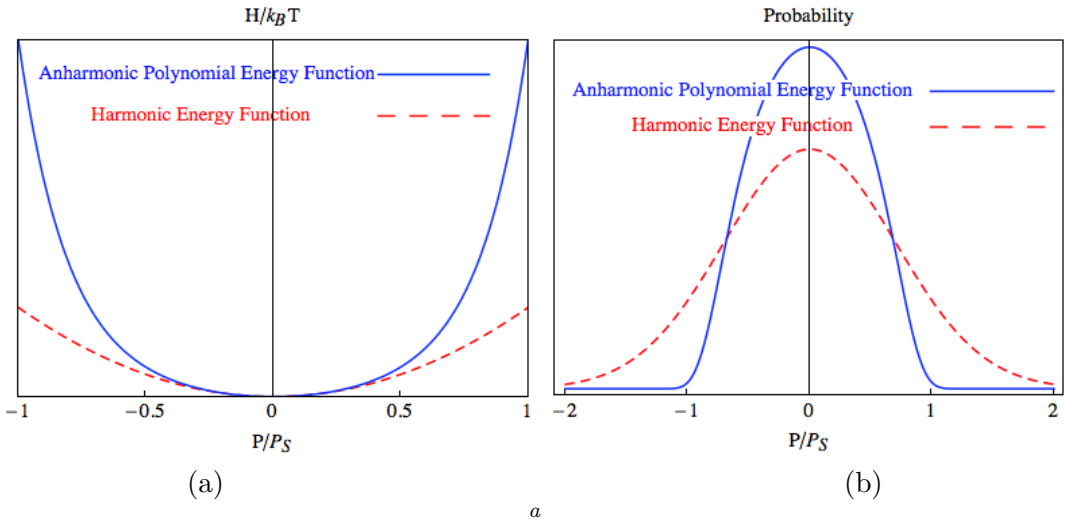

Figure 2.2.1: (a): Comparison of linear and nonlinear energy costs for change in polarization field. (b): Comparison of probability distributions for the linear and nonlinear dielectrics.

[a](a): Comparison of linear and nonlinear energy costs for change in polarization field. The blue curve is representing the nonlinear behavior, and mimics the hard (walls) restrictions on the fluctuations
(b): Comparison of probability distributions for the linear and nonlinear dielectrics. The higher order terms in the energy formulation make the smaller values of the polarization more probable and consequently decreases the fluctuations.

shown in Figure 2.2.1(a). Furthermore, the energy cost for the change in polarization field is compared for the cases of linear and non-linear behavior in Figure 2.2.1(a). Specifically, by taking into account the higher order terms of the polynomial function $g(P)$, the energy cost increases rapidly for the change in polarization field approaching P_S.

As a result of using the new energy function(2.2.2), the distribution of the fluctuating polarization field is no longer Gaussian. Basic statistical mechanics tells us that the probability of occurrence of a certain change of polarization can be expressed as an exponential function

$$p(P) \propto \exp(-H(P)/k_BT), \tag{2.2.5}$$

indicating that, the higher polarization values (with the attendant larger energy cost) are less probable. Accordingly, the nonlinear function $g(P)$ ensures lower probability for largers value of the polarization. We have shown this qualitatively in Figure2.2.1(b). Our modified

Hamiltonian, which accounts for the nonlinear dielectric behavior, essentially *confines* the thermal fluctuations of the polarization field in a finite range of $|P/P_S| \leqslant 1$. For such a non-Gaussian distribution of the fluctuating field, the equipartition theorem is inapplicable, and analytical solutions are hard to come by. However, we develop here a variational approximation to obtain an estimation of the fluctuations—that yields analytical expressions. It is worthwhile to remark that the subject of thermal-mechanical fluctuations of the membranes has been extensively investigated. For example, in a pioneering work, [2, 68] proposed that the thermal fluctuations of a membrane soften the renormalized bending modulus. Also, in the context of dealing with non-quadratic Hamiltonians, Nelson et. al.[18] have discussed the crumpling transition in polymerized membranes, Guitter et. al.[69] studied the fluctuations of self avoiding tethered membranes and Bowick et. al.[70] investigated the tubular transition of self avoiding anisotropic membranes. Several other examples abound which we avoid citing for the sake of brevity. Furthermore, in the context of the somewhat more complicated and *hard* membrane materials, the reader is referred to the following sample of works: investigation of graphene fluctuations by Gao and co-workers [71], DNA, by Su and Purohit [72], and twin-boundaries in crystalline metals by Chen and Kulkarni [73].

2.3 Thermal fluctuations

The Hamiltonian of the system (2.2.2) can be rewritten as

$$H = H^q + H^{nq}, \tag{2.3.1}$$

where H^q is the quadratic part of the Hamiltonian that includes the first three terms of (2.2.2), and H^{nq} is the last term of (2.2.2) ("Non-quadratic"). Due to the presence of the non-quadratic terms, the equipartition theorem is not applicable; it is hopeless to compute the exact free energy and thermal fluctuations in closed-form. Nevertheless, we can employ a variational approximation based on the Bogoliubov inequality [8] that asserts the following

$$F \leqslant F_{\text{var}} := F_0 + \langle H - H_0 \rangle_{H_0}, \tag{2.3.2}$$

where F is the actual free energy of the system, $H_0[P,h]$ is any Hamiltonian, F_0 is the free energy associated with the Hamiltonian H_0:

$$F_0 = -k_B T \log Z_0, \quad Z_0 = \int e^{-H_0[P,h]/k_B T} D[P,h], \tag{2.3.3}$$

and $\langle\ \rangle_{H_0}$ denotes the expectation value with respect to the Hamiltonian H_0.

To make analytical progress, we select a quadratic Hamiltonian H_0 that in Fourier $\mathbf{q}$-space is given by

$$\begin{aligned} H_0[P,h] =& \frac{L^2}{2} \sum_{\mathbf{q}\in\mathcal{K}} \Big\{ G_h(\mathbf{q}) |h_{\mathbf{q}}|^2 + G_P(\mathbf{q}) |P_{\mathbf{q}}|^2 \\ &+ G_f(\mathbf{q}) h_{\mathbf{q}} P_{-\mathbf{q}} \Big\}, \end{aligned} \tag{2.3.4}$$

where $\mathcal{K} := \{\mathbf{q} = \frac{2\pi}{L}(\nu_x, \nu_y) : \nu_x, \nu_y \in \mathbb{Z}, \frac{2\pi}{L} \le |\mathbf{q}| \le \frac{2\pi}{d}\}$, $G_h(\mathbf{q})$, $G_P(\mathbf{q})$ and $G_f(\mathbf{q})$ are set of propagators that will be determined later, and $h_{\mathbf{q}}$ ($P_{\mathbf{q}}$) is the Fourier transformation of $h(\mathbf{x})$ ($P(\mathbf{x})$)

$$\begin{aligned} h_{\mathbf{q}} &= \frac{1}{L^2} \int_{\mathbb{S}} h(\mathbf{x}) \exp(-\imath \mathbf{q}.\mathbf{x}) d\mathbf{x}, \\ P_{\mathbf{q}} &= \frac{1}{L^2} \int_{\mathbb{S}} P(\mathbf{x}) \exp(-\imath \mathbf{q}.\mathbf{x}) d\mathbf{x}. \end{aligned} \tag{2.3.5}$$

For the Hamiltonian (4.2.5), by the equipartition theorem we find the free energy F_0 to be

$$F_0 = \alpha_F + \sum_{\mathbf{q}} \frac{k_B T}{2} \log(4 G_h(\mathbf{q}) G_P(\mathbf{q}) - G_f(\mathbf{q})^2), \tag{2.3.6}$$

where α_F is a constant of no consequence. Also, for simplicity we consider only the first two terms in (2.2.3). Then, to within a constant,

$$\begin{aligned} \langle H - H_0 \rangle_{H_0} = \frac{L^2}{2} \sum_{\mathbf{q}\in\mathcal{K}} \Big\{ & \kappa_b |\mathbf{q}|^4 \langle |h_{\mathbf{q}}|^2 \rangle_{H_0} \\ & + a \langle |P_{\mathbf{q}}|^2 \rangle_{H_0} + 2f |\mathbf{q}|^2 \langle |h_{\mathbf{q}} P_{-\mathbf{q}}| \rangle_{H_0} - \frac{k_B T}{L^2} \Big\} \\ & + a \int_{\mathbb{S}} \langle \varepsilon_4 \frac{P^4}{P_s^2} + \varepsilon_6 \frac{P^6}{P_s^4} \rangle_{H_0} \, d\mathbf{x}. \end{aligned} \tag{2.3.7}$$

All the quadratic correlations can be calculated using the equipartition theorem

$$\begin{aligned}
\langle |h_{\mathbf{q}}|^2 \rangle_{H_0} &= \frac{4k_BTG_P(\mathbf{q})}{L^2(4G_h(\mathbf{q})G_P(\mathbf{q}) - G_f(\mathbf{q})^2)}, \\
\langle |P_{\mathbf{q}}|^2 \rangle_{H_0} &= \frac{4k_BTG_h(\mathbf{q})}{L^2(4G_h(\mathbf{q})G_P(\mathbf{q}) - G_f(\mathbf{q})^2)}, \\
\langle h_{\mathbf{q}} P_{-\mathbf{q}} \rangle_{H_0} &= \frac{-2k_BTG_f(\mathbf{q})}{L^2(4G_h(\mathbf{q})G_P(\mathbf{q}) - G_f(\mathbf{q})^2)}.
\end{aligned} \tag{2.3.8}$$

The last two terms of (2.3.7), which are higher order correlations, can be estimated by invoking Wick's theorem [65] as below

$$\langle P^4 \rangle_{H_0} = 3\langle P^2 \rangle_{H_0}^2, \quad \langle P^6 \rangle_{H_0} = 15\langle P^2 \rangle_{H_0}^3, \tag{2.3.9}$$

in which $\langle P^2 \rangle_{H_0} = \sum_{\mathbf{q}\in\mathcal{K}} \langle P_{\mathbf{q}}^2 \rangle_{H_0}$. Minimization of the variational free energy F_{var} with respect to the unknown propagators furnishes an upper bound of the exact free energy. Now let $\eta = \sum_{\mathbf{q}\in\mathcal{K}} \langle P_{\mathbf{q}}^2 \rangle_{H_0}$ and $\chi(\mathbf{q}) = 4G_h(\mathbf{q})G_P(\mathbf{q}) - G_f(\mathbf{q})^2$. Then substituting (2.3.8) and (2.3.9) into F_{var} (2.3.2), results in the following simplified form

$$\begin{aligned}
F_{\text{var}} = \sum \mathbf{q} \in \mathcal{K} \frac{k_BT}{2} \log(\chi(\mathbf{q})) + \frac{2k_BT}{\chi(\mathbf{q})} \left(\mathbf{q}^4 \kappa_b G_P(\mathbf{q}) + aG_h(\mathbf{q}) + f\mathbf{q}^2 G_f(\mathbf{q}) \right) \\
+ \frac{3a\eta^2 L^2 \epsilon_4}{P_s^2} + \frac{15a\eta^3 L^2 \epsilon_6}{P_s^4}.
\end{aligned} \tag{2.3.10}$$

We minimize the free-energy with respect to $G_h(\mathbf{q}), G_P(\mathbf{q})$ and $G_f(\mathbf{q})$ and obtain

$$
\begin{aligned}
0 &= \frac{\partial F_{\text{var}}}{\partial G_h(\mathbf{q})} \\
&= -2k_BT\Big\{a\frac{12G_f(\mathbf{q})^2\epsilon_4 P_s^2\eta + 90a\eta^2 G_f(\mathbf{q})^2\epsilon_6}{P_s^4\chi(\mathbf{q})^2} \\
&+ \frac{aG_f(\mathbf{q})^2 + 4G_P(\mathbf{q})^2|\mathbf{q}|^4\kappa_b}{\chi(\mathbf{q})^2} \\
&+ \frac{G_P(\mathbf{q})(4fG_f(\mathbf{q})|\mathbf{q}|^2 + G_f(\mathbf{q})^2)}{\chi(\mathbf{q})^2} \\
&- \frac{4G_h(\mathbf{q})G_P(\mathbf{q})^2}{\chi(\mathbf{q})^2}\Big\} \\
0 &= \frac{\partial F_{\text{var}}}{\partial G_P(\mathbf{q})} \\
&= -2k_BT\Big\{a\frac{48\eta\epsilon_4 P_s^2 G_h(\mathbf{q})^2 + 360\eta^2\epsilon_6 G_h(\mathbf{q})^2}{P_s^4\chi(\mathbf{q})^2} \\
&+ G_h(\mathbf{q})\frac{4G_h(\mathbf{q})(a - G_P(\mathbf{q})) + 4f|\mathbf{q}|^2 G_f(\mathbf{q})}{\chi(\mathbf{q})^2} \\
&+ \frac{(G_h(\mathbf{q}) + |\mathbf{q}|^4\kappa_b)G_f(\mathbf{q})^2}{\chi(\mathbf{q})^2}\Big\} \\
0 &= \frac{\partial F_{\text{var}}}{\partial G_f(\mathbf{q})} \\
&= k_BT\Big\{\frac{24a\eta G_f(\mathbf{q})G_h(\mathbf{q})(2\epsilon_4 P_s^2 + 15\eta\epsilon_6)}{P_s^4\chi(\mathbf{q})^2}, \\
&+ \frac{4G_f(\mathbf{q})}{\chi(\mathbf{q})^2}\Big(G_h(\mathbf{q})(a - G_P(\mathbf{q})) + |\mathbf{q}|^4\kappa_b G_P(\mathbf{q})\Big), \\
&+ \frac{8f|\mathbf{q}|^2 G_h(\mathbf{q})G_P(\mathbf{q}) + 2f|\mathbf{q}|^2 G_f(\mathbf{q})^2 + G_f(\mathbf{q})^3}{\chi(\mathbf{q})^2}\Big\},
\end{aligned}
\tag{2.3.11}
$$

wherein for differentiating the higher order correlations $\langle P^4\rangle_{H_0} = 3\eta^2$ and $\langle P^6\rangle_{H_0} = 15\eta^3$ we used the chain rule to write

$$
\frac{\partial\eta^n}{\partial G} = n\eta^{n-1}\sum_{\mathbf{q}\in\mathcal{K}}\frac{\partial\eta}{\partial G(\mathbf{q})} = n\eta^{n-1}\sum_{\mathbf{q}\in\mathcal{K}}\frac{\partial}{\partial G(\mathbf{q})}\langle P^2(\mathbf{q})\rangle_{H_0}. \tag{2.3.12}
$$

Solving the equations in (2.3.11) for the unknown propagators yields

$$\begin{aligned} G_h(\mathbf{q}) &= |\mathbf{q}|^4 \kappa_b \\ G_P(\mathbf{q}) &= a(1 + \frac{12\eta\epsilon_4}{P_s^2} + \frac{90\eta^2\epsilon_6}{P_s^4}) \\ G_f(\mathbf{q}) &= -2f|\mathbf{q}|^2. \end{aligned} \tag{2.3.13}$$

Subsequent substation in the expression for η, gives us

$$\begin{aligned} \eta &= \langle P^2 \rangle_{H_0} \\ &= \frac{1}{L^2} \int \langle P^2(\mathbf{x}) \rangle_{H_0} d\mathbf{x} = \frac{1}{L^2} \int \sum_{\mathbf{q},\mathbf{q}' \in \mathcal{K}} \langle P_{\mathbf{q}} P_{\mathbf{q}'} e^{\imath(\mathbf{q}+\mathbf{q}')\cdot\mathbf{x}} \rangle_{H_0} d\mathbf{x} \\ &= \frac{1}{L^2} \sum_{\mathbf{q},\mathbf{q}' \in \mathcal{K}} \delta(\mathbf{q}+\mathbf{q}') \langle P_{\mathbf{q}} P_{\mathbf{q}'} \rangle_{H_0} \int d\mathbf{x} = \sum_{\mathbf{q} \in \mathcal{K}} \langle P_{\mathbf{q}}^2 \rangle_{H_0} \\ &= \sum_{\mathbf{q} \in \mathcal{K}} \frac{4k_B T G_h(\mathbf{q})}{L^2(4G_h(\mathbf{q})G_P(\mathbf{q}) - G_f(\mathbf{q})^2)} \\ &= \sum_{\mathbf{q} \in \mathcal{K}} \frac{k_B T \kappa_b}{L^2(\kappa_b \xi - f^2)}, \end{aligned} \tag{2.3.14}$$

where $\xi = a(1 + \frac{90\eta^2\epsilon_6}{P_s^4} + \frac{12\eta\epsilon_4}{P_s^2})$ and η can be solved for to estimate the polarization fluctuation. Further details on the variational approach and its accuracy in the context of the current problem are provided in the Appendix.

2.4 Thermal fluctuations of the electric field

The computation of polarization correlation in Section 2.3 allows the estimation of the root mean square electric field. The polarized membrane induces an electric field that can be calculated using Maxwell's equations. Here we may consider two ideal boundary conditions: (1) non-conducting boundary conditions, in which the membrane exterior has the permittivity of vacuum and (2) conducting boundary condition, in which the surrounding electrolyte is perfectly conductive. The real boundary conditions are somewhere between these two extremes—we will find that our final results (at the level of approximation we are interested in) are insensitive to these two bounding boundary conditions. Accordingly,

we feel justified in avoiding the more complex nonlinear Poisson-Boltzmann framework. In the first case, we write the Maxwell equation as below

$$\mathrm{div}(-\epsilon_0 \nabla\phi + \frac{P}{d}\chi(z)\mathbf{e}_z) = 0, \tag{2.4.1}$$

where

$$\chi(z) = 1 \quad \text{if} \quad z \in [-\frac{d}{2}, \frac{d}{2}], \quad \text{otherwise} \quad = 0.$$

The solution can be conveniently found in Fourier space

$$\begin{aligned} \phi(\mathbf{x}, z) &= \sum_{\mathbf{q}\in\mathcal{K}} \hat{\phi}(\mathbf{q}, z)\mathbf{e}^{\imath\mathbf{q}.\mathbf{x}}, \\ \hat{\phi}(\mathbf{q}, z) &= \frac{\hat{P}_{\mathbf{q}}}{2d\epsilon_0|\mathbf{q}|}(e^{|\mathbf{q}|z} - e^{-|\mathbf{q}|z})e^{-|\mathbf{q}|d/2}. \end{aligned} \tag{2.4.2}$$

The ensuing voltage difference across the thickness of the membrane is

$$\begin{aligned} \Delta\hat{\phi}(\mathbf{q}) &= \hat{\phi}(\mathbf{q}, d/2) - \hat{\phi}(\mathbf{q}, -d/2) \\ &= \frac{P_{\mathbf{q}}(1 - e^{-d|\mathbf{q}|})}{d\epsilon_0|\mathbf{q}|}. \end{aligned} \tag{2.4.3}$$

The autocorrelation of the potential can be obtained by summing over all possible modes

$$\begin{aligned} \langle V^2\rangle &= \sum_{\mathbf{q}\in\mathcal{K}} \langle\Delta\hat{\phi}(\mathbf{q})^2\rangle \\ &= \sum_{\mathbf{q}\in\mathcal{K}} \frac{\langle P_{\mathbf{q}}^2\rangle(1 - e^{-d|\mathbf{q}|})^2}{d^2\epsilon_0^2|\mathbf{q}|^2}. \end{aligned} \tag{2.4.4}$$

The above sum can be approximately calculated by replacing it with an integration. For conducting boundary conditions, equation (2.4.4) simply reduces to

$$\langle V^2\rangle = \frac{1}{\epsilon_0^2}\sum_{\mathbf{q}\in\mathcal{K}} \langle P_{\mathbf{q}}^2\rangle. \tag{2.4.5}$$

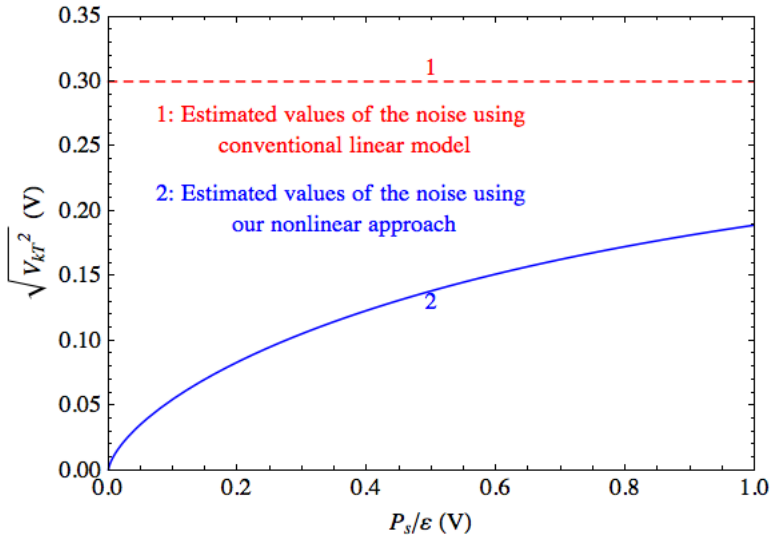

Figure 2.4.1: Calculated values of noise with different P_s

2.5 Power spectrum of the fluctuating electric field

The power spectrum of the electric field is the ensemble average of the time average of the power dissipation per unit frequency bandwidth and may be used to estimate the frequency dependence of our results [74]. This is necessary since experimental results indicate the noise threshold to be sensitive to the frequency of the applied field. This can be explained physically by considering the fact that the membrane is heavily occupied by fluctuating charges and dipoles, that can dissipate energy and generate noise during conformational transitions. Since the external fields are mostly time dependent–usually sinusoidal– it is best to compare the frequency spectrum of the thermal noise with that of the external field. In this section we calculate the power spectrum of the fluctuating voltage, from which we can estimate the Nyquist noise of the membrane. To this end, we assume a relaxation time, τ, during which the state of the system does not change. The relaxation time in biological membranes, depends on the diffusion constants of the membrane, dipoles and charges, and is roughly of the order of a millisecond [5]. This level of approximation, as will be seen in Section 2.6 where we present our results, suffices to draw experimentally relevant conclusions.

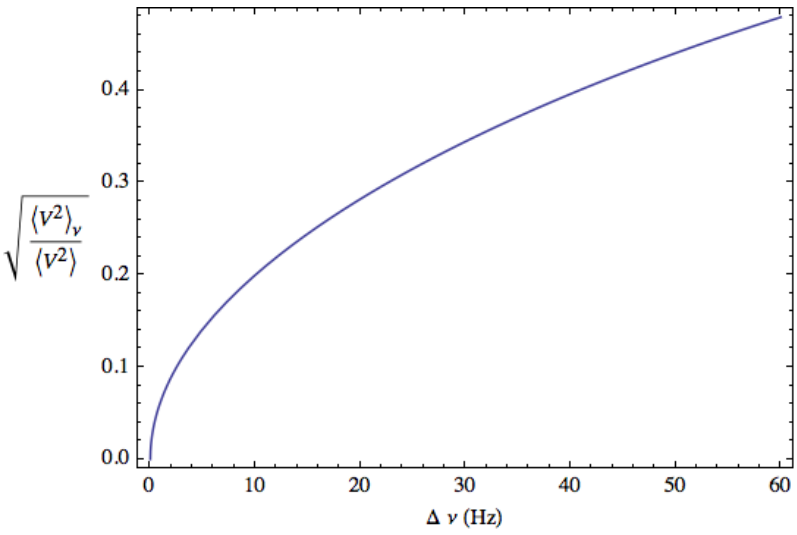

a

Figure 2.5.1: Calculated thermal noise in the presence of time-dependent fields.

[a]The relaxation time is considered to be 1 milli-second. Typically the frequencies of imposed electric fields do not exceed 60Hz, and most are, usually, lower. For frequencies less than 10Hz, the effect of frequency is quite significant.

The relaxation process is well-known to be an exponential decay in the effect of random fields

$$C(\tau) \propto e^{-t/\tau}. \tag{2.5.1}$$

Then the power spectrum of the fluctuating electric field is obtained as

$$\begin{aligned} G(\nu) &= 4\int_0^\infty \langle V^2\rangle e^{-t/\tau}\cos(2\pi\nu t)dt \\ &= \frac{4\langle V^2\rangle\tau}{1+(2\pi\nu\tau)^2}. \end{aligned} \tag{2.5.2}$$

This value is equivalent to the Nyquist noise power in a resistor — $4Rk_BT$. For low frequency ranges in which $\nu\tau \ll 1$, the power is almost constant — frequency-independent— and the fluctuating voltage is considered to be white noise. In this case the Nyquist noise for different frequency bandwidth can be calculated by simply multiplying the power by the frequency bandwidth: $\langle V^2\rangle_\nu = 4Rk_BT\triangle\nu$. However, at high frequencies, since the power spectrum is no longer a constant, the Nyquist noise should be calculated by integrating

equation (2.5.2) over all possible values of the frequency. Assuming that the frequencies from external electrical fields do not exceed 60Hz, to draw a comparison with the thermal noise, we have calculated the noise, $\langle V^2 \rangle_\nu$ for different frequency bandwidth, up to 60Hz—the results is shown in Figure 2.5.1. As evident, at very low frequencies (0-10Hz), the noise threshold can be as much an order of magnitude smaller than the associated high-frequency value, $\langle V^2 \rangle$.

2.6 Relevance to real biological membranes

So far, we have considered model fluid membranes. Real biological membranes are highly heterogeneous and are covered with a large fraction of proteins. In such a crowded environment, polarization is spatially correlated within its plane. This non-locality of the polarization may play a significant role. One simple (and completely *phenomenological*) way to take this into account is to add a term proportional to the spatial gradient of the polarization. This notion is inspired from similar considerations in crystalline ferroelectrics and approximations made in the quantum mechanical density functional theory. Let δ be the smallest correlation length. Then we can modify the quadratic part of the original Hamiltonian (2.2.2) as follows

$$H^q = \int_{\mathbb{S}} \tfrac{1}{2}\kappa_b(\nabla^2 h(\mathbf{x}))^2 + \tfrac{1}{2}aP(\mathbf{x})^2 + \tfrac{1}{2}a\delta^2|\nabla P(\mathbf{x})|^2 + fP(\mathbf{x})\nabla^2 h(\mathbf{x})d\mathbf{x}. \tag{2.6.1}$$

To estimate the strength of the polarization gradient term or alternatively, the order of magnitude of δ, we make two distinct arguments—both lead to similar results and are likely to bound the actual value: (1) We may consider the polarization correlation to be linked with the tension correlation. The rationale is that the electromechanical conformation of the mechanosensitive channels are coupled to the tension of the membrane [75]. (2) A geometrical argument may be made that δ ought to scale with the average inter-protein distance. Based on the first argument, using a result given by [17], we consider the ratio of

Table 2.6.1: Estimated values of thermal noise limit in cell membranes. The noise was calculated for a cell of size $L \approx 150\mu m$.

Frequency (Hz)	Experimental values(V/cm)	Linear dielectric model (V/cm)	Nyquist noise in the equivalent RC circuit (V/cm)	Present model for a pure lipid bilayer[a] (V/cm)	Predicted values for a real biomembrane (V/cm)
	Chicken fibroblasts* [59]				
1	0.6	6.1×10^5	3.6×10^3	1×10^3	100
	Bovine fibroblasts* [58]				
10^{-1}	300	6.1×10^5	1.1×10^3	320	30
1	2.1	6.1×10^5	3.6×10^3	1×10^3	100
10^1	1.5	6.1×10^5	1.1×10^4	3.2×10^3	300
10^2	30	6.1×10^5	3.6×10^4	9.5×10^3	900
10^3	600	6.1×10^5	1.1×10^5	1.5×10^4	1400

[a]Considering the thickness of the membrane to be $d \approx 5nm$, we have converted the reported cell-level value to the membrane noise value.

the two-point tension-correlation with respect to self-correlation

$$\eta = \frac{\langle|\nabla h(0)\nabla h(\delta)|\rangle}{\langle|\nabla h(0)|^2\rangle} = \frac{\sum_{\mathbf{q}}\langle q^2 h_{\mathbf{q}}^2\rangle \mathbf{e}^{\imath \mathbf{q}\cdot\delta}}{\sum_{\mathbf{q}}\langle q^2 h_{\mathbf{q}}^2\rangle}, \tag{2.6.2}$$

where δ is the relative position vector between two points. By integrating over all modes, for different values of δ, we find that for $\delta \geqslant 5d$ the ratio is less than 0.1, which is essentially negligible. Therefore, we conclude that for biological membranes, the minimum correlation length is at least $5d$.

According to [5], biological membranes are extremely crowded. They estimate that 30-55% of the area of the lipid membrane is occupied by various types of protein channels. The radius of the channels in their open state is roughly about 2-3nm. Using these values, the average distance between the centers of the proteins can be estimated to be about 6-12 nm. This argument provides an alternative way to estimating δ.

Recalculating the fluctuations of polarization, using equation (2.6.1) for the quadratic part of the total Hamiltonian (2.3.1), gives the estimated noise for different values of δ. For

$\delta \approx 10nm$, we obtain values of noise voltage which is almost one order of magnitude smaller than what we obtained earlier in Section 2.4.

2.7 Results and Discussion

For quantitative results, we must estimate P_s. The breakdown voltage of the membrane is around $1V$—-and the polarization corresponding to this represents a strict upper bound. As it can be appreciated from Figure 2.2.1(a), significantly higher electric fields are required to polarize a membrane close to P_s. Evidently $P_s \to \infty$, represents the linear case which corresponds to the quadratic Hamiltonian. Indeed, our nonlinear numerical results coincide with the linear estimates discussed in the introduction of the paper if P_s is taken to be very large. The variation of the noise threshold with respect to choice of P_s is shown in Figure 2.4.1 where the abscissa corresponds to the voltage corresponding to P_s. To solve the Maxwell equation in Section 2.4, we used the conducting boundary condition, since it gives us the upper bound of the voltage noise. In our calculations, we have assumed that $\kappa_b = 25k_BT$, $\epsilon = 2\epsilon_0 =$, $f^2/\kappa_b \approx a/2$. For the higher order terms, since the dominant parameter is P_s we have set ε_i equal to 1. We have verified that this does not significantly alter our results. The linear framework yields noise threshold around 0.3V. Even if we adopt the excessively simple model that the dielectric response is almost linear up until the strict upper limit of the breakdown voltage, our models predict a noise threshold that is still much lower than 0.3V. To further refine our estimate of P_s, we take recourse in recent experimental work [76] that has documented nonlinear dielectric properties for a specific biomembrane (of outer hair cells in the ear). There is significant diversity among biological membranes, however, their linear dielectric behavior is markedly similar *and* since our primary interest is the in the order of magnitude estimates, we used the experimental estimate of P_s by [76] as a representative value. According to their model, the length change of the outer hair cell with voltage, can be explained by a nonlinear relationship between the flexoelectric coefficient and the applied electric field. To explain the nonlinear dependence of flexoelectric coefficient on the membrane voltage, they proposed a nonlinear relationship between the polarization density and the electric field. Their work suggest that for dipole

moments less than 10D, the dielectric behavior of the membrane is linear. Considering the dipole density of such membranes to be about $6000/\mu m^2$, we estimate P_s/ϵ to be less than 10 mV. Using these estimates, our calculations of the noise threshold appear in Table 2.6.1 where a comparison is also made with known experimental results and other models. We have converted the estimated voltage noise to the electric field noise, by using the thickness of the membrane: $\overline{E}_{k_BT} = \overline{V}_{k_BT}/d$. Some comments related to the frequency effect and the consideration of gradient of polarization (relevant for real biological membranes) are warranted. Consideration of both effectively reduce the noise threshold estimates by an order of magnitude. For example, consideration of the gradient of polarization term along with the estimate of $\delta = 10nm$ (see Section 2.6) leads to the noise threshold estimate that is almost 10 times smaller that for a model fluid membrane. The experimental values in the second column evidently have significant scatter. The notable aspect however, as already emphasized briefly in the Introduction, is how low these are compared to the estimates from conventional models (column 3). We note that in the cited experimental references and prior works, the noise estimates were made for the entire cell. In Table 2.6.1, we have converted the noise values from the cell level to the membrane level through the following relations: $E_{mem} \approx E_{cell} \times L/d$, in which L is the size(radius) of the cell. Here, we have assumed that the electric field is uniform across the thickness of the membrane and cell, and used the equation: $\overline{V}_{k_BT} = \overline{E}_{mem} \times d = \overline{E}_{cell} \times L$. The fourth column is the Nyquist noise at different frequencies. The results of our model for pure lipid bilayers are shown in column 5. In the last column, we have provided the estimated values of noise in real biological membranes, where we have (phenomenologically) considered the interactions between the channels and other physical inhomogeneities, using $\delta \approx 10nm$.

2.8 Concluding Remarks

In summary, we have pointed out the rather large discrepancy that exists between the (experimentally estimated) minimum electric field that an ideal fluid membrane can detect and what the existing theoretical models predict. A consistent accounting for the influence of the nonlinear dielectric behavior of membranes on the thermal fluctuations of the mem-

brane electric field appears, in large part, to address this issue. The dielectric nonlinearity can be explained physically by the dipole saturation phenomena, and the consequent fact that there is an upper limit, P_S to which a membrane is capable of being polarized. Our mathematical framework yields analytical solution for the thermal electrical noise of membranes. In real biological membranes (as opposed to fluid membranes), we must contend with more complex situations. Proteins, salts, charged objects, ionic flux and the polarized double layers are some of the items that may contribute to the fluctuations of electric field in real biological membranes. To some extent, phenomenologically, we consider the effect of inhomogeneities through an added energetic term that sets the scale for the membrane in-plane correlations of polarization. The predictions of our theoretical framework provide noise estimates that are of the same order of magnitude as experiments. In particular, our work provides both a benchmark estimate for model fluid membranes (which should be experimentally testable) and reasonable predictions for biological membranes (where significantly more complexity may be expected). Further experimental studies are required to understand and clarify the quantitative aspects of dielectric nonlinearity in biological membranes and settle the rather large scatter in the existing experimental data.

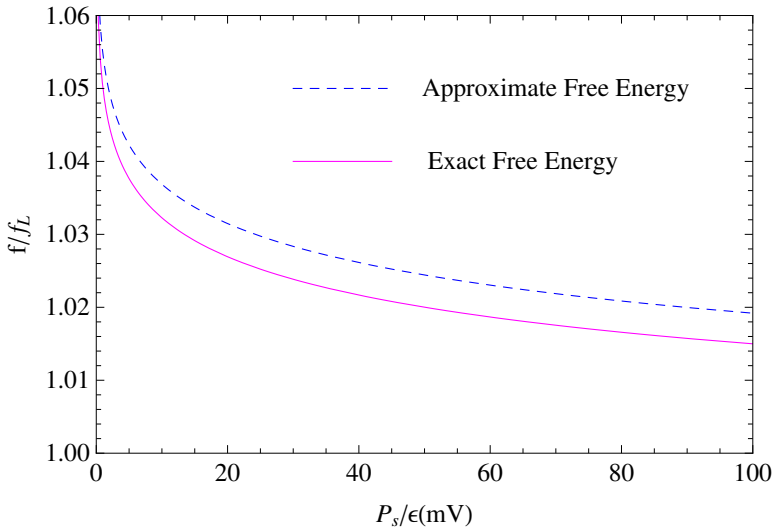

Figure 2.8.1: Comparison of the exact free energy and the corresponding approximate one

Appendix: Details on the variational approximation

Kleinert and co-workers introduced the so-called variational perturbation method (VPT) to handle the statistical mechanics of anharmonic Hamiltonians [65]. A straightforward perturbation approach (expanded around, say, a quadratic Hamiltonian) results in a divergent series. On the other hand, variational approximation using trial function, while effective, works best if the trial function is an "inspired" guess. The VPT combines both approaches and it has been shown that the resulting series converges exponentially. In the present work, we have used the VPT while retaining only the first term. This approach is extensively used to deal with thermal fluctuations of fluid membranes in different contexts [8, 24].

In this appendix we present some calculations that provide some assurance to the quality of our approximation. Consider the following Hamiltonian which, while anharmonic in the polarization field, ignore the mechanical displacement fields

$$H = \int \tfrac{1}{2} a P^2 + \tfrac{a\varepsilon_4}{P_S^2} P^4. \tag{2.8.1}$$

The advantage of the Hamiltonian in (2.8.1) that includes a fourth order polarization term (but no field derivatives) is that the partition function and the free energy can be obtained in closed-form and therefore provides a simple (but related) test case to assess

the approximation we have used in this work. To deal with the path integral in the partition function, we first discretize the Hamiltonian (2.8.1). To this end we assume that the membrane consists of 2N molecules located at $\mathbf{x} \in \mathcal{L} = \Lambda(n_1, n_2) : n_1, n_2 = 1, \cdots, m$, where $\Lambda = L/m$. The total number of degrees of freedom are $N = m^2$ and each has an area of $A_0 = \Lambda^2$. Given that the area density of the dipole moment at point $\mathbf{x}$ is $P(\mathbf{x})$, the dipole moment $\tilde{P}(\mathbf{x})$ at this point can be calculated by: $\tilde{P}(\mathbf{x}) = P(\mathbf{x})A_0$. Substituting this into equation (2.8.1) and summing over all degrees of freedom, we obtain

$$H = \textstyle\sum_{\mathbf{x}\in\mathcal{L}} \frac{1}{2} a \frac{\tilde{P}^2(\mathbf{x})}{A_0} + a\varepsilon_4 \frac{\tilde{P}^4(\mathbf{x})}{A_0^3 P_S^2}. \tag{2.8.2}$$

The partition function is

$$\begin{aligned} Z = \int \exp(-\beta H) &= \int \exp(-\beta(\textstyle\sum_{\mathbf{x}\in\mathcal{L}} \frac{1}{2} a \frac{\tilde{P}^2(\mathbf{x})}{A_0} + a\varepsilon_4 \frac{\tilde{P}^4(\mathbf{x})}{A_0^3 P_S^2})) \textstyle\prod_{\mathbf{x}\in\mathcal{L}} d\tilde{P}(\mathbf{x}) \\ &= \textstyle\prod_{\mathbf{x}\in\mathcal{L}} \frac{e^{\frac{aA_0\beta P_S^2}{32\epsilon_4}} A_0 P_S K_{\frac{1}{4}}\left(\frac{a\beta A_0 P_S^2}{32\epsilon_4}\right)}{2\sqrt{2\epsilon_4}}, \end{aligned} \tag{2.8.3}$$

where $K_{\frac{1}{4}}$ is the modified Bessel function of the second kind. The free energy per unit area is

$$\begin{aligned} f = \frac{F}{NA_0} &= -\frac{k_B T}{NA_0} \log Z \\ &= -\frac{aP_S^2}{32\epsilon_4} - \frac{k_B T}{A_0} \log \frac{A_0 P_S K_{\frac{1}{4}}\left(\frac{aA_0 P_S^2}{32 k_B T \epsilon_4}\right)}{2\sqrt{2\epsilon_4}}. \end{aligned} \tag{2.8.4}$$

In the limits of $P_S \to \infty$ or $\epsilon_4 \to 0$, which corresponds to the quadratic Hamiltonian, we obtain

$$f_L = -\tfrac{k_B T}{2A_0} \log \tfrac{2\pi k_B T A_0}{a}. \tag{2.8.5}$$

Also the fluctuations of the dipole moment at each point $\mathbf{x}' \in \mathcal{L}$ can be obtained using

the partition function (2.8.3)

$$\begin{aligned}\langle \tilde{P}^2(\mathbf{x}')\rangle &= \tfrac{1}{Z}\int \tilde{P}^2(\mathbf{x}')\exp(-\beta(\textstyle\sum_{\mathbf{x}\in\mathcal{L}}\tfrac{1}{2}a\frac{\tilde{P}^2(\mathbf{x})}{A_0}+a\varepsilon_4\frac{\tilde{P}^4(\mathbf{x})}{A_0^3P_S^2}))\prod_{\mathbf{x}\in\mathcal{L}}d\tilde{P}(\mathbf{x})\\ &= \frac{A_0^2P_S^2}{8\epsilon_4}\left(\frac{K_{\frac{3}{4}}\left(\frac{aA_0P_S^2}{32k_BT\epsilon_4}\right)}{K_{\frac{1}{4}}\left(\frac{aA_0P_S^2}{32k_BT\epsilon_4}\right)}-1\right).\end{aligned} \tag{2.8.6}$$

The root mean square of the voltage across the membrane is given by

$$V_{\text{exact}} = \sqrt{\langle V^2\rangle} = \frac{\sqrt{\langle \tilde{P}^2(\mathbf{x}')\rangle}}{A_0\epsilon_0}. \tag{2.8.7}$$

To compare the exact results with that of the variational approximation, we calculate the free energy per unit area and the root mean square of the voltage across the membrane, by minimizing the right hand side of the inequality (2.3.2) with respect to the trial parameter. To start, consider the trial Hamiltonian as below

$$H_0 = \textstyle\sum_{\mathbf{x}\in\mathcal{L}}\tfrac{1}{2}\bar{a}\tilde{P}^2(\mathbf{x}), \tag{2.8.8}$$

where $\bar{a}$ is the trial dielectric parameter. Using the above Hamiltonian, we calculate the right hand side of the inequality (2.3.2) as below

$$\begin{aligned}F_{\text{var}} &= \alpha_F + \tfrac{k_BT}{2}\textstyle\sum_{\mathbf{x}\in\mathcal{L}}\log\bar{a} + \sum_{\mathbf{x}\in\mathcal{L}}\frac{a}{2A_0}\langle\tilde{P}^2(\mathbf{x})\rangle_{H_0} + \sum_{\mathbf{x}\in\mathcal{L}}\frac{a\epsilon_4}{A_0^3P_S^2}\langle\tilde{P}^4(\mathbf{x})\rangle_{H_0}\\ &= \alpha_F + \tfrac{k_BT}{2}\textstyle\sum_{\mathbf{x}\in\mathcal{L}}\log\bar{a} + \sum_{\mathbf{x}\in\mathcal{L}}\frac{a}{2A_0}\frac{k_BT}{\bar{a}} + \sum_{\mathbf{x}\in\mathcal{L}}\frac{3a\epsilon_4}{A_0^3P_S^2}\left(\frac{k_BT}{\bar{a}}\right)^2,\end{aligned} \tag{2.8.9}$$

where we have used Wick's theorem to obtain the higher order correlation function $\langle\tilde{P}^4(\mathbf{x})\rangle_{H_0} = 3\langle\tilde{P}^2(\mathbf{x})\rangle_{H_0}^2$. Also, we have directly used the equipartition theorem to calculate the correlation function: $\langle\tilde{P}^2(\mathbf{x})\rangle_{H_0} = k_BT/\bar{a}$. Minimization of the variational free energy with respect to the trial dielectric parameter, provides us with an upper bound of the exact free energy

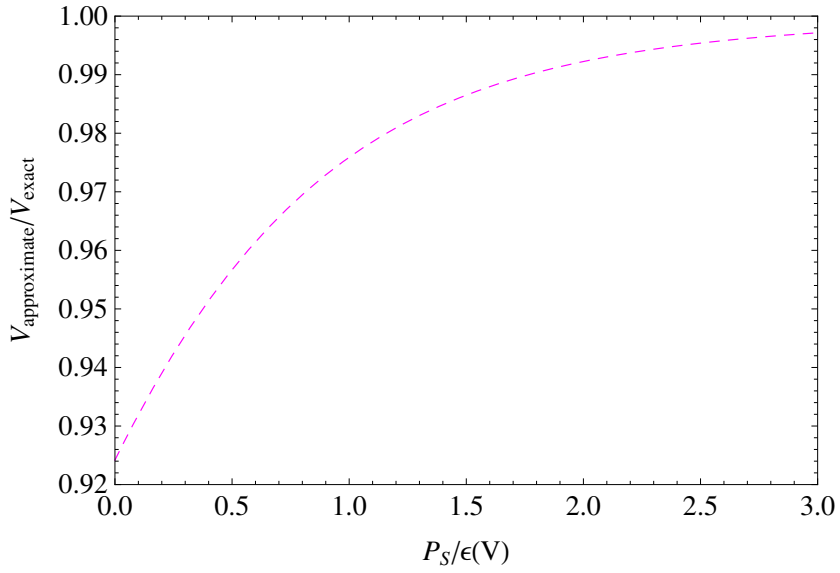

Figure 2.8.2: Comparison of exact root mean square of the voltage and the corresponding approximate one

$$\frac{\partial F}{\partial \bar{a}} = \sum_{\mathbf{x}\in\mathcal{L}} \left(\frac{k_B T}{2\bar{a}} - \frac{k_B T a}{2A_0 \bar{a}^2} - \frac{6a\epsilon_4}{A_0^3 P_S^2 \bar{a}^3} (k_B T)^2 \right)$$
$$:= 0. \tag{2.8.10}$$

The solution of equation (2.8.10) will give us the renormalized dielectric parameter as below

$$\bar{a} = \frac{a}{2A_0} \left(1 + \sqrt{1 + \frac{48 k_B T \epsilon_4}{a A_0 P_S^2}} \right). \tag{2.8.11}$$

The renormalized dielectric parameter may be substituted in (2.8.8) and by recourse to the equipartition theorem, we may calculate the free energy per unit area, fluctuations of the dipole moment, and eventually the root mean square of the voltage across the membrane. A comparison between the variational approximation obtained using (2.8.11), and the exact values of the free energy per unit area and the root mean square of the voltage, from equations (2.8.4) and (2.8.7), respectively, is depicted in Figures 2.8.1 and 2.8.2. In Figure 2.8.1, the free-energies are normalized with respect to the one obtained from

the quadratic Hamiltonian (the linear dielectric case, (2.8.5)). The variational free energy which is shown is dashed blue is always above the exact free energy (magenta). On the other hand, since the variational free energy is always greater than the exact free energy, the estimated fluctuations (obtained from variational method) will be always smaller than the exact fluctuations. We have also compared the estimated and the exact root mean square of the voltage in figure 2.8.2. The vertical axis in this plot is the ratio of the variational estimate with respect to the exact value. For any values of P_S, the error is less than 10%. In case more accurate results are of interest, progressing to the second order of the variational perturbation method[65] is required.

Chapter 3

Thermal Fluctuations of Vesicles and Nonlinear Curvature Elasticity—Implications for Size-dependent Renormalized Bending Rigidity and Vesicle Size Distribution

Both closed and open biological membranes noticeably undulate at physiological temperatures. These thermal fluctuations influence a broad range of biophysical phenomena, ranging from self-assembly to adhesion. In particular, the experimentally measured thermal fluctuations spectra also provides a facile route to the assessment of mechanical and certain other physical properties of biological membranes. The theoretical assessment of thermal fluctuations, be it for closed vesicles or the simpler case of flat open lipid bilayers, is predicated on assuming that the elastic curvature energy is a quadratic functional of the curvature tensor. However, a qualitatively correct description of several phenomena

such as binding-unbinding transition, vesicle-to-bicelle transition, appearance of hats and saddles among others, appear to require consideration of constitutively nonlinear elasticity that includes fourth order curvature contributions rather than just quadratic. In particular, such nonlinear considerations are relevant in the context of large-curvature or small-sized vesicles. In this work we discuss the statistical mechanics of closed membranes (vesicles) incorporating both constitutive and geometrical nonlinearities. We derive results for the renormalized bending rigidity of small vesicles and show that significant *stiffening* may occur for sub-20 nm vesicle sizes. Our closed-form results may also be used to determine nonlinear curvature elasticity properties from either experimentally measured fluctuation spectra or microscopic calculations such as molecular dynamics. Finally, in the context of our results on thermal fluctuations of vesicles and nonlinear curvature elasticity, we reexamine the problem of determining the size distribution of vesicles and obtain results that reconcile well with experimental observations. However, our results are somewhat paradoxical. Specifically, the molecular dynamics predictions for the thermo-mechanical behavior of small vesicles of prior works, appear to be inconsistent with the nonlinear elastic properties that we estimate by fitting to the experimentally determined vesicle size-distribution trends and data.

3.1 Introduction

Biological membranes are ubiquitous in life, and form the envelope through which cells and organelles interact with their surroundings [77]. Lipid bilayers, which primarily consist of self-assembled phospholipid molecules, often form closed vesicles [78]. Usually just a few nanometers thick, the membranes serve as the gatekeepers for the cells and vesicles and aid in the transport of chemicals, facilitate mechanical and electrical signaling, transduction and adhesion. The vesicles, depending on the specific membrane composition and the surrounding environment, can exhibit a diversity of morphologies and of course serve as multi-purpose carriers that are capable of facilitating communication among cells, transporting functional genetic information as well as management of cellular waste. Aside from fundamental biological studies, lipid-based vesicles are often also created artificially in the

laboratory for applications in drug design and delivery.

Although membranes are microscopically quite complex, their mechanical behavior is reasonably well-described by the phenomenological theory of elasticity and just a few continuum parameters such as the bending moduli and surface tension. Specifically, the oft-used Canham-Helfrich's theoretical framework parametrizes the energy cost of the deformation of a tension-less membrane patch by the following quadratic form [1, 2, 79, 80, 81][1]

$$F_b = \int_{\mathbb{S}} \frac{1}{2}\kappa_b(H - H_o)^2 + \bar{\kappa}(K - K_o). \tag{3.1.1}$$

Here κ_b and $\bar{\kappa}$ are the bending moduli that, respectively, parametrize the energy change due to changes in the mean (H) and Gaussian (K) curvatures. The corresponding spontaneous curvatures are denoted by H_o and ${K_o}^2$. The elastic energy scale is set by the bending modulus and surface tension. Their typical values are such that membranes are usually hard to stretch but bend (curve) quite easily [4, 5]. Typical bending modulus of most lipid-bilayers is between 5 and $25k_BT$—-small enough compared to the thermal energy scale that membranes undulate or fluctuate noticeably at physiological temperatures [4, 5, 6, 7, 8]. The study of these experimentally observed and widely studied thermal fluctuations has been one of the cornerstones of biophysical research on membranes [6, 7, 8, 82, 83]. Statistical mechanics of open (nearly) flat membranes is well-developed and, to a comparatively lesser degree of exhaustiveness, several works also exist that describe the thermal fluctuations of closed vesicles [28, 29, 30, 31, 7]. The reason for the interest in thermal fluctuations of membranes is simple; aside from fundamental scientific curiosity, the fluctuations have been found to be responsible for the so-called entropic (steric) repulsive force between mem-

[1]This specific form is not quite the same as that originally presented by Canham or Helfrich. Several researchers have motivated the Helfrich-Canham Hamiltonian from fundamental grounds i.e. both as a derivation from three-dimensional solid or liquid crystal elasticity or statistical mechanics [79, 80, 81]. The specific form in Equation (6.1.1) is taken from Maleki and Fried [80] and as motivated by them, inclusion of spontaneous Gaussian curvature is important in certain situations.

[2]We emphasize a point which is sometimes glossed over but quite clearly highlighted by Maleki and Fried [80]. H_o can be ascribed to two contributions, geometric or constitutive. While the former corresponds to asymmetries between the bilayer leaflets, the latter denotes the stable equilibrium state of a membrane, which is zero for a flat membrane and can be nonzero for spherical vesicles.

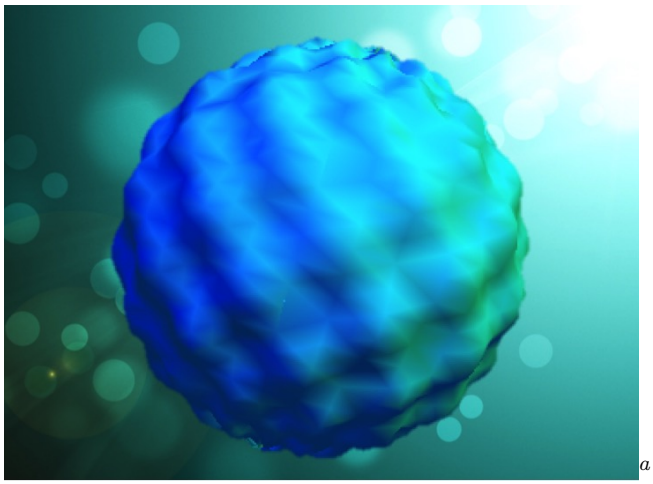 [a]

Figure 3.1.1: A schematic showing fluctuations of a spherical vesicle.

[a]Due to the small bending stiffness of biological membranes, compared with the thermal energy scale, such vesicles undergo considerable undulations at physiological temperatures. Experimental measurement of the amplitude of the fluctuations provides a facile route to the determination of the bending stiffness of the vesicles.

branes [84, 33, 34] and strongly influence phenomena such self-assembly, adhesion, binding-unbinding transitions, membrane fusion and many others [6, 85, 86, 87]. In particular, the experimentally measured fluctuation spectra or calculated via microscopic methods such as molecular dynamics, has provided a facile route to estimate mechanical and other related properties of membranes [13, 14, 15, 16]. For instance, in the case of a large, nearly flat membranes, the following result for the fluctuations of the out of plane displacement field h, can be easily derived based on the linearized version of the quadratic Hamiltonian described in Equation (6.1.1) : $\langle h^2 \rangle \propto k_B T/\kappa_b$ [5]. This basic result has been extended to numerous other physically relevant contexts providing an avenue to extract useful information e.g. incorporation of electromechanical coupling, tilt of lipids, presence of proteins or inclusions, proximity to substrates or other vesicles among others [17, 18, 19, 20, 21, 22, 23, 24].

For very large cells and/or vesicles, assuming that the membrane is nearly flat is a reasonable assumption and considerably simplifies the statistical mechanics analysis. However, this assumption is certainly in error for even moderately sized vesicles and may conceal some interesting physical effects due to the presence of finite curvature. For instance Morse

and Milner [29] showed that the free-energy of a single vesicle *increases* logarithmically with vesicle size, if finite-size contributions are incorporated, as opposed to a logarithmic *decrease* predicted for a nearly-flat membrane. Accordingly, several works have devoted attention to the more difficult problem of understanding the fluctuation behavior of closed membranes [28, 29, 30, 31, 7]. In particular, one motivating factor has been the experimentally observed size-distribution of vesicles [88]. A collection of a fixed number of vesicles with different sizes can freely exchange amphiphilic molecules until a thermodynamic equilibrium state is reached. Typically, the experimentally observed size distribution of an ensemble of vesicles at equilibrium is a Gaussian in nature, with a rather large cut-off radius of about 10–20 nm. Theoretical models that purport to explain vesicle size-distribution trends, do so based on contributions from the elastic bending energy and the chemical potential of the amphiphilic molecules that is required to create a vesicle. However, such models—-which are predicated on the quadratic Helfrich Hamiltonian described in (6.1.1)—appear to be unable to completely explain all features of the experimentally observed vesicle size-distribution.

Our work is motivated by the following observations and questions:

- How does the bending modulus get renormalized for high-curvature or small-sized vesicles? Ostensibly, for small vesicles, nonlinear curvature elasticity properties should play a significant role; do they indeed do so?

- In analogy with what has been done in the case of quadratic Helfrich-Canham Hamiltonian, it would also be desirable to have closed-form expressions for the thermal fluctuation spectra of nonlinear curvature elasticity to readily extract nonlinear elastic properties via experiments or molecular dynamics.

- The experimentally observed size-distributions of vesicles appear to be at odds with all theoretically derived distributions. Helfrich speculated and (qualitatively) proposed that nonlinear curvature elasticity may play a role in the correct prediction of vesicle size-distribution. However, a derivation of vesicle size distribution that includes thermal fluctuations within a nonlinear curvature elasticity framework is still missing in

the literature.

- Development of the statistical mechanics of closed membranes, incorporating fourth order nonlinear curvature elasticity, may be useful to understand various biophysical phenomena for small vesicles e.g. adhesion, modification of repulsive forces, binding-unbinding among others.

To address the aforementioned issues, in the present work, we develop the statistical mechanics of closed spherical vesicles that are described by fourth order constitutively nonlinear curvature elasticity and may be suitable for the study of small-sized vesicles. The outline of the paper is as follows: Nonlinear fourth order curvature elasticity is described in Section II along with several aspects of the problem setup. The statistical mechanics of closed vesicles is developed in Section III, where we present the results for the renormalization of bending modulus of small vesicles followed by, in Section IV, the implications of our work for the assessment of size-distribution of vesicles. Our results appear to be paradoxical in light of some past computation of nonlinear elasticity properties. This, along with other issues, are discussed in the Section V where we also conclude the work.

3.2 Nonlinear Curvature Elasticity and Problem Setup

Consider a closed vesicle described by an enclosing surface $\mathbb{S}$. The elastic energy density may be represented by $\psi = \bar{\psi}(H, K)$. As has been discussed elsewhere[80], treatment of the vesicle surface as an isotropic fluid membrane and the foundational principles of continuum mechanics restrict the dependence of ψ solely to (H, K). Assuming conservation of area and volume, in the absence of external forces, the total potential energy of the vesicle can be written as

$$E = \int_{\mathbb{S}} (\psi + \sigma) d\mathbb{S} + \int_V p dV, \tag{3.2.1}$$

where σ and p are the surface tension and osmotic pressure, respectively. The conventional vesicle equations, as usually found in the literature, are obtained by assuming a quadratic form for ψ i.e. Equation (6.1.1). The equilibrium equations, derivable by means of variational calculus, however can proceed without the actual specification of ψ and has been carried out by a number of authors [7, 89, 90, 91, 92, 93]. We quote below the result in the form presented by Biria et al. [94]

$$\begin{aligned}&\bar{\psi}_H(2H^2-K)+\frac{1}{2}\Delta_S\bar{\psi}_H+2\bar{\psi}_K HK+2\Delta_S(\bar{\psi}_K H)\\&-\operatorname{div}_S(\mathbf{L}\nabla_S\bar{\psi}_K)-2(\nabla_S H)\cdot(\nabla_S\bar{\psi}_K)-2\bar{\psi}_K\Delta_S H\\&-2H(\psi+\sigma)=p.\end{aligned}\tag{3.2.2}$$

Here, the subscript H (and K) denote the derivative with respect to H (and K). Further, $\mathbf{L}$ is the curvature tensor and ∇_S, Δ_S and div_S correspond to surface gradient, surface Laplacian and surface divergence operators[3], respectively [94].

Fourth order nonlinear curvature elasticity is obtaining by considering all the invariants of the curvature tensor $\mathbf{L}$ up to fourth order. Ignoring the spontaneous curvature, this leads to

$$\bar{\psi}(H,K)=\frac{1}{2}\kappa_b H^2+\overline{\kappa}K+\frac{1}{2}\gamma_1 H^4+\frac{1}{2}\gamma_2 H^2K+\frac{1}{2}\gamma_3 K^2,\tag{3.2.3}$$

where γ_i are the fourth order moduli.

In linearized curvature elasticity (i.e. the quadratic Helfrich theory), assuming that the

[3]Let $\mathbf{n}$ be the normal vector to the surface $\mathbb{S}$. A surface projection tensor may be defined as:

$$\mathbf{P}=\mathbf{I}-\mathbf{n}\otimes\mathbf{n},$$

where $\mathbf{I}$ is the identity tensor. The surface gradient, surface Laplacian and surface divergence of a scalar field f and a vector field $\mathbf{g}$ can then be defined in terms of $\mathbf{P}$ and their smooth extensions f^e and $\mathbf{g}^e$ as [94]

$$\begin{aligned}&\nabla_S f=\mathbf{P}\nabla f^e, \qquad \nabla_S\mathbf{g}=(\nabla\mathbf{g}^e)\mathbf{P},\\&\operatorname{div}_S\mathbf{g}=\mathbf{P}\cdot\nabla\mathbf{g}^e, \qquad \Delta_S f=\operatorname{div}_S(\nabla_S f).\end{aligned}$$

Finally, the curvature tensor takes the following form: $\mathbf{L}=-\nabla_S\mathbf{n}$.

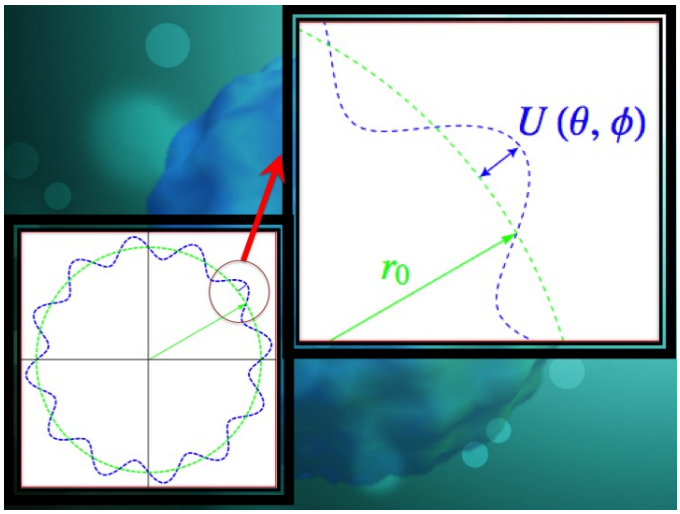

Figure 3.2.1: Displacement field fluctuations of the surface of a spherical membrane. We have assumed that the fluctuations are normal to the surface. The fluctuating mid-plane displacement is normalized as $u(\theta, \phi) = U(\theta, \phi)/r_0$

vesicle is a sphere of radius R, the Young-Laplace equation takes the form: $R = 2\sigma/p$. In the nonlinear setting however, due to the presence of higher order moduli, this relation is modified. Assuming that sphere is the stable state, Equation (3.2.2) results in

$$-\frac{\gamma_1}{R^5} + \frac{\gamma_3}{R^5} = p - \frac{2\sigma}{R}, \tag{3.2.4}$$

which implies that for a certain range of pressure, there may be more than one sphere solution, that might be either stable or unstable depending on the values of γ_i. In this paper we will not focus on the stability of different morphologies in the context of nonlinear elasticity. It is assumed that the conditions (based on the values of surface tension, pressure and the elastic properties) ensure that a spherical vesicle is stable. For further details on this topic, the reader is referred to references [95, 96, 97].

In what follows, we will assume that the topology of the membrane does not change as it undergoes thermal fluctuations and accordingly, the contribution of the Gaussian curvature to the free energy may be neglected. [4]

[4]In the conventional (linear) model, according to Gauss-Bonnet theorem, the integration of the Gaussian curvature over the surface is invariant under any deformation and hence the contribution of the Gaussian curvature to the bending energy may be ignored. This is, however a global constraint on the topology of the

We rescale the fourth-order moduli to emphasize the fact that nonlinear curvature elasticity introduces an intrinsic length scale—-in sharp contrast to the conventional Helfrich-theory: $\gamma_c = \kappa_b \ell_c^2$ where ℓ_c is the critical length scale that determines when the nonlinearity may be ignored, $\ell_c H \ll 1$. Typically, ℓ_c is assumed to be in the same order of magnitude as the thickness of the membrane. Note that when the size of the vesicle approaches the thickness of the membrane, the assumptions of 2D curvature elasticity are no longer satisfied. In this case one need to consider the correction of higher order terms in the bending energy function. We will focus on the fluctuations of a closed vesicle in the shape of a perfect sphere—-as has been done by nearly all works that precede us. The fluctuating spherical vesicle (Figure. 3.1.1) with a mean radius of r_0, surface defined as $\mathbb{S} := \{\mathbf{r} \in \mathbb{R}^3 : |\mathbf{r}| = r_0\}$ has a membrane of thickness d. Consider a small but arbitrary perturbation of the surface of the vesicle. The position of each point on the *perturbed* surface of the sphere can be described as

$$\tilde{\mathbf{r}} = \mathbf{r} + \varepsilon U \mathbf{n}, \tag{3.2.6}$$

where we have assumed that the perturbation is only along the normal direction as shown in Figure. 4.1.1. Here $\varepsilon \in \mathbb{R}$ is a small number and $U(\theta, \phi) : \mathbb{S} \to \mathbb{R}$ denotes the magnitude of the normal perturbation. The mean curvature and the Jacobian of the perturbed surface

membrane, which is necessary but not sufficient. Strictly speaking, the Gaussian curvature at any point on the surface depends only on the metric tensor which is constrained by the intrinsic topology of the surface. To capture the effect of such strict local topological constraint, one need to fix the metric tensor's components, using local Lagrange multipliers in the total Hamiltonian. This will guarantee that the Gaussian curvature will not change at any point on the surface, and therefore all the contributions of the Gaussian curvature in the free energy can be neglected. In this manner, the total bending energy density in nonlinear framework can be modified as below

$$\bar{\psi} = \frac{1}{2}\kappa_b H^2 + \frac{1}{2}\gamma_c H^4 + \lambda \cdot (\mathbf{g} - \mathbf{g}^0), \tag{3.2.5}$$

where γ_c is the only fourth order constant. Also, $\mathbf{g}^0$ and $\mathbf{g}$ correspond to the metric tensors of the undeformed and deformed surfaces respectively. Further, λ is a set of Lagrange multipliers accounting for the constraints on the metric tensor components. Imposing such local topological constraints, for the simplest example of an unstretchable flat sheet, it has been shown that constraining the metric tensor components results in a significant modification to the shape equation [98, 99]. This notion is critical when the deformations may result in topological changes. For our specific problem, since the fluctuations are considered to take place for a fixed (*and* stable) topology– and that is a stable sphere will remain a sphere in the absence of external forces– implementing the topological constraints is unimportant. Accordingly, in the remainder of the work, the additional Lagrange multiplier term in Equation (3.2.5) is dropped.

can be expressed as

$$\begin{aligned}\tilde{H} &= H + \delta H \\ \tilde{J} &= 1 + \delta J,\end{aligned} \tag{3.2.7}$$

where, H is the mean curvature of the undeformed surface. Up to second order in ϵ, the variations of H and J may be expanded as [92, 100]

$$\begin{aligned}\delta J &= -2HU\varepsilon + (\frac{1}{2}|\nabla_S U|^2 + KU^2)\varepsilon^2 + O(\varepsilon^2) \\ \delta H &= ((2H^2 - K)U + \frac{1}{2}\Delta_S U)\varepsilon \\ &\quad + (HU\Delta_S U - \frac{1}{2}\nabla_S U \cdot (H\nabla_S U) + (4H^2 - 3K)HU^2)\varepsilon^2 \\ &\quad + O(\varepsilon^2).\end{aligned} \tag{3.2.8}$$

Neglecting the contribution of the Gaussian curvature, the bending energy per unit area of the perturbed surface can be written as

$$\bar{\psi}[\tilde{H}] = \frac{1}{2}\kappa_b \tilde{H}^2 + \frac{1}{2}\gamma_c \tilde{H}^4. \tag{3.2.9}$$

Using Equations (3.2.7) and (3.2.8) and integrating the above expressions over the surface of the membrane, we obtain

$$\begin{aligned}\mathcal{E}^{\text{tot}}[U, H] &= \int_{\mathbb{S}} \bar{\psi}[\tilde{H}]\tilde{J} dA_0 \\ &= \int_{\mathbb{S}} \left(E(\varepsilon^0) + E(\varepsilon^2) + E(\varepsilon^4) + O(\varepsilon^4)\right) dA_0,\end{aligned} \tag{3.2.10}$$

in which we have retained up to fourth order terms. The leading terms in the expressions for $E(\varepsilon^i)$ are as follows

$$
\begin{aligned}
E(\varepsilon^0) &= \frac{1}{2}\kappa_b H^2\left(1+\ell_c^2 H^2\right)\\
E(\varepsilon^2) &= \frac{1}{8}\kappa_b(\Delta_S U)^2(1+6H^2\ell_c^2)\\
&\quad+\frac{1}{4}\kappa_b U\Delta_S U(5H^2-2K+3H^2(7H^2-4K)\ell_c^2)+\cdots\\
E(\varepsilon^4) &= \frac{1}{32}\kappa_b\ell_c^2(\Delta_S U)^4+\cdots .
\end{aligned}
\tag{3.2.11}
$$

Specializing to the case of a perfect sphere of radius r_0, the equilibrium mean and Gaussian curvatures are $H^{-1}=-r_0$ and $K^{-1}=r_0^2$. Moreover, we define the normalized mid-plane displacement as: $u=U/r_0$. For notational simplicity, we use $\underline{\Delta}:=\Delta_S(r_0=1)$ as the surface laplacian operator on the unit sphere. Assuming that θ and ϕ are polar and azimuthal angles, we can write the area element as: $dA_0=r_0^2 d\Omega$, where $d\Omega=\sin(\theta)d\theta d\phi$. Then, integrating the terms in (3.2.11) over the area of the sphere, we obtain[5]

[5]In spherical coordinates, using $(\mathbf{e}_r,\mathbf{e}_\theta,\mathbf{e}_\phi)$ as the basis vectors, the perturbed surface of the sphere is $\tilde{\mathbf{r}}=r_0(1+u(\theta,\phi))\mathbf{e}_r$ and the area element and normal vector of the perturbed surface are

$$
\begin{aligned}
\tilde{J}dA_0 &= |\partial_\theta\tilde{\mathbf{r}}\times\partial_\phi\tilde{\mathbf{r}}|\;d\theta d\phi\\
&= \sqrt{1+\left(\frac{\partial u}{\partial\theta}\right)^2+\left(\frac{1}{\sin\theta}\frac{\partial u}{\partial\phi}\right)^2}\,r_0^2\sin\theta\;d\theta d\phi\\
\mathbf{n} &= \frac{\partial_\theta\tilde{\mathbf{r}}\times\partial_\phi\tilde{\mathbf{r}}}{|\partial_\theta\tilde{\mathbf{r}}\times\partial_\phi\tilde{\mathbf{r}}|}.
\end{aligned}
$$

Also the mean curvature is

$$
\tilde{H}=-\frac{1}{2}\,\mathrm{div}_S\;\mathbf{n}.
$$

The surface operators are defined as

$$
\begin{aligned}
\overline{\nabla} &:= \frac{\partial}{\partial\theta}\mathbf{e}_\theta+\frac{1}{\sin\theta}\frac{\partial}{\partial\phi}\mathbf{e}_\phi\\
\underline{\Delta} &:= \frac{1}{\sin\theta}\frac{\partial}{\partial\theta}\left(\sin\theta\frac{\partial}{\partial\theta}\right)+\frac{1}{\sin^2\theta}\frac{\partial^2}{\partial\phi^2}.
\end{aligned}
$$

The area element and the mean curvature can then be expressed as

$$
\begin{aligned}
\tilde{J}dA_0 &= r_0^2(1+2u+u^2+\frac{1}{2}|\overline{\nabla}u|^2+\cdots)\sin\theta\;d\theta d\phi\\
\tilde{H} &= -\frac{1}{r_0}\left(1-u-\frac{1}{2}\underline{\Delta}u+u^2+u\underline{\Delta}u-\frac{1}{2}|\overline{\nabla}u|^2+\cdots\right).
\end{aligned}
$$

$$
\begin{aligned}
E_0 &= \int_{\mathbb{S}} E(\varepsilon^0) dA_0 = 2\pi\kappa_b \left(1 + \frac{\ell_c^2}{r_0^2}\right) \\
E_2 &= \int_{\mathbb{S}} E(\varepsilon^2) dA_0 \\
&= \int_{\mathbb{S}} \left[\frac{1}{8}\kappa_b \left(1 + \frac{6\ell_c^2}{r_0^2}\right) (\underline{\Delta} u)^2 + \frac{3}{4}\kappa_b \left(1 + \frac{5\ell_c^2}{r_0^2}\right) u \underline{\Delta} u\right] d\Omega \\
E_4 &= \int_{\mathbb{S}} E(\varepsilon^4) dA_0 = \int_{\mathbb{S}} \left[\frac{1}{32 r_0^2}\kappa_b \ell_c^2 (\underline{\Delta} u)^4\right] d\Omega.
\end{aligned} \tag{3.2.12}
$$

For notational simplicity, in what follows, we set $\kappa_1 = \frac{1}{8}\kappa_b(1+6\ell_c^2/r_0^2)$, $\kappa_2 = \frac{3}{4}\kappa_b(1+5\ell_c^2/r_0^2)$, and $\kappa_3 = \frac{1}{32}\kappa_b\ell_c^2/r_0^2$. Evidently, E_0 is the ground state energy, corresponding to the equilibrium state. A small perturbation of the surface (3.2.6), requires an additional elastic energy that can be expressed as: $E_{pert} = E_2 + E_4$. Up to second order, the energy function E_2 within the linearized curvature elasticity framework has been derived earlier by many authors. Here, we have generalized it to include the effects of constitutive nonlinearities. In the following section we will use the energy function (3.2.12) to study the thermal fluctuations of the displacement field for a spherical vesicle.

3.2.1 Thermal Fluctuations in the Context of Nonlinear Elasticity and the Renormalized Bending Rigidity of Small Vesicles

There exists a rich and extensive literature on thermal fluctuations of membranes [101, 84, 102, 85, 103]. In the context of lipid bilayers and biological membranes, the vast majority of the works use Helfrich's classical quadratic Hamiltonian (i.e. linearized curvature elasticity) as the starting point. Specifically, constitutive nonlinearity—as detailed in the preceding section, has hitherto not been accounted for. Unfortunately, carrying out statistical mechanics of non-quadratic Hamiltonians is a daunting task to say the least; and closed-form solutions are frequently unobtainable. The equipartition theorem, which is the essential result used by nearly all the analytical statistical mechanics works on biological membranes, is not applicable.

Several methods have been introduced in the literature for treating non-quadratic Hamil-

tonians. Perhaps, the most straightforward approach is the perturbation expansion [65] wherein the non-quadratic part of the Hamiltonian is considered to be a small perturbation compared to the quadratic part for which an exact solution is known. If the perturbation term is small enough, and under certain conditions, a rapid convergence of the free energy expansion may be achieved. Nevertheless, for low temperatures, divergent contributions may appear from second order corrections [65]. Improved results may be obtained by the so-called variational perturbation theory (VPT) which has been successfully employed to remove divergencies in several canonical problems of quantum and statistical physics [65, 104, 105, 106, 66]. This method is based on the so-called principle of minimum sensitivity [107] and involves the use of a trial quadratic Hamiltonian with a variational coupling parameter. The requirement that an infinite perturbation expansion series should not depend on the variational parameter, the variational coupling parameter is "optimized" so that a truncated series solution depends minimally on it. The convergence of this method has been shown to be excellent when compared to all-numerical calculations and fairly reasonable closed-form analytical solutions may be obtained with just first or second order expansions in many cases [65, 108][6]. Renormalization group [109] (RG) is also another approach to treat the divergencies in perturbation expansions. This method is based on scaling techniques and some universal properties of materials near critical phenomena. In most of the cases, RG involves numerical calculations to estimate the free energy, and is often unable to produce analytical expressions for the correlation functions.

In what follows, we employ the variational perturbation approach and retain terms only up to the first order. Higher order corrections are cumbersome to incorporate but may be included if required. Our choice of the approach is dictated by our desire to obtain closed-form yet reasonably accurate solutions. The perturbed energy function, introduced in (3.2.12) is split in two parts; quadratic (E_2) and a non-quadratic (E_4) part that is not tractable via the equipartition theorem. We express the original Hamiltonian in the

[6]This approach, if only a first-order expansion is used, is also known more popularly as the Gibbs-Bogoliubov variational method which is frequently used in several classes of quantum and classical statistical mechanics problems [109, 8, 24, 110, 111, 112].

following modified form:

$$\mathbb{H}(\lambda) = \mathbb{H}_0 + \lambda \mathbb{H}_I, \tag{3.2.13}$$

where λ is a control parameter, such that $0 \leqslant \lambda \leqslant 1$. We remark that $\mathbb{H}$ is *exactly* the original non-quadratic Hamiltonian when $\lambda = 1$. Also, $\mathbb{H}_0$ is a *trial* Hamiltonian, that is analytically soluble and $\mathbb{H}_I$ is the correction term. Using the concept of the canonical ensemble, the partition function is

$$Z(\lambda) = \int \exp\left(-\beta \mathbb{H}(\lambda)\right) \mathcal{D}[u], \tag{3.2.14}$$

where $\beta = \frac{1}{k_B T}$ and $\mathcal{D}[u]$ represents the *functional integration measure* [65]. The Helmholtz free energy can be obtained as

$$F(\lambda) = -\frac{1}{\beta} \log Z(\lambda). \tag{3.2.15}$$

Differentiating the above free-energy, with respect to λ, we obtain

$$\begin{aligned} \frac{\partial F(\lambda)}{\partial \lambda} &= \frac{\int \mathbb{H}_I \exp(-\beta(\mathbb{H}_0 + \lambda \mathbb{H}_I)) \mathcal{D}[u]}{\int \exp(-\beta(\mathbb{H}_0 + \lambda \mathbb{H}_I)) \mathcal{D}[u]} \\ &= \langle \mathbb{H}_I \rangle. \end{aligned} \tag{3.2.16}$$

The second derivative of the free-energy, with respect to λ yields

$$\begin{aligned} \frac{\partial^2 F(\lambda)}{\partial \lambda^2} &= -\beta(\langle \mathbb{H}_I^2 \rangle - \langle \mathbb{H}_I \rangle^2) \\ &= -\beta \langle (\mathbb{H}_I - \langle \mathbb{H}_I \rangle)^2 \rangle, \end{aligned} \tag{3.2.17}$$

which is always a negative value; $\frac{\partial^2 F(\lambda)}{\partial \lambda^2} \leqslant 0$. This implies that the free energy is a concave function for all values of λ, and thus, the function $F(\lambda)$ is always below the tangent to $F(\lambda)$ at $\lambda = 0$. Using the Taylor expansion around $\lambda = 0$ we can write

$$F(\lambda) \leqslant F_0 + \left(\frac{\partial F}{\partial \lambda}\right) |_{\lambda=0} \lambda + \frac{1}{2!} \left(\frac{\partial^2 F}{\partial \lambda^2}\right) |_{\lambda=0} \lambda^2 + \cdots . \tag{3.2.18}$$

We may now set $\lambda = 1$ to retrieve the free-energy corresponding to the original Hamiltonian. Also we can write the correction term in terms of the trial Hamiltonian $\mathbb{H}_0$ and the exact Hamiltonian $\mathbb{H}$ as: $\mathbb{H}_I = \mathbb{H} - \mathbb{H}_0$. The infinite Taylor series in the right hand side of Equation (3.2.18) should match the exact free energy—regardless of the choice of the trial Hamiltonian $\mathbb{H}_0$. In practice, however, the series is truncated up to a finite order M to obtain an estimate of the free energy. Let F_M be the truncated series (3.2.18) up to M-th order. Then using cumulant averages we can write the explicit form for F_M as

$$F_{\mathrm{M}} = F_0 - \frac{1}{\beta}\sum_{k=1}^{M}\frac{(-\beta)^k}{k!}\langle[\mathbb{H} - \mathbb{H}_0]^k\rangle^c_{H_0}, \tag{3.2.19}$$

where, $\langle\cdot\rangle_{\mathbb{H}_0}$ denotes the phase average with respect to $\mathbb{H}_0$ and the superscript c corresponds to cumulant averages[65][7]. Unlike the infinite series expansion in Equation (3.2.18), the truncated series F_M *does* depend on the choice of the trial Hamiltonian $\mathbb{H}_0$. Accordingly, in order to obtain an optimized estimate, we need to minimize the *sensitivity* of the truncated series to the trial Hamiltonian. Suppose now that the trial Hamiltonian $\mathbb{H}_0$ in Fourier space is defined as

$$\mathbb{H}_0 = \sum_{\mathbf{q}\in\mathcal{K}_N} u(\mathbf{q})G(\mathbf{q})u(\mathbf{q})^*, \tag{3.2.20}$$

with $\mathbf{q}$ representing the modes of fluctuations, $u(\mathbf{q})$ being the fluctuating field in mode $\mathbf{q}$ and $G(\mathbf{q})$ is an unknown trial function that defines the form of interactions between the degrees of freedom. Then, to obtain the optimal form of $G(\mathbf{q})$, we must set[65]

$$\frac{\partial F_M}{\partial G(\mathbf{q})} := 0. \tag{3.2.21}$$

[7]The cumulant averages of a function $\mathbb{X}$ with respect to $\mathbb{H}_0$ up to third order is defined as [65]

$$\begin{aligned}
&\langle\mathbb{X}\rangle^c_{\mathbb{H}_0} = \langle\mathbb{X}\rangle_{\mathbb{H}_0}\\
&\langle\mathbb{X}^2\rangle^c_{\mathbb{H}_0} = \langle\mathbb{X}^2\rangle_{\mathbb{H}_0} - \langle\mathbb{X}\rangle^2_{\mathbb{H}_0}\\
&\langle\mathbb{X}^3\rangle^c_{\mathbb{H}_0} = \langle\mathbb{X}^3\rangle_{\mathbb{H}_0} - 3\langle\mathbb{X}^2\rangle_{\mathbb{H}_0}\langle\mathbb{X}\rangle_{\mathbb{H}_0} + 2\langle\mathbb{X}\rangle^3_{\mathbb{H}_0}.
\end{aligned}$$

In a rather good approximation, the result for the truncated series of the variational free energy from this method will converge i.e. $F_M \approx F_{M+1}$ and the series (3.2.19) achieves its minimal sensitivity to the trial function. We remark that restricting calculations to first order in the truncated series (3.2.19) yields just the well-known *Bogoliubov theorem*[8] for the upper bound of the exact free energy

$$F \leqslant F_0 + \langle \mathbb{H} - \mathbb{H}_0 \rangle_{\mathbb{H}_0}. \tag{3.2.22}$$

In what follows, we will use this approach up to first order to obtain a closed form solution for the free energy of the system.

As can be appreciated, the original Hamiltonian may be split into a trial and a correction term in an infinite number of ways. The next step involves choosing the optimal trial quadratic Hamiltonian. To achieve this, we start with the Fourier decomposition of the perturbation field on the sphere. To this end we expand the displacement in terms of spherical harmonics. Let N be the total number of degrees of freedom and

$$\mathcal{K}_N := \{(l,m) | (l,m) \in \mathbf{Z} \times \mathbf{Z}, l \geqslant 2, l(l+1) < N, -l < m < l\}.$$

Then we can expand the normalized perturbation field in terms of spherical harmonics as below

$$u(\theta, \phi) = \sum_{(l,m) \in \mathcal{K}_N} u_{l,m} Y_{l,m}, \tag{3.2.23}$$

where Y_{lm}[8] are spherical harmonics [113] with eigenvalues

$$\nabla^2 Y_{l,m} = -q_{l,m}^2 Y_{l,m} = -l(l+1)Y_{l,m}, \tag{3.2.24}$$

and $u_{l,-m} = u_{l,m}^*$ are the Fourier transformation of $u(\theta, \phi)$

$$u_{l,m} = \int_{\mathbb{S}} u(\theta, \phi) Y_{lm}^* d\Omega. \tag{3.2.25}$$

We select the general form for the quadratic trial Hamiltonian $\mathbb{H}_0$ in Fourier space as defined in Equation (3.2.20). The goal now is to match the exact free-energy as closely as possible by finding an optimal match for the form of the propagator $G(\mathbf{q})$. To this end we set [8, 65]

$$\frac{\partial}{\partial G(\mathbf{q})} \left(F_0 + \langle \mathbb{H} - \mathbb{H}_0 \rangle_{\mathbb{H}_0} \right) := 0. \tag{3.2.26}$$

The partition function and the free energy corresponding to the trial quadratic Hamiltonian $\mathbb{H}_0$ in Equation (3.2.20) is obtained as

$$\begin{aligned} Z_0 &= \int e^{-\beta \mathbb{H}_0[u]} \mathcal{D}[u], \\ F_0 &= \alpha_F + \frac{k_B T}{2} \sum_{\mathbf{q} \in \mathcal{K}_N} \log(G(\mathbf{q})), \end{aligned} \tag{3.2.27}$$

where α_F is a constant independent of the propagator $G(\mathbf{q})$. Calculating F_0 from (3.2.27) and substituting it into the L.H.S. of Equation (3.2.22), we obtain the variational free energy

[8] We have excluded the modes corresponding to $l = 0$ and $l = 1$, since these modes represent the area change and the rigid body motion of the vesicle and hence do not contribute to the total energy. We also recall the two important properties of the spherical harmonics, which will be used later in our calculations. They are orthonormal

$$\int_{\mathbb{S}} Y_{lm} Y_{l'm'}^* d\Omega = \delta_{ll'} \delta_{mm'},$$

and separable:

$$Y_{lm} = P_l^m(\theta) e^{\imath m \phi},$$

where $P_l^m(\theta)$ is the Legendre polynomial corresponding to the mode (l, m). In what follows, for the eigenvalues of the spherical harmonics, we use the notation $\mathbf{q} = q_{l,m}$ wherein $\mathbf{q}^2 = q_{l,m}^2 = l(l+1)$.

F_{var} as

$$\begin{aligned} F_{\text{var}} &= F_0 + \langle \mathbb{H} - \mathbb{H}_0 \rangle_{\mathbb{H}_0} \\ &= \alpha_F + \frac{k_B T}{2} \sum_{\mathbf{q} \in \mathcal{K}_N} \log(G(\mathbf{q})) \\ &+ \sum_{\mathbf{q} \in \mathcal{K}_N} (\kappa_1 \mathbf{q}^4 - \kappa_2 \mathbf{q}^2) \langle u(\mathbf{q})^2 \rangle_{\mathbb{H}_0} \\ &+ 4\pi\kappa_3 \langle (\nabla^2 u)^4 \rangle_{\mathbb{H}_0}. \end{aligned} \tag{3.2.28}$$

The mean square value of the perturbation field in each mode of the fluctuation can be obtained using the equipartition theorem [114]

$$\langle u(\mathbf{q})^2 \rangle_{\mathbb{H}_0} = \frac{k_B T}{2G(\mathbf{q})}. \tag{3.2.29}$$

Also the last term in (3.2.28) which is a higher order correlation function, may be calculated by invoking Wick's theorem[114]

$$\langle (\nabla^2 u)^4 \rangle_{\mathbb{H}_0} = 3 \langle (\nabla^2 u)^2 \rangle^2_{\mathbb{H}_0}. \tag{3.2.30}$$

Minimization of the variational free energy in (3.2.28) with respect to the unknown propagator $G(\mathbf{q})$ provides an upper bound for the exact free energy. Then, solving Equation (3.2.26) gives us the following form for $G(\mathbf{q})$

$$G(\mathbf{q}) = \left((\kappa_1 + 24\pi\eta\kappa_3)\mathbf{q}^2 - \kappa_2 \right) \mathbf{q}^2, \tag{3.2.31}$$

where,

$$\eta = \langle (\nabla^2 u)^2 \rangle_{\mathbb{H}_0} = \frac{1}{4\pi} \sum_{\mathbf{q} \in \mathcal{K}_N} \mathbf{q}^4 \langle u(\mathbf{q})^2 \rangle_{\mathbb{H}_0}, \tag{3.2.32}$$

which should be calculated by integrating over all undulation modes. For brevity we rewrite

Equation (3.2.31) as

$$G(\mathbf{q}) = \frac{1}{8}(c_1\mathbf{q}^4 - c_2\mathbf{q}^2), \tag{3.2.33}$$

where c_1 and c_2 are the corresponding coefficients of $\mathbf{q}^4$ and $\mathbf{q}^2$ in (3.2.31), respectively. The unknown value of η in the expression for c_1, should be calculated from the implicit equations of (3.2.29), (3.2.31) and (3.2.32)

$$\begin{aligned}
\eta &= \frac{1}{4\pi}\sum_{\mathbf{q}\in\mathcal{K}_N} \mathbf{q}^4\langle u(\mathbf{q})^2\rangle_{\mathbb{H}_0} \\
&= \frac{k_BT}{4\pi}\sum_{\mathbf{q}\in\mathcal{K}_N} \frac{\mathbf{q}^4}{2G(\mathbf{q})} \\
&= \frac{k_BT}{\pi c_1}\sum_{\mathbf{q}\in\mathcal{K}_N} \left(1 + \frac{c_2}{c_1\mathbf{q}^2} + \cdots\right),
\end{aligned} \tag{3.2.34}$$

where, to further simplify our calculations, we have dropped the term $\frac{1}{\mathbf{q}^2}$ since it is negligible compared to one– $\mathbf{q}^2 \gg 1$. To compute the summation we replace it with an integral

$$\sum_{\mathbf{q}\in\mathcal{K}_N} := \sum_l (2l+1) \approx \int (2l+1)dl, \tag{3.2.35}$$

where l_{max} can be easily obtained from the total number of modes (degrees of freedom)

$$N = \sum_l (2l+1) = \frac{4\pi r_0^2}{A_0}, \tag{3.2.36}$$

in which A_0 is the area associated with each degree of freedom, and is typically of the same order of magnitude as d^2 with d is the thickness of the membrane. Substituting the solution of Equation (3.2.34) for η into the expression for $G(\mathbf{q})$ in Equation (3.2.33) gives us the following form for the coefficients c_1 and c_2

$$\begin{aligned}
c_1 &= \frac{1}{2}\kappa_b\left(1 + \frac{6\ell_c^2}{r_0^2} + \chi\right) \\
c_2 &= 6\kappa_b\left(1 + \frac{5\ell_c^2}{r_0^2}\right),
\end{aligned} \tag{3.2.37}$$

where,

$$\chi = \sqrt{1 + \frac{12\ell_c^2}{r_0^2} + \frac{36\ell_c^4}{r_0^4} + \frac{24\ell_c^2 N}{\beta\kappa_b r_0^2}}. \tag{3.2.38}$$

Note that the $\mathbf{q}^4$ contribution in (3.2.31) is equivalent to the bending rigidity (c_1) of a vesicle studied in the context of linearized curvature elasticity, and according to (3.2.37), can be significantly larger than the bare modulus κ_b. We also note that there is a curvature-dependent suppression of thermal fluctuations in the nonlinear context and accordingly larger vesicles experience stronger fluctuations, compared to smaller vesicles. On the other hand, the $\mathbf{q}^2$ term in Equation (3.2.33) has softening effects, that arise from geometric nonlinearities. In the remainder of this section, we aim to study the softening effects of the thermal fluctuations on the bending rigidity. This topic has been well appreciated since the early and pioneering work by Helfrich [115, 102, 100, 116]. Considering geometric nonlinearity and using first order approximations, Helfrich [115] explained that the renormalized bending rigidity in linearized curvature elasticity (for nearly flat membranes) can be written as:[9]

$$\kappa_{\text{eff}} = \kappa_b + \frac{\alpha}{2\pi} k_B T \log N, \tag{3.2.39}$$

wherein α is a universal constant and N is the number of molecules in the system. Assuming weak rippling in nearly flat membranes, he predicted $\alpha = -1$. Peliti and Leibler [102] also reexamined this problem and obtained α as -3. Later on, Kleinert [100] rigorously discussed the origins of these discrepancies and highlighted the care needed in choosing the integration measures in path integrals as well as some algebraic errors in expanding the energy formulation in terms of the fluctuation field. He confirmed that $\alpha = -3$. In the following, we will revisit this problem to study the coupled effects of geometric and

[9] We highlight that in many works on this topic, the bending energy density is assumed to have the form of $\frac{1}{2}\kappa_b'(1/R_1 + 1/R_2)^2$ in which R_1 and R_2 are the principle curvatures radiuses. In this form, the mean curvature is considered to be: $H' = 1/R_1 + 1/R_2$, while in the present work, we consider half of this value as mean curvature— $H = (1/R_1 + 1/R_2)/2$. Accordingly, the bending energy of a sphere, based on our assumption is obtained as: $2\pi\kappa_b$, while in some works, the bending energy is assumed to be $8\pi\kappa_b'$. Therefore, the change in the bending modulus in some of the references we have cited is: $\frac{\alpha}{8\pi} k_B T \log N$. A comparison between these two forms, shows that any variation in κ_b, used in our model, is four times larger than those in other works [115, 102, 100, 116].

constitutive nonlinearities. We note in passing that, in a somewhat controversial and later work, [116], argued for the use of *curvature* as the proper integration measure and obtained $\alpha = +1$. This result is however widely disputed.

Consider now a spherical vesicle (described by linearized elasticity) with a bending rigidity of c_1 and radius r_0. The bending energy can be computed to be: $\int \frac{1}{2} c_1 \frac{1}{r_0^2} dA_0 = 2\pi c_1$. Also, at finite temperature, the free energy of the vesicle can be obtained using Equations (3.2.27) and (3.2.33)

$$\begin{aligned} F_0 &= -k_B T \log Z_0 \\ &= \alpha_F + \frac{k_B T}{2} \sum_{\mathbf{q} \in \mathcal{K}_N} \log G(\mathbf{q}) \\ &= \alpha_F + \frac{k_B T}{2} \sum_{\mathbf{q} \in \mathcal{K}_N} \left(\log c_1 \mathbf{q}^4 - \frac{c_2}{c_1 \mathbf{q}^2} + \cdots \right). \end{aligned} \tag{3.2.40}$$

The above expression shows that contribution of geometric nonlinearity, produces additional terms in the Taylor expansion of the free-energy. The "additional free energy" can be interpreted as the change in apparent bending stiffness

$$\begin{aligned} \Delta F &= \frac{1}{2} k_B T \sum_{\mathbf{q} \in \mathcal{K}_N} \left(\frac{c_2}{c_1 \mathbf{q}^2} + \frac{c_2^2}{2 c_1^2 \mathbf{q}^4} + \cdots \right) \\ &:= 2\pi (c_1 - \kappa_{\text{eff}}). \end{aligned} \tag{3.2.41}$$

Thus, the effective bending stiffness, can be calculated up to first order as

$$\kappa_{\text{eff}} = c_1 - \frac{c_2}{4\pi c_1} k_B T \sum_{\mathbf{q} \in \mathcal{K}_N} \frac{1}{\mathbf{q}^2}. \tag{3.2.42}$$

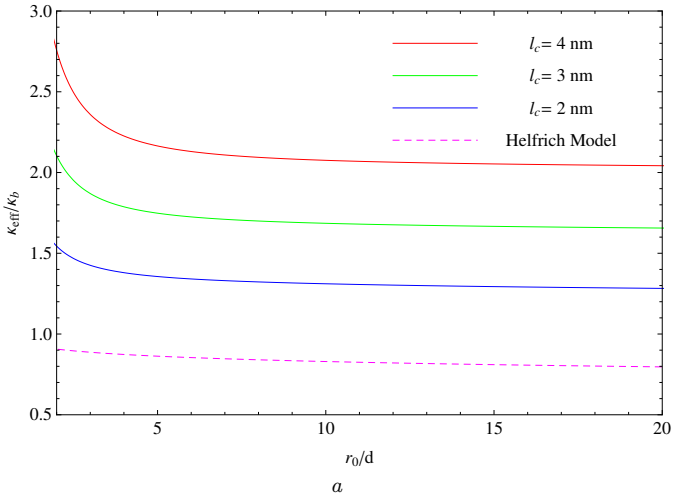

a

Figure 3.2.2: Renormalized bending modulus for different values of ℓ_c.

[a]Solid red, green and blue correspond to $\ell_c = 4$nm, $\ell_c = 3$nm and $\ell_c = 2$nm, respectively. Dashed line is obtained from Helfrich linear model in which $\ell_c = 0$. The data has been calculated with $\kappa_b = 20 k_B T$ and $d = 5$nm.

The summation is calculated using integration over all possible modes

$$\begin{aligned}\sum_{\mathbf{q}\in\mathcal{K}_N} \frac{1}{\mathbf{q}^2} &= \int \frac{2l+1}{l(l+1)} dl \\ &= \log N. \end{aligned} \tag{3.2.43}$$

Substituting the above integral into Equation (3.2.42), we obtain the effective bending rigidity as

$$\kappa_{\text{eff}} = \frac{1}{2}\kappa_b \left(1 + \frac{6\ell_c^2}{r_0^2} + \chi\right) - \frac{\alpha'}{4\pi} k_B T \log N, \tag{3.2.44}$$

where χ has been previously defined in (3.2.38) and α' is:

$$\begin{aligned}\alpha' &= \frac{c_2}{c_1} \\ &= \frac{12 + \frac{60\ell_c^2}{r_0^2}}{1 + \frac{6\ell_c^2}{r_0^2} + \chi} \end{aligned} \tag{3.2.45}$$

Note that in the limit of $\ell_c \to 0$ the above expression reduces to that of conventional

linearized curvature elasticity model [100]. For quantitative comparisons, we have calculated the bending stiffness, for a range of vesicle size with different values of ℓ_c. The results are shown in Figure. 3.2.2 where we compare four different cases. The horizontal axis is the normalized radius of the vesicle r_0/d where we set $d = 5$nm. Solid blue, green and red lines correspond to $\ell_c = 2$nm, $\ell_c = 3$nm and $\ell_c = 4$nm, respectively. The dashed line corresponds to the case of $\ell_c = 0$ which reduces to Helfrich quadratic model[115]. As can be readily observed, for small vesicles that have high curvatures, the effect of nonlinearity become quite significant. Even for a small value of $\ell_c = 3$nm—less than the typical thickness of the membrane—the apparent bending rigidity becomes significantly *stiffer* for sub-20 nm vesicles. Also, the effect of nonlinearity does not vanish in the limit of the flat membrane, when $H \to 0$. The corresponding limits of the normalized effective bending rigidity $\kappa_{\text{eff}}/\kappa_b$ for the cases of $\ell_c = 2$nm, $\ell_c = 3$nm and $\ell_c = 4$nm are found to be 1.42, 1.76 and 2.13, respectively.

3.2.2 Size Distribution of Vesicles

Vesicles can be artificially made across a broad range of diameters. However, if an ensemble of vesicles are allowed to freely exchange molecules—artificial or nature-made—the size of the vesicles will change for some period, until they become thermodynamically stable. At this state, it is very unlikely to find vesicles beyond certain sizes, i.e. there is discernible maximum and minimum size-limit for the radius of the vesicles. Depending on the experimental methods used for the preparation of vesicles, these size limits may slightly vary in the beginning, but eventually the experimentally observed size distributions appear to become independent of the method of preparation and are determined by macroscopic mechanical and entropic properties of the vesicles [117]. Several experimental efforts have been dedicated to this subject [117, 118, 119]. The most common method to determine the size distribution of vesicles is via dynamic light scattering (DLS) measurements. Another well-known method is to use cryo-TEM images [120, 121, 122] and obtain the size distribution histogram using statistical analysis. In a recent work Xu et al.[88] have used a combination of these two approaches and obtained the size distribution for a set of lauric

acid vesicles. They confirmed that the size of the vesicles is distributed within a finite range with a remarkably large cut-off radius of about $20nm$. In this section, using the results derived in the preceding sections, we aim to study the qualitative effects of mechanical properties and their corresponding entropic effects on the size distributions of small unilamellar vesicles.

Table 3.2.1: Comparison between the previous models of size distribution and the present work.

Model[a]	ζ	f(N)	Cut-off radius (r_c)
$E = 2\pi\kappa_b + \mu N$	$\zeta = 0$	AN	$r_c = 0$
Helfrich linear model: Eq.(3.2.50)	$\zeta = 1$	AN	$r_c = 0$
Helfrich nonlinear model: Eq. (3.2.51)	$\zeta = 1$	$AN + B/N$	$r_c > 0$
Morse and Milner: Eq. (3.2.53)	$\zeta = -7/8$	AN	$r_c = 0$
Kleinert: Eq. (3.2.54)	$\zeta = 4/3$	AN	$r_c = 0$
Present model: Eq. (3.2.57)	$\zeta \leqslant 3$	$A_0N + A_1/N$ $+\sqrt{A_2 + A_3/N + A_4/N^2}$	$r_c > 0$

[a] In general, the distribution function can be expressed as: $w(N) \propto N^{\zeta} \exp(-f(N))$. The second column in this table shows various values for the exponent ζ in different models. Also, various forms of the function $f(N)$ are shown in the third column. The symbols A and B are constants, representing the chemical potential and those associated with fourth order moduli, respectively. Further, A_i in the last row are constants, corresponding to coefficients of renormalized bending stiffness in the present model. A comparison between the listed models, shows that Helfrich nonlinear model and the present model provide more realistic predictions of the cut-off radius in the size distribution of vesicles. Unlike Helfrich's nonlinear model, in the present work, the entropic effects of the constitutive nonlinearity, are taken into account to further modify the predicted size distribution.

In the following we assume that the vesicles can exchange amphiphilic molecules, while the total number of the vesicles remains fixed. Also the spontaneous curvature is considered to be zero, and that there is always non-zero amount of energy cost for any non-zero curvature. Given that N is the number of amphiphilic molecules in a vesicle, the size distribution of the vesicles, $w(N)$ is determined by the total free energy F and the Boltzmann factor

$$w(N) \propto \exp(-F/k_BT). \tag{3.2.46}$$

We first briefly review the predictions for Equation (3.2.46) made by conventional approaches before discussing the results unique to this work.

The bending energy of a sphere in linearized curvature elasticity is alway: $2\pi\kappa_b$ which is independent of the vesicle size. This implies that regardless of the size of two vesicles, the transfer of surfactant molecules from one vesicle to another does not change the total bending energy. This, results in a flat distribution for the vesicles' sizes (3.2.46). The total free energy for the vesicle with N number of amphiphilic molecules and chemical potential μ can then be written as

$$F = 2\pi\kappa_b + N\mu. \tag{3.2.47}$$

Equation (3.2.47) gives rise to an exponentially decaying distribution, with *zero* size, being the most probable size—a rather glaring problem. To further modify the result of Equation (3.2.46), Helfrich[68] proposed to include the entropic effects in the elastic energy. As discussed in the last section, in the conventional linear framework, the thermal undulations lead to softening effects on the effective bending modulus [115]. The corresponding effective bending modulus is provided in Equation (3.2.39). To account for the entropic effects, Helfrich [68] substituted the bare value of bending modulus κ_b by the renormalized bending stiffness κ_{eff}

$$w(N) \propto \exp(\frac{-\mu N - 2\pi\kappa_{\text{eff}}}{k_B T}). \tag{3.2.48}$$

The above expression has been extensively used to predict the size distribution of the vesicles. In general, using the expression for the effective bending rigidity (3.2.39), the following size distribution is obtained

$$w(N) \propto N^{-\alpha} \exp(-\mu N/k_B T). \tag{3.2.49}$$

The major differences between prior theoretical works on this topic, arise from the diversity in predicting the universal constant α. Using $\alpha = -1$ and normalizing the size distribution

to 1, Helfrich [68] obtained the size distribution as

$$w(N) = \left(\frac{2}{\overline{N}}\right)^2 N \exp(-\frac{2N}{\overline{N}}), \tag{3.2.50}$$

where $\overline{N}$ is the mean number of molecules per vesicle and is determined by the chemical potential μ. As well-evident, the final distribution function described in Equation (3.2.50) is *independent* of the mechanical properties of the vesicles. Furthermore, since the vesicles cannot deform beyond a certain curvature and there is always a cut-off radius for the size distribution of the small vesicles, such a distribution is not compatible with experimental observations. To resolve the inconsistency, Helfrich [68] suggested that fourth order curvature elasticity terms should be incorporated in the bending energy formulation. Using a rather crude approximation, he demonstrated that accounting the fourth order term can alter the size distribution to make smaller sizes less probably. He modified the probability density distribution in the following form

$$w(N) \propto N e^{-AN-B/N}. \tag{3.2.51}$$

The above distribution although slightly shifts the mean value of the diagram to a larger size, and suggests smaller probability for smaller sizes, is incapable of predicting the correct value for the experimentally observed cut-off radius.

In a different work, Morse and Milner [29] suggested that the free energy, due to translational and rotational entropy[10], increases logarithmically with the size of the vesicle in the following form

$$F(N) = F_0 + \alpha k_B T \log N, \tag{3.2.52}$$

[10]We note that in the present work for pure lipid membranes, we assume that there is no entropic contributions from tilting or area change.

for which they evaluate $\alpha = +\frac{7}{8}$. Based on this, they obtained the size distribution as

$$w(N) \propto N^{-7/8} e^{-\mu N}. \tag{3.2.53}$$

Unfortunately, this predicted size-distribution renders smaller vesicles more probably not less and is somewhat contradictory to the experimental observation that there exists a minimal vesicle size.

Finally, we note that Kleinert [100] also revisited this problem. Renormalizing the mean and Gaussian and spontaneous curvature constants, and considering their effects together within a harmonic approximation, he obtained the following form for the size distribution

$$w(N) \propto N^{7\rho^2 - 6\rho + 4/3} e^{-AN}, \tag{3.2.54}$$

in which he introduced the so called *elastic fraction* $\rho \in (0, 1)$ that essentially captures the combined entropic effects of mean, Gaussian and spontaneous curvatures. It can be readily seen that the exponent of N has a maximum of $7/3$. Nevertheless for pure bending of the lipid membranes that does not involve any tilt or area change, the maximum is found to be $4/3$. As a result, compared to (3.2.50) and (3.2.53) the distribution (3.2.54) predicts smaller probability for small sizes, however, is still far from the experimental observations.

We now turn to the use of the thermal fluctuations results we have derived in the preceding section, in the context of fourth order nonlinear elasticity, to derive the size-distribution. Consider the following general form of the size distribution

$$w(N) \propto N^{\zeta} \exp\left(-f(N)\right), \tag{3.2.55}$$

wherein ζ and $f(N)$ determine different forms of the distributions and their dependences on N in various models. Prior models as well as ours (to be described) may be described by appropriate specification of ζ and $f(N)$.

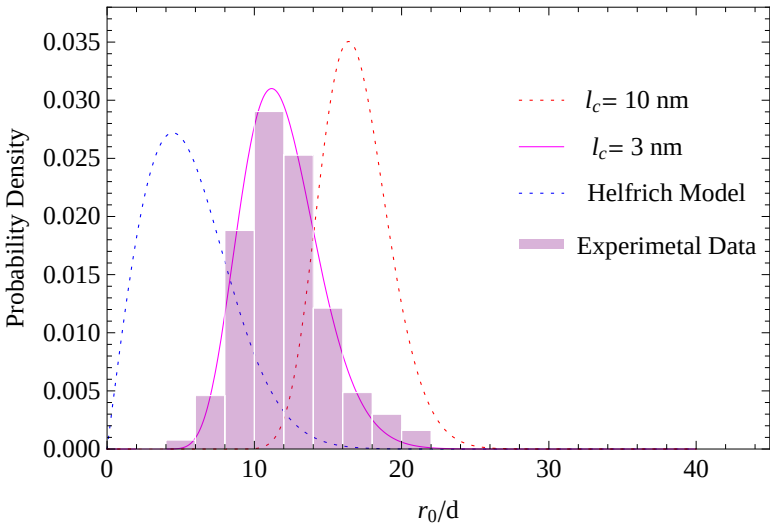

a

Figure 3.2.3: Size distribution of vesicles with different values of ℓ_c.

[a]In this figure, the horizontal axis is the normalized radius of the vesicle $\xi = r_0/d$ and the vertical axis is the probability of finding vesicles within a certain radius. Dotted blue curve corresponds to the size distribution as predicted by linear curvature elasticity[68]. The solid magenta is obtained assuming $\ell_c = 3$nm, which results in a shift in the size distribution, to larger sizes. Also the dotted red line corresponds to $\ell_c = 10$nm which dramatically changes the cut-off radius as well as the mean radius of the vesicles. Based on the experimental data[88], shown in purple color, we have estimated the characteristic length for this kind of lauric acid vesicles to be about $\ell_c = 3$nm. For our calculations, we have set $\kappa_b = 20 k_B T$ and $d = 5$nm.

In our model, substituting Equation (3.2.44) into Equation (3.2.47), the total free-energy for a given size of the vesicle can be written as

$$\begin{aligned} F &= 2\pi\kappa_{\text{eff}} + \mu N \\ &= \pi\kappa_b \left(1 + \frac{6\ell_c^2}{r_0^2} + \chi\right) - \frac{\alpha'}{2} k_B T \log N + \mu N, \end{aligned} \tag{3.2.56}$$

where χ and α' are defined in (3.2.38) and (3.2.45) respectively. Using Equation ((3.2.48)) we propose the following size-distribution

$$w(N) \propto N^{\alpha'/2} \exp\left(-f(N)\right), \tag{3.2.57}$$

where

$$f(N) = \frac{1}{k_B T}\left(\mu N + \frac{A_1}{N} + \sqrt{A_3 + \frac{A_4}{N} + \frac{A_5}{N^2}}\right). \tag{3.2.58}$$

Here we have substituted r_0^2 in (3.2.56) by $NA_0/4\pi$ where A_0 is the area per amphiphilic molecule. Other A_i are coefficients that depend on κ_b and ℓ_c. Note that the exponent α' in Equation (3.2.57) is not a *constant* and varies with the radius of the vesicle. On the other hand, in addition to the term $1/N$, the contribution of the term $1/\sqrt{N}$ in the exponential function dramatically reduces the probability for finding small vesicles. These two effects together result in a notable shift in the size-distribution diagram towards larger sizes when compared to other models [100, 68, 29].

A comparison between the results of our model with experimental data [88] is made in Figure. 3.2.3, where we have plotted the size distribution for three different cases. In this figure, the horizontal axis is the normalized radius of the vesicle r_0/d and the vertical axis is the probability of finding vesicles with a certain radius. Dotted blue curve corresponds to the size distribution within linear curvature elasticity [68] as presented in Equation (3.2.50). The solid magenta is obtained from the present nonlinear model, assuming $\ell_c = 3$nm and the dotted red line corresponds to $\ell_c = 10$nm. Finally, we may estimate the characteristic length ℓ_c to fit our results to those obtained from the experiments. A comparison between our results and experimental data [88] in Figure. 3.2.3 shows that the corresponding characteristic length for this type of composition is roughly about $\ell_c = 3$nm. Even though this value is in the same order as the thickness of the membrane, at finite temperature it can dramatically change the size distribution of the vesicles through thermal fluctuations. Finally, the experimentally observed cut-off radius is clearly evident in our model.

3.2.3 Discussion and Concluding Remarks

One of the main results derived in this paper is a closed-form expression for the spectra of the thermal fluctuations of spherical vesicles duly incorporating nonlinear curvature elasticity terms. In conjunction with our results, either molecular dynamics simulations or experimental flicker spectroscopy may now be used to extract nonlinear elasticity properties. The renormalized bending rigidity due to thermal fluctuations is found to be size-dependent and a dramatic stiffening is predicted to occur for small sub-20 nm vesicle sizes.

The conventional models (based on linear curvature elasticity) that purport to describe vesicle size-distributions typically fail to adequately capture a few qualitative aspects of the distribution for small vesicle sizes. We have used our analytical expression for the renormalized bending stiffness in the nonlinear framework, to study the size distribution of vesicles. Although, all the existing models predict a Gaussian size distribution, the problem of the cut-off radius–below which the vesicles are not likely to exist– is inadequately predicted and as evident from our predictions, the size-distribution is considerably more complex. A possible explanation for the instability of vesicles with sizes below the cut-off radius is the entropic repulsive forces between the amphiphilic molecules.

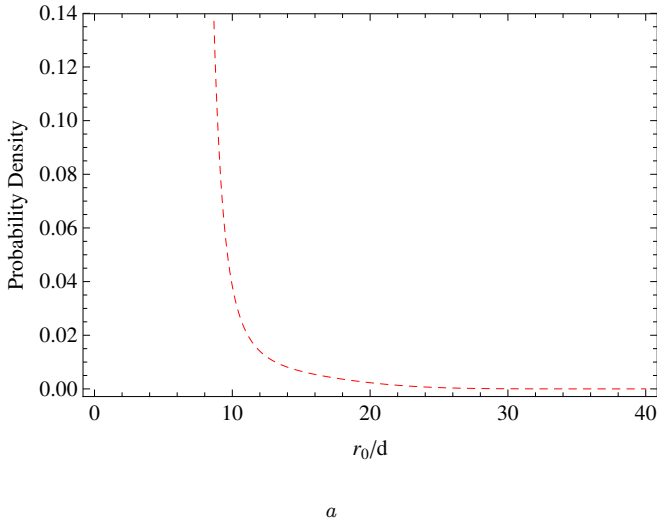

a

Figure 3.2.4: Size distribution of vesicles with negative fourth order modulus is shown qualitatively in this figure.

[a] In sharp contrast to experimental observations known so far, the distribution is discontinuous and is not a Gaussian distribution. Small-size vesicles are *more* probable not less. Finally, beyond a certain size, the vesicle becomes unstable. This plot is obtained by $\ell_c = 2$nm. For larger values of ℓ_c, the unstable region is shifted to larger sizes.

In the following we summarize the key issues related to fourth-order moduli as discussed in prior works put in the context of what we have found:

- The first one is regarding the magnitude and significance of the fourth order modulus. Typically ℓ_c is assumed to be of the order of the thickness of the membrane. Based

on this assertion, the higher order contributions of the bending energy are usually ignored in studying the mechanical response of the vesicles. Our results, however, demonstrate that thermal fluctuations of small unilamellar vesicles are significantly influenced by the higher order modulus even for small values of ℓ_c. Furthermore, for nearly flat membranes, wherein the curvature dependency vanishes, the nonlinearity can still significantly suppress the undulations and hence increase the apparent rigidity. For example, using $\ell_c = 2$nm which is less than the thickness of the membrane, a correction of about 40% is obtained in the apparent bending rigidity. In order to highlight some of the discrepancies between our results with the prior works the reader is referred to a recent work by Harmandaris and Deserno [123]. Using molecular dynamics simulations, these authors employed the well-known idea of tether-pulling experiments [124, 125] to study the fourth order correction of the bending energy for cylindrical vesicles consist of pure DPPC lipid molecules. Their results indicate that the quadratic energy function proposed by Helfrich is valid for a wide range of curvature radii up to the thickness of the membrane. The entropic effects are assumed to be intrinsically embedded in the simulations. Nevertheless, we speculate that, for tethered membranes, due to the high surface tension, the undulations are significantly suppressed and hence the role of entropic effects in the apparent bending stiffness were not adequately taken into account. This can be explained by recognizing the fact that the fluctuations of the out of plane displacement field in the presence of surface tension vary as: $\langle h^2 \rangle \propto 1/\sigma$. According to the relation between the surface tension and the radius of the vesicle $R \propto 1/\sqrt{\sigma}$, to reduce the size of the vesicle to just a few times of the thickness of the membrane, a relatively high tension field is required to overcome the entropic effects. It has been observed in experiments that if such tension field is abruptly removed, the vesicle will undergo an entropic instability[126].

In a different work Li et al.[127], also using molecular dynamic simulations, have computed the elastic properties of the membrane, including fourth order moduli. Unlike the work by Harmandaris and Deserno [123], these authors carried the their

simulations for various volume fractions of hydrophilic molecules. Interestingly, their results on free energy calculation also demonstrate that the higher order contribution of bending energy, is relatively small and the difference between their results and those obtained within Helfrich model is no more than 10%. Also, they obtained values for the fourth order moduli which surprisingly depend on the topology of the vesicles– negative values for spherical and positive values for cylindrical vesicles. This is puzzling to us since the properties, in principle, or for the underlying material not a topological structure. A possible explanation for observation of such contradictory results in their analysis is that the contribution of the intrinsic topology— spontaneous Gaussian and mean curvatures— is not taken into account. Strictly speaking, a flat membrane does not transform to spherical shape, unless an energy cost is considered for fission or fusion. In this manner all the free energy should not be referred to only bending energy. Hence, the free energy of cylindrical and spherical shapes should be analyzed using the different reference states.

- The second issue regarding the fourth order modulus is related to the *sign* of the modulus. In the present work, the higher order modulus is assumed to be positive from the outset. However, it has been argued that the fourth order modulus is negative when dealing with different co-surfactants [128]. Also it has been argued that a negative fourth order elastic modulus is a possible explanation for the mechanism of lipid protein sorting [129]. We note that, in the presence of different compositions, various stable phases might be observed that can be described in terms of different spontaneous mean and Gaussian curvatures or alternatively different bending stiffnesses. We however, believe that a change in the molecular structure of the membrane, results in both mechanical and topological transformations. For pure lipid membranes, a positive fourth order correction of bending energy is *required* to explain the experimentally observed size distribution of vesicles—as evident from Figure. 3.2.4 which clearly demonstrates how unrealistic the size-distribution results will be if a negative fourth order modulus is used.

- Finally, we note that, when the area-size of the membrane becomes comparable with

its thickness, the notion of high-q cutoff necessary in the functional integration becomes dubious. For the smallest size vesicles, we come dangerously close to that limit. However, given the close agreement of our results with experimentally observed vesicle size-distributions, we speculate that our results are at least qualitatively reasonable.

Chapter 4

Entropic Pressure Inside Biological Vesicles

Biological membranes fluctuate noticeably at physiological temperatures. These thermal fluctuations give rise to an entropic repulsive force between fluctuating flat membranes. This entropic repulsive force, and thermal fluctuations in general, influence a broad range of biological phenomena, such as cell adhesion, binding-unbinding transition, self-assembly, stabilization of multi-lamellar vesicles among others. In this work, we examine the entropic force due to the fluctuations of a curved biological membrane fully accounting for geometric nonlinearities. Our results find immediate application towards the resolution of the entropic pressure and stability of multi-lamellar vesicles.

4.1 Introduction

Biological membranes are generally quite flexible and fluctuate freely and notably at physiological temperatures. When an external object approaches a membrane, it hinder the membrane's out-of-plane fluctuations. This hinderance decreases the entropy which depends on the distance between the membrane and the external object. This leads to a repulsive force that tends to push the membrane and the particle apart. The most well-known example of such forces is the entropic force between two biological membrane that has

been extensively studied in the literature. Helfrich [84], for the first time, postulated that the entropic force between two biological membranes varies as $1/d^3$. Since Helfrich's proposal, biophysicists have used the existence of this repulsive force to explain and understand a variety of phenomena related to membrane interactions. The entropic force has been found to have significant role to control the adhesion of particles on biological membrane as well. This is, however, has not received much attention in the literature compared to the interactions between two membranes. Unlike a flat membrane, the topology of a particle might not be flat and indeed in most cases these particles are curved—spherical or cylindrical. During wrapping transition, the membrane deforms to a curved configuration. Entropic force has been also found to have a crucial role in stabilizing small and unilamellar vesicles. When the size of the vesicles are relatively small, the fluctuations of the molecules are confined within the radius of the vesicle. The effect of entropic pressure in stabilizing the small vesicles has been observed in experiments. Typically, a tension-less vesicle cannot be stable in very small sizes. In the presence of surface tension, the fluctuations are strongly suppressed and hence the effect of entropic pressure become negligible. It has been observed in the experiments that if this surface tension, is suddenly removed, the vesicle undergoes an entropic expulsion[126, 130]. Multilamellar vesicles are also found to be metastable when the distance between the vesicles are small. These are all examples of biological phenomena's that are involved with entropic contributions on curved geometries. In this paper, we aim to revise the entropic force for spherical topologies.

4.2 Set up of the statistical mechanics problem

Consider a spherical particle approaching a membrane. During wrapping transition, the membrane transforms into a semi-spherical shape until fully enclose the particle. We aim to have an estimation of the entropic repulsive force between the particle and membrane, during this process. To this end, we assume that the part of the membrane that is affected by the entropic pressure, is a part of a larger spherical vesicle, that fully envelops the particle as shown in Figure. 4.1.1. The fluctuating spherical vesicle (Fig. 4.1.1) with a mean radius of r_0, surface defined as $\mathbb{S} := \{\mathbf{r} \in \mathbb{R}^3 : |\mathbf{r}| = r_0\}$??— has a membrane of thickness d.

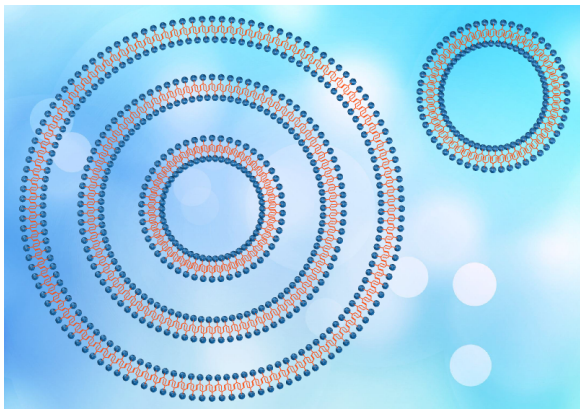

[a]

Figure 4.1.1: Fluctuations on spherical surface.

[a]The out-of-plane fluctuations of the membrane is confined within the distance between the membranes (or the radius of the membrane). This leads to a decrease in entropy that results in steric pressure inside the spherical membrane.

Consider a small but arbitrary pertur- bation of the surface of the vesicle. The position of each point on the perturbed surface of the sphere can be described as

$$\tilde{\mathbf{r}} = \mathbf{r} + \varepsilon U \mathbf{n}, \tag{4.2.1}$$

where, we have assumed that the perturbation is only along the normal direction. Here $\varepsilon \in \mathbb{R}$ is a small number and $U(\theta, \phi) : \mathbb{S} \to \mathbb{R}$ denotes the magnitude of the normal perturbation. The mean curvature and the Jacobian of the perturbed surface can be expressed as

$$\begin{aligned} \tilde{H} &= H + \delta H \\ \tilde{J} &= 1 + \delta J, \end{aligned} \tag{4.2.2}$$

where, H is the mean curvature of the undeformed surface. Up to second order in ϵ, the variations of H and J may be expanded as[92, 100]

$$\begin{aligned}
\delta J &= -2HU\varepsilon + (\frac{1}{2}|\nabla_S U|^2 + KU^2)\varepsilon^2 + O(\varepsilon^2) \\
\delta H &= ((2H^2 - K)U + \frac{1}{2}\Delta_S U)\varepsilon \\
&\quad + (HU\Delta_S U - \frac{1}{2}\nabla_S U \cdot (H\nabla_S U) \\
&\quad + (4H^2 - 3K)HU^2)\varepsilon^2 + O(\varepsilon^2).
\end{aligned} \tag{4.2.3}$$

Neglecting the contribution of the Gaussian curvature, the elastic energy per unit area of the perturbed surface can be written as

$$\bar{\psi} = \frac{1}{2}\kappa_b \tilde{H}^2 + \sigma, \tag{4.2.4}$$

where σ is the surface tension of the membrane. Using Equations (4.2.2) and (4.2.3) and integrating the above expressions over the surface of the membrane, we obtain

$$\begin{aligned}
\mathcal{E}^{\text{tot}}[U, H] &= \int_{\mathbb{S}} \bar{\psi}\tilde{J} dA_0 \\
&= \int_{\mathbb{S}} \left(E(\varepsilon^0) + E(\varepsilon^2) + O(\varepsilon^2)\right) dA_0,
\end{aligned} \tag{4.2.5}$$

in which we have retained up to fourth order terms. The leading terms in the expressions for $E(\varepsilon^i)$ are as follows

$$\begin{aligned}
E(\varepsilon^0) &= \frac{1}{2}\kappa_b H^2 \\
E(\varepsilon^2) &= \frac{1}{8}\kappa_b(\Delta_S U)^2 + \frac{1}{4}\kappa_b U\Delta_S U(5H^2 - 2K) + \cdots .
\end{aligned} \tag{4.2.6}$$

Specializing to the case of a perfect sphere of radius R_0, the equilibrium mean and Gaussian curvatures are $H^{-1} = -R_0$ and $K^{-1} = R_0^2$. Moreover, we define the normalized mid-plane displacement as: $u = U/R_0$. For notational simplicity, we use $\underline{\Delta} := \Delta_S(R_0 = 1)$ as the surface laplacian operator on the unit sphere. Assuming that θ and ϕ are polar and azimuthal angles, we can write the area element as: $dA_0 = R_0^2 d\Omega$, where $d\Omega = \sin(\theta)d\theta d\phi$.

Then, integrating the terms in (4.2.6) over the area of the sphere, we obtain

$$\mathcal{E}^{\text{tot}}[u, R_0] = 2\pi\kappa_b + \int_{\mathbb{S}} \frac{1}{8}\Big[\kappa_b(\underline{\Delta}u)^2 + (6\kappa_b - 4\sigma R_0^2)u\underline{\Delta}u + 8\sigma R_0^2 u^2\Big]\, d\Omega. \tag{4.2.7}$$

Now let $\eta = r_0/R_0$ where, r_0 is the radius of the particle inside the spherical membrane. Then, the displacement field on the surface of the membrane would be restricted within the distance to the particle as

$$\eta - 1 < u < 1 - \eta. \tag{4.2.8}$$

Then from the definition[74] the partition function and the free energy of the system can be written as a functional integral

$$\begin{aligned} Z &= \int_{\eta-1}^{1-\eta} \exp(-\beta\mathcal{E}^{\text{tot}}[u, R_0])\mathcal{D}[u] \\ F &= -k_B T \log Z, \end{aligned} \tag{4.2.9}$$

where $\beta = 1/k_B T$. Consequently, the entropic pressure on the spherical membrane occupying a volume of $V = \frac{4}{3}\pi(R_0^3 - r_0^3)$ is obtained as

$$\begin{aligned} p &= -\frac{\partial F}{\partial V} = -\frac{\partial F}{\partial \eta}\frac{\partial \eta}{\partial V} \\ &= \frac{1}{4\pi R_0^3 \eta}\frac{\partial F}{\partial \eta}. \end{aligned} \tag{4.2.10}$$

Now note that the partition function in (4.2.9) is not a Gaussian integral and hence cannot be analytically carried out. However, using numerical methods, such as Monte Carlo, one can get a good estimation of the partition function to impose the hard constraint (4.2.8) on the path integral. Nevertheless, using a slight modification in the energy formulation, we can get analytical estimation for the partition function and the free energy. The procedure is as follows: 1) we add a potential energy term to the original elastic energy in (4.2.7) to

mimic the effects of the steric pressure on suppression of the fluctuations and instead, carry out the partition function integration within $(-\infty, \infty)$, 2) we optimize the potential energy, in such a way that

$$\langle u^2 \rangle < (1-\eta)^2, \tag{4.2.11}$$

which is a softer constraint compared to (4.2.8). Now let

$$\tilde{\mathcal{E}} = \mathcal{E}^{\text{tot}}[u, R_0] + V[u] \tag{4.2.12}$$

be the total energy, including the potential energy $V[u]$. In general, $V[u]$ can be expanded in a polynomial form as

$$\begin{aligned} V[u] = \int_{\mathbb{S}} \alpha_2 \left(\frac{u}{1-\eta}\right)^2 + \alpha_4 \left(\frac{u}{1-\eta}\right)^4 \\ + \alpha_6 \left(\frac{u}{1-\eta}\right)^6 + \cdots . \end{aligned} \tag{4.2.13}$$

Basic statistical mechanics tells us that the probability of occurrence of a certain change of displacement field can be expressed as an exponential function

$$\rho(u) \propto \exp(-\tilde{\mathcal{E}}/k_B T), \tag{4.2.14}$$

indicating that, the higher values of u (with the attendant larger energy cost) are less probable. Accordingly, the potential energy $V[u]$ ensures lower probability for larger values of u and eventually, decreases the fluctuations. To make analytical progress, we keep only the quadratic term in $V[u]$.

$$V[u] = \int_{\mathbb{S}} \alpha \left(\frac{u}{1-\eta}\right)^2 d\Omega. \tag{4.2.15}$$

Now the coefficient α should be found in such a way that

$$\langle u^2 \rangle_{\tilde{\mathcal{E}}} = \delta^2 (1-\eta)^2, \tag{4.2.16}$$

where $\delta^2 < 1$ is used to ensure that the inequality (5.1.2) is satisfied. Also the subscript, denotes averaging with respect to the total energy, including the potential energy. In the next section, we proceed to use the potential energy (4.2.15) to get an estimate of the entropic pressure on a spherical membrane.

4.3 Entropic force on a spherical membrane

The total Hamiltonian of a fluctuating spherical membrane, in the vicinity of an external hinderance, up to quadratic order is expressed as

$$\begin{aligned}\tilde{\mathcal{E}} &= \mathcal{E}^{\text{tot}}[u, R_0] + V[u] \\ &= \int_{\mathbb{S}} \frac{1}{8} \Big[\kappa_b(\underline{\Delta} u)^2 + (6\kappa_b - 4\sigma R_0^2) u \underline{\Delta} u \\ &\qquad + 8(\sigma R_0^2 + \frac{\alpha}{(1-\eta)^2}) u^2\Big] \, d\Omega. \end{aligned} \tag{4.3.1}$$

We start with the Fourier decomposition of the perturbation field on the sphere. To this end we expand the displacement in terms of spherical harmonics. Let N be the total number of degrees of freedom and

$$\mathcal{K}_N := \{(l,m) | (l,m) \in \mathbf{Z} \times \mathbf{Z}, l \geqslant 2, l(l+1) < N, -l < m < l\}.$$

Then we can expand the normalized perturbation field in terms of spherical harmonics as below

$$u(\theta, \phi) = \sum_{(l,m) \in \mathcal{K}_N} u_{l,m} Y_{l,m}, \tag{4.3.2}$$

where Y_{lm} are spherical harmonics[**?**] with eigenvalues

$$\nabla^2 Y_{l,m} = -q_{l,m}^2 Y_{l,m} = -l(l+1) Y_{l,m}, \tag{4.3.3}$$

and $u_{l,-m} = u^*_{l,m}$ are the Fourier transformation of $u(\theta, \phi)$

$$u_{l,m} = \int_{\mathbb{S}} u(\theta, \phi) Y^*_{l,m} d\Omega. \tag{4.3.4}$$

We have excluded the modes corresponding to $l = 0$ and $l = 1$, since these modes represent the area change and the rigid body motion of the membrane and hence do not contribute to the total energy. We also recall the two important properties of the spherical harmonics, which will be used later in our calculations. They are orthonormal

$$\int_{\mathbb{S}} Y_{lm} Y^*_{l'm'} d\Omega = \delta_{ll'} \delta_{mm'},$$

and separable

$$Y_{lm} = P^m_l(\theta) e^{im\phi},$$

where $P^m_l(\theta)$ is the Legendre polynomial corresponding to the mode (l, m). In what follows, for the eigenvalues of the spherical harmonics, we use the notation $\mathbf{q} = q_{l,m}$ wherein $\mathbf{q}^2 = q^2_{l,m} = l(l+1)$.

The total Hamiltonian, then can be expanded in Fourier space as below

$$\begin{aligned} \tilde{\mathcal{E}} = \frac{\pi}{4} \sum_{(l,m) \in \mathcal{K}_N} \Big[& \kappa_b \mathbf{q}^4 - (6\kappa_b - 4\sigma R_0^2) \mathbf{q}^2 \\ & + 8(\sigma R_0^2 + \frac{\alpha}{(1-\eta)^2}) \Big] |u(\mathbf{q})|^2. \end{aligned} \tag{4.3.5}$$

The partition function of the system can be then obtained as below

$$\begin{aligned} Z &= \int_{-\infty}^{\infty} \exp(-\tilde{\mathcal{E}}/k_B T) \prod_{\mathbf{q} \in \mathcal{K}_N} du(\mathbf{q}) \\ &= \prod_{\mathbf{q} \in \mathcal{K}_N} \frac{2}{\sqrt{\beta}} \\ &\times \frac{1}{\sqrt{\Big(\kappa_b \mathbf{q}^4 - (6\kappa_b - 4\sigma R_0^2) \mathbf{q}^2 + 8(\sigma R_0^2 + \frac{\alpha}{(1-\eta)^2}) \Big)}}. \end{aligned} \tag{4.3.6}$$

Accordingly, the free energy is obtained as

$$\begin{aligned} F &= -k_B T \log Z \\ &= \alpha_F + \frac{k_B T}{2} \sum_{\mathbf{q}\in\mathcal{K}_N} \log \Big[\kappa_b \mathbf{q}^4 - (6\kappa_b - 4\sigma R_0^2)\mathbf{q}^2 \\ &\qquad +8(\sigma R_0^2 + \frac{\alpha}{(1-\eta)^2}\Big], \end{aligned} \tag{4.3.7}$$

wherein α_F is a constant of no consequence. Further, the fluctuations of the normalized out-of-plane displacement in each mode is calculated using equipartition theorem

$$\langle |u(\mathbf{q})|^2 \rangle = \frac{2k_B T}{\pi \left(\kappa_b \mathbf{q}^4 - (6\kappa_b - 4\sigma R_0^2)\mathbf{q}^2 + 8(\sigma R_0^2 + \frac{\alpha}{(1-\eta)^2})\right)}. \tag{4.3.8}$$

The autocorrelation function of the displacement field can be obtained by summing over all possible modes

$$\begin{aligned} \langle u^2 \rangle &= \frac{1}{4\pi} \int_{\mathbb{S}} \langle u(\theta,\phi)^2 \rangle d\Omega \\ &= \frac{1}{4\pi} \int_{\mathbb{S}} \sum_{\mathbf{q},\mathbf{q}'\in\mathcal{K}_N} \langle u(\mathbf{q}) u(\mathbf{q}') \rangle Y_{\mathbf{q}} Y_{\mathbf{q}'} d\Omega \\ &= \frac{1}{4\pi} \int_{\mathbb{S}} \sum_{\mathbf{q},\mathbf{q}'\in\mathcal{K}_N} \langle u(\mathbf{q}) u(\mathbf{q}') \rangle \delta(\mathbf{q}, -\mathbf{q}') d\Omega \\ &= \sum_{\mathbf{q}\in\mathcal{K}_N} \langle |u(\mathbf{q})|^2 \rangle. \end{aligned} \tag{4.3.9}$$

To compute the summation we replace it with an integral

$$\sum_{\mathbf{q}\in\mathcal{K}_N} := \sum_l (2l+1) \approx \int (2l+1) dl, \tag{4.3.10}$$

where l_{max} can be easily obtained from the total number of modes (degrees of freedom):

$$N = \sum_l (2l+1) = \frac{4\pi R_0^2}{A_0}, \tag{4.3.11}$$

in which A_0 is the area associated with each degree of freedom, and is typically of the same

order of magnitude as d^2 with d is the thickness of the membrane. Now, let

$$\begin{aligned}
A_1 &= 4(\eta-1)^2 R_0^2\sigma\left(R_0^2\sigma - 5\kappa_b\right)\\
A_2 &= \kappa_b\left(9(\eta-1)^2\kappa_b - 8\alpha\right)\\
A_3 &= \frac{8\alpha\kappa_b}{(\eta-1)^2} - \left(2R_0^2\sigma - 9\kappa_b\right)\left(2R_0^2\sigma - \kappa_b\right)\\
A_4 &= (\eta-1)^2\left(\kappa_b + 2R_0^2\sigma\right)\\
\theta &= \mathrm{Arctan}(\frac{A_1+A_2}{A_4\sqrt{A_3}}).
\end{aligned} \tag{4.3.12}$$

Then, the summation in (4.3.9) can be evaluated as

$$\begin{aligned}
&\sum_{\mathbf{q}\in\mathcal{K}_N}\langle|u(\mathbf{q})|^2\rangle =\\
&\frac{2k_BT}{\pi}\int\frac{2\pi q dq}{\kappa_b\mathbf{q}^4 - (6\kappa_b - 4\sigma R_0^2)\mathbf{q}^2 + 8(\sigma R_0^2 + \frac{\alpha}{(1-\eta)^2})}\\
&= \frac{2k_BT\theta}{\pi\sqrt{32\kappa_b\left(\frac{\alpha}{(\eta-1)^2} + R_0^2\sigma\right) - 4\left(2R_0^2\sigma - 3\kappa_b\right)^2}}.
\end{aligned} \tag{4.3.13}$$

As it is mentioned earlier, the fluctuations should be restricted within the distance between the membrane and the particle. Hence, one can solve for α from the following equation

$$\begin{aligned}
&\frac{2k_BT\theta}{\pi\sqrt{32\kappa_b\left(\frac{\alpha}{(\eta-1)^2} + R_0^2\sigma\right) - 4\left(2R_0^2\sigma - 3\kappa_b\right)^2}}\\
&= \delta^2(1-\eta)^2.
\end{aligned} \tag{4.3.14}$$

Note that, depending on the sign of A_3, θ can be hyperbolic or inverse trigonometric function. In the following we will investigate both cases separately, to solve the above equation for α, and the entropic pressure.

Case I: Small radius, large $\alpha \rightarrow A_3 > 0$

When $A_3 > 0$, we will have

$$\frac{8\alpha\kappa_b}{(\eta-1)^2} > \Big(2R_0^2\sigma - 9\kappa_b\Big)\Big(2R_0^2\sigma - \kappa_b\Big), \tag{4.3.15}$$

which holds when α is large enough. This happens in the close distances (or large values of η) when the entropic pressure is relatively large. In this case, for θ we will have: $0 < \theta < \pi/2$ while the denominator of (4.3.14) has a sharper variation with respect to the α. Therefore, we approximately keep the numerator in (4.3.14) as a constant θ and solve for η using the expression in the denominator. We obtain

$$\begin{aligned}\alpha = &\frac{\theta^2(k_BT)^2}{8\pi^2\delta^4(\eta-1)^2\kappa_b} \\ &+ \frac{(\eta-1)^2\left(2R_0^2\sigma - 9\kappa_b\right)\left(2R_0^2\sigma - \kappa_b\right)}{8\kappa_b}.\end{aligned} \tag{4.3.16}$$

Substituting the above expression into Equation (4.3.7) and taking the derivative with respect to the volume, we will have

$$\begin{aligned}p &= -\frac{\partial F}{\partial V} = -\frac{\partial F}{\partial \eta}\frac{\partial \eta}{\partial V} \\ &= \frac{1}{4\pi R_0^3\eta^2}\frac{\partial F}{\partial \eta} \\ &= \frac{1}{4\pi R_0^3\eta^2}\frac{\theta^2(k_BT)^2}{8\pi^2\delta^4(\eta-1)^5\kappa_b} \\ &\times \sum_{\mathbf{q}\in\mathcal{K}_N}\frac{k_BT}{2\left(\kappa_b\mathbf{q}^4 - (6\kappa_b - 4\sigma R_0^2)\mathbf{q}^2 + 8(\sigma R_0^2 + \frac{\alpha}{(1-\eta)^2})\right)} \\ &= \frac{1}{4\pi R_0^3\eta^2}\frac{\theta^2(k_BT)^2}{8\pi^2\delta^4(\eta-1)^5\kappa_b} \times \delta^2(1-\eta)^2 \\ &= \frac{\lambda_A}{(1-\eta)^3},\end{aligned} \tag{4.3.17}$$

where λ is the resulting coefficient. As it can be seen, the power law for the steric pressure is $1/(1-\eta)^3$, which is the same as the interaction between two flat membrane. This is true for small distances, when η is relatively large.

Case II: Large radius, small $\alpha \rightarrow A_3 < 0$

When $A_3 < 0$, we will have

$$\frac{8\alpha\kappa_b}{(\eta-1)^2} < \left(2R_0^2\sigma - 9\kappa_b\right)\left(2R_0^2\sigma - \kappa_b\right), \tag{4.3.18}$$

which holds when α is small enough. This happens in the large distances (or small values of η) when the entropic pressure is relatively small. Note that the expression in the (4.3.14) can be written in terms of A_3

$$\langle u^2\rangle = \frac{k_B T\theta}{\pi\sqrt{A_3}}\text{Arctan}(\frac{A_1+A_2}{A_4\sqrt{A_3}}). \tag{4.3.19}$$

When $A_3 < 0$, the above function transform to

$$\begin{aligned}\langle u^2\rangle &= \frac{k_B T\theta}{\pi\sqrt{-A_3}}\text{Arctanh}(\frac{A_1+A_2}{A_4\sqrt{-A_3}}) \\ &= \frac{k_B T\theta}{2\pi\sqrt{-A_3}}\log\left(\frac{A_1+A_2+A_4\sqrt{-A_3}}{-A_1-A_2+A_4\sqrt{-A_3}}\right) \\ &= \lambda_B \log\left(\frac{A_1+A_2+A_4\sqrt{-A_3}}{-A_1-A_2+A_4\sqrt{-A_3}}\right).\end{aligned} \tag{4.3.20}$$

Here, $\lambda_B = \frac{k_B T\theta}{2\pi\sqrt{-A_3}}$ and since α is considered to be very small, λ is assumed to be a constant. In this manner, solving for α gives us

$$\begin{aligned}\alpha &= \frac{(\eta-1)^2\text{sech}^2\left(\frac{\delta^2(\eta-1)^2}{2\lambda_B}\right)}{8\kappa_b} \\ &\times\left[4\kappa_b\left(\kappa_b - 3R_0^2\sigma\right)\cosh\left(\frac{\delta^2(\eta-1)^2}{\lambda_B}\right)\right. \\ &\left.+5\kappa_b^2 - 8R_0^2\sigma\kappa_b + 4R_0^4\sigma^2\right] \\ &\approx (\eta-1)^2\exp\left(-\frac{\delta^2(\eta-1)^2}{\lambda_B}\right) + \cdots .\end{aligned} \tag{4.3.21}$$

Substituting the above expression into Equation (4.3.7) and taking the derivative with respect to the volume, we will have

$$\begin{aligned} p &= -\frac{\partial F}{\partial V} = -\frac{\partial F}{\partial \eta}\frac{\partial \eta}{\partial V} \\ &= \frac{1}{4\pi R_0^3 \eta^2}\frac{\partial F}{\partial \eta} \\ &\approx (1-\eta)^3 \exp\left(\frac{\delta^2(1-\eta)^2}{\lambda_B}\right) + \cdots . \end{aligned} \tag{4.3.22}$$

The above expression shows an exponential decaying of the steric pressure. Such behavior was previously observed in Monte-Carlo simulations [67] for the interaction of two flat membranes, however, the form of the function was found to be slightly different. In a recent work, Hanlumyuang et al.[67] observed an exponential decaying trend of the repulsive force in Monte Carlo calculations. Though their model did not account for geometric nonlinearities or surface tension, we speculate that such exponential trend is because of fixing the area and inhibiting the in-plane motions. In this manner, an artificial surface tension will affect the results. This issue, becomes more important at larger inter membrane distances when the membrane undergoes larger fluctuations, which requires higher surface tension to maintain the fixed area.

Chapter 5

Thermal Fluctuations and Effective Bending Stiffness of Nonlinearly Elastic Graphene and Solid Membranes: An Analytical and Atomistic Investigation

The study of statistical mechanics of thermal fluctuations of graphene—the prototypical two-dimensional material—is rendered rather complicated due to the necessity of accounting for geometric deformation nonlinearity in its deformation. Unlike fluid membranes such as lipid bilayers, coupling of stretching and flexural modes leads to a highly anharmonic elastic Hamiltonian. Existing treatments heavily draw on analogies that exist in the high-energy physics literature. In this study, using a variational perturbation method, we present a "mechanics-oriented" novel treatment of the thermal fluctuations of graphene, fully accounting for deformation nonlinearities, and evaluate their effect on the effective bending stiffness. We compare the results from our approach to both molecular dynamics simulations as well as other analytical methods in the literature.

5.1 Introduction

During the past decade, statistical mechanics of interfaces and two dimentional membranes has been one of the most attractive topic of research in physics and material science. Despite the well-known Mermin-Wagner theorem, these 2D materials are found to be stable at finite temperature. The stability of these 2D materials at finite temperature has attracted much attention after the discovery of graphene monolayer—as a prototype two dimensional crystalline membrane. Due to the unusual flexibility and the ability to sustain large deformations, graphene monolayers are found to be suitable for a number of fascinating applications in areas such as electronics, energy harvesting, biological systems among many others. They are mechanically described as elastic sheets that are resilient to areal change (in-plane deformations), but are quite flexible to undergo large curvatures—simillar to fluid (biological) membranes. Specifically, the energy cost for their bending deformation can be parametrized by a quadratic function of curvature

$$F_b = \int \frac{1}{2}\kappa_b(H - H_0)^2 + \kappa_G(K - K_0), \tag{5.1.1}$$

where, κ_b and $\bar{\kappa}$ are the bending moduli that, respectively, correspond the energy change due to changes in the mean (H) and Gaussian (K) curvatures. The corresponding spontaneous curvatures are denoted by H_o and K_o. Equation (5.1.1) has been also used in the context of biological membranes [1, 2, 6, 8]. Bending stiffnesses κ_b of both graphene and biological membranes are typically very low—$(10 - 60)k_BT$— hence, the energy cost for their out-of-plane deformations can be easily provided by thermal energy at room temperature. Thus, these 2D membranes, experience noticeable fluctuations at room temperature that can be observed and measured in experiments or molecular dynamic simulations. Based on the linearized version of the Equation (6.1.1)— $H = -\nabla^2 h$, with h being the out-of-plane displacement field— the ensemble average of the fluctuations for a membrane of size L^2 can be obtained as: $\langle h^2 \rangle \propto k_BTL^2/\kappa_b$. In particular, this basic result has provided a facile route to estimate mechanical and other related properties of biological membranes [13, 14, 15, 16].

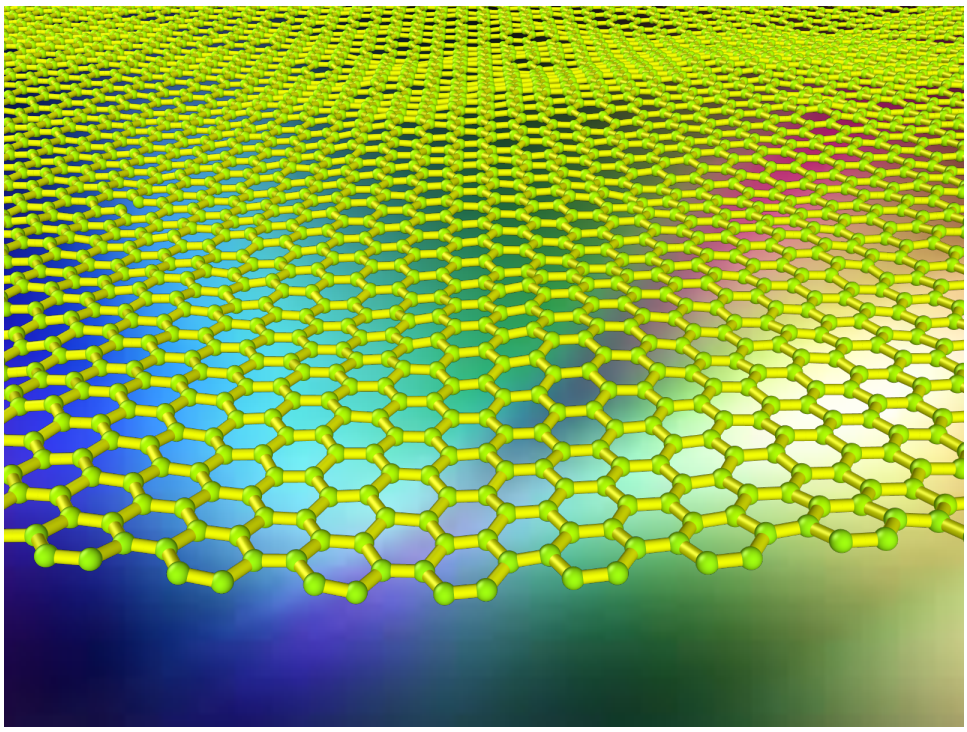

Figure 5.1.1: Snapshot of molecular dynamics simulation of a graphene monolayer.

Unlike biological membranes, reported values for bending stiffness of graphene are all evaluated at zero Kelvin, where there is no fluctuations and temperature effects [9, 10, 11]. In fact, the fluctuations spectra cannot be used to determine the bending modulus of graphene. This is due to the fact that elasticity of graphene is somewhat more complicated, compared to fluid (biological) membranes. The von-Karman nonlinear plate theory [131] is usually employed to describe the elasticity of 2D solid materials. Accordingly, in addition to bending energy in (6.1.1), the elastic energy cost for their in-plane deformations must be also accounted for and is nonlinearly coupled to the out-of-plane displacement field. As a result of the nonlinear coupling of in- and out-of-plane deformations, graphene sheets appeared to have intrinsic ripples at finite temperature. Further, the fluctuations in graphene monolayers are found to be suppressed when compared to fluid (biological) membranes [132]. Molecular dynamics simulations of graphene monolayers, with periodic boundary conditions in all directions, show that the apparent bending stiffness of graphene at finite temperature is much larger than its bare value—at zero kelvin [71]. Typically, the out-of-plane fluctuations for solid membranes are described as a power law; i.e. $\langle h^2 \rangle \propto L^{\eta}$, with L being the in-plane

size of the sheet. Within the harmonic approximation, the exponent η is equal to 2. Due to nonlinearity, η is smaller than 2 for solid membranes. Several works have numerically studied this scaling and its entropic consequences [71, 132, 133, 134, 135]. Typical values of η for graphene are found to range from $(0.7-1.2)$ [71, 132, 133, 134, 135]. The anomalous effects of finite temperature in graphene, can be also represented in the so-called *renormalized* or *effective* bending stiffness that depends on the mode of deformation, i.e. $\kappa^{\text{eff}} := \kappa^{\text{eff}}(q)$[1]. It has been first, studied by Nelson and Peliti [132] that the effective bending stiffness diverges from the bare value of bending modulus κ_b for long wave-length fluctuations. Generally, the mode-dependence of κ^{eff} can be expressed as a power law, i.e. $\kappa^{\text{eff}}(q) \sim q^{-\delta}$. Using a one-loop self-consistent method, Nelson and Peliti[132] obtained $\delta = 1$. Later on, several following works appeared to revisit this problem using different advanced theoretical and numerical methods that are well-developed in high-energy physics literature. Reported values for δ in literature range $(0.65 - 1.1)$ [71, 132, 133, 134, 135].

In general, thermal fluctuations may have contradictory softening and stiffening effects on 2D materials. Several works have studied the softening effects in the context of fluid (biological) membranes [100, 102, 115]. The so-called *apparent* bending stiffness is expressed as[115]

$$\kappa_{\text{eff}} = \kappa_b + \frac{\alpha}{8\pi} k_B T \log N, \tag{5.1.2}$$

wherein $\alpha = -3$[100] is a universal constant and N is the number of degrees of freedom in the system. Though, this softening effect has been primarily studied for fluid membranes it appears universally in all 2D materials including fluid and solid membranes. In addition to softening effects of thermal fluctuations, solid membranes experience anomalous stiffening at finite temperature due to nonlinear elasticity[2]. The competition between softening and stiffening effects of thermal fluctuations at very long wave-length ($q \to 0$), that leads to crumpling phase in graphene monolayers, has been also the subject of interest for physicists.

[1] Within harmonic approximation, the effective bending stiffness is simply equivalent to the bare value of the bending modulus and is mode-independent, i.e. $\kappa^{\text{eff}} := \kappa_b$

[2] In contrast to the softening effect, the stiffening effect is pecular to only solid membranes and not fluid membranes.

Most of the treatments in the area of statistical mechanics of solid or polymerized membranes are originated in high-energy physics and very little has been understood among mechanics community. In this work, we revisit this topic using a variational perturbation method to study the stiffening effects of thermal fluctuations in graphene. In Section 5.2 on overview of the energy formulation in nonlinear elasticity is presented. To start with a simpler model, we study the one-dimensional version of the problem in Section 5.3. Our results in this part demonstrate that despite of non-linearities, this problem can be solved exactly analytically in one dimension. We later expand the problem in two dimensions, for which there is no exact analytical solution in Section 5.4. An approximate method is used to evaluate the effective bending stiffness in Section 5.5. We compare our theoretical result with data from molecular dynamic simulations in Section 5.6.

5.2 Energy Formulation within Nonlinear Elasticity

Consider a rectangular graphene sheet occupying a domain of size $\mathbb{S} = (0, L)^2$ on the xy plane. The configuration of the sheet is described by the state variables $\{u_x(\mathbf{x}), u_y(\mathbf{x}), w(\mathbf{x}) : \mathbb{S} \to \mathbb{R}\}$, where u_x and u_y are the in-plane displacement fields along the x and y directions, respectively. Furthermore, w is the out-of-plane displacement field. Also, $\mathbf{x} = (x, y)$ refers to the coordinates of the points on the sheet. The kinematic of the deformation of such 2D structure, is analogous to nonlinear von Karman plate theory when the thickness is vanishing. Accordingly, the components of the Green-Lagrangian strain tensor are obtained as

$$\varepsilon_{\gamma\delta} = \frac{1}{2}\left(\frac{\partial u_\gamma}{\partial x_\delta} + \frac{\partial u_\delta}{\partial x_\gamma} + \frac{\partial w}{\partial x_\gamma}\frac{\partial w}{\partial x_\delta} + \frac{\partial u_k}{\partial x_\gamma}\frac{\partial u_k}{\partial x_\delta}\right), \tag{5.2.1}$$

where the subscripts γ, δ or k represents x or y. It is noted that the last term leading to nonlinear contributions from the in-plane displacement field is typically neglected compared to other terms. This is due to fact that the in-plane elastic stiffness of the graphene is notably larger than its flexural stiffness. In this paper, henceforth, we disregard the last term in

Equation (6.4.1) and instead focus on the consequences of the nonlinear contribution of the out-of-plane displacement. Having the strain field in (6.4.1), the resulting stress tensor can be written as

$$\sigma_{\gamma\delta} = \frac{E}{1+\nu}\left(\varepsilon_{\gamma\delta} + \frac{\nu}{1-\nu}\varepsilon_{kk}\delta_{\gamma\delta}\right). \tag{5.2.2}$$

Let E and ν be the elastic Young modulus and poisson ratio of the graphene sheet, respectively. Then, using the above stress field and the strain field in (6.4.1), the in-plane strain energy can be written as

$$\begin{aligned} U_s &= \int \frac{1}{2}\sigma_{\gamma\delta}\varepsilon_{\gamma\delta} \\ &= \int_{\mathbb{S}} \left\{ \frac{E}{2(1-\nu^2)}\left(I_1 + 2\nu I_2\right) + \frac{E}{1+\nu} I_3 \right\}, \end{aligned} \tag{5.2.3}$$

where $I_1 = \varepsilon_{xx}^2 + \varepsilon_{yy}^2$, $I_2 = \varepsilon_{xx}\varepsilon_{yy}$, and $I_3 = \varepsilon_{xy}^2$. Furthermore, the bending energy of the deformed graphene sheet, U_b is a function of the two invariants of the curvature tensor; mean and Gaussian curvatures, which are the trace and determinant of the curvature tensor, respectively. Within linear approximation, mean (H) and Gaussian (K) curvatures are described as

$$\begin{aligned} H &= \frac{\partial^2 w}{\partial x^2} + \frac{\partial^2 w}{\partial y^2} \\ K &= \frac{\partial^2 w}{\partial x^2}\frac{\partial^2 w}{\partial y^2} - \left(\frac{\partial^2 w}{\partial x \partial y}\right)^2. \end{aligned} \tag{5.2.4}$$

The corresponding bending energy U_b, then can be written as

$$U_b = \int_{\mathbb{S}} \frac{1}{2}\kappa_b H^2 + \kappa_G K, \tag{5.2.5}$$

in which κ_b and κ_G are the corresponding bending stiffnesses. Due to the Gauss-Bonnet theorem, the integration of Gaussian curvature over the area is fixed when the topology of the system does not change in the deformed configuration. Hence, we can disregard the second term in integration (5.2.5).

The total elastic energy of the membrane is the summation of the in-plane strain energy and bending energy, i.e. $U = U_s + U_b$. In order to obtain the total elastic energy in terms of the displacement fields, we start by deriving the components of the strain tensor

$$\begin{aligned}
\varepsilon_{xx} &= \frac{\partial u_x}{\partial x} + \frac{1}{2}\left(\frac{\partial w}{\partial x}\right)^2 \\
\varepsilon_{yy} &= \frac{\partial u_y}{\partial y} + \frac{1}{2}\left(\frac{\partial w}{\partial y}\right)^2 \\
\varepsilon_{xy} &= \frac{1}{2}\left(\frac{\partial u_x}{\partial y} + \frac{\partial u_y}{\partial x} + \frac{\partial w}{\partial x}\frac{\partial w}{\partial y}\right).
\end{aligned} \tag{5.2.6}$$

It can be readily seen that employing the nonlinear strain tensor (6.4.1) results in a rather complicated form of the elastic energy. The complexity appears in two parts; first, the contribution of the fourth order terms of the out of plane deformation, and second, the coupling terms between the in-plane and out of plane displacements. Consequently, the total elastic energy[3] can be split into three parts: harmonic terms U_{h}, coupling (between in and out-of-plane displacement fields) terms U_{c}, and anharmonic term U_{anh}. Hence we have

$$U = U_{\mathrm{h}} + U_{\mathrm{c}} + U_{\mathrm{anh}}, \tag{5.2.8}$$

[3]The resulting expressions for I_1, I_2, and I_3 are derived as

$$\begin{aligned}
I_1 &= \varepsilon_{xx}^2 + \varepsilon_{yy}^2 \\
&= \frac{1}{4}\left\{\left(\frac{\partial w}{\partial x}\right)^4 + \left(\frac{\partial w}{\partial y}\right)^4\right\} + \frac{\partial u_x}{\partial x}\left(\frac{\partial w}{\partial x}\right)^2 + \frac{\partial u_y}{\partial y}\left(\frac{\partial w}{\partial y}\right)^2 + \left(\frac{\partial u_x}{\partial x}\right)^2 + \left(\frac{\partial u_y}{\partial y}\right)^2
\end{aligned} \tag{5.2.7a}$$

$$\begin{aligned}
I_2 &= \varepsilon_{xx}\varepsilon_{yy} \\
&= \frac{1}{4}\left(\frac{\partial w}{\partial x}\frac{\partial w}{\partial y}\right)^2 + \frac{1}{2}\frac{\partial u_x}{\partial x}\left(\frac{\partial w}{\partial y}\right)^2 + \frac{1}{2}\frac{\partial u_y}{\partial y}\left(\frac{\partial w}{\partial x}\right)^2 + \frac{\partial u_x}{\partial x}\frac{\partial u_y}{\partial y}
\end{aligned} \tag{5.2.7b}$$

$$\begin{aligned}
I_3 &= \varepsilon_{xy}^2 \\
&= \frac{1}{4}\left(\frac{\partial w}{\partial x}\frac{\partial w}{\partial y}\right)^2 + \frac{1}{2}\frac{\partial w}{\partial x}\frac{\partial w}{\partial y}\left(\frac{\partial u_x}{\partial y} + \frac{\partial u_y}{\partial x}\right) + \frac{1}{2}\left(\frac{\partial u_x}{\partial y} + \frac{\partial u_y}{\partial x}\right)^2.
\end{aligned} \tag{5.2.7c}$$

in which

$$U_{\rm h} = \frac{1}{2}\kappa_b(\nabla^2 w)^2 + \frac{E}{2(1-\nu^2)}\left(|\nabla \mathbf{u}|^2 + 2\nu\frac{\partial u_x}{\partial x}\frac{\partial u_y}{\partial y}\right) + \frac{E}{2(1+\nu)}\left(\frac{\partial u_x}{\partial y} + \frac{\partial u_y}{\partial x}\right)^2 \tag{5.2.9a}$$

$$U_{\rm c} = \frac{E}{2(1-\nu^2)}\left(\frac{\partial u_x}{\partial x}\left(\frac{\partial w}{\partial x}\right)^2 + \frac{\partial u_y}{\partial y}\left(\frac{\partial w}{\partial y}\right)^2 + \nu\frac{\partial u_x}{\partial x}\left(\frac{\partial w}{\partial y}\right)^2 + \nu\frac{\partial u_y}{\partial y}\left(\frac{\partial w}{\partial x}\right)^2\right) + \frac{E}{2(1+\nu)}\frac{\partial w}{\partial x}\frac{\partial w}{\partial y}\left(\frac{\partial u_x}{\partial y} + \frac{\partial u_y}{\partial x}\right) \tag{5.2.9b}$$

$$U_{\rm anh} = \frac{E}{8(1-\nu^2)}\left(\left(\frac{\partial w}{\partial x}\right)^4 + \left(\frac{\partial w}{\partial y}\right)^4 + 2\left(\frac{\partial w}{\partial x}\frac{\partial w}{\partial y}\right)^2\right) = \frac{E}{8(1-\nu^2)}|\nabla w|^4. \tag{5.2.9c}$$

Our goal in this work is to study the statistical mechanics of the fully coupled nonlinear system including all the coupling and anharmonic terms in (5.2.9). We start with a one dimensional case where $u_y = 0$ and $(u_x, w) = (u_x(x), w(x))$. We later expand our analysis to the actual two dimensional problem.

5.3 Statistical mechanics of a nonlinear elastic sheet in one dimension

Consider a sheet of size L^2, under one dimensional deformation, i.e. the displacement field is solely a function of x as: $(u_x, w) = (u_x(x), w(x))$ while $u_y = 0$. Therefore, the strain tensor will have only one component

$$\varepsilon_x = \frac{\partial u_x}{\partial x} + \frac{1}{2}\left(\frac{\partial w}{\partial x}\right)^2. \tag{5.3.1}$$

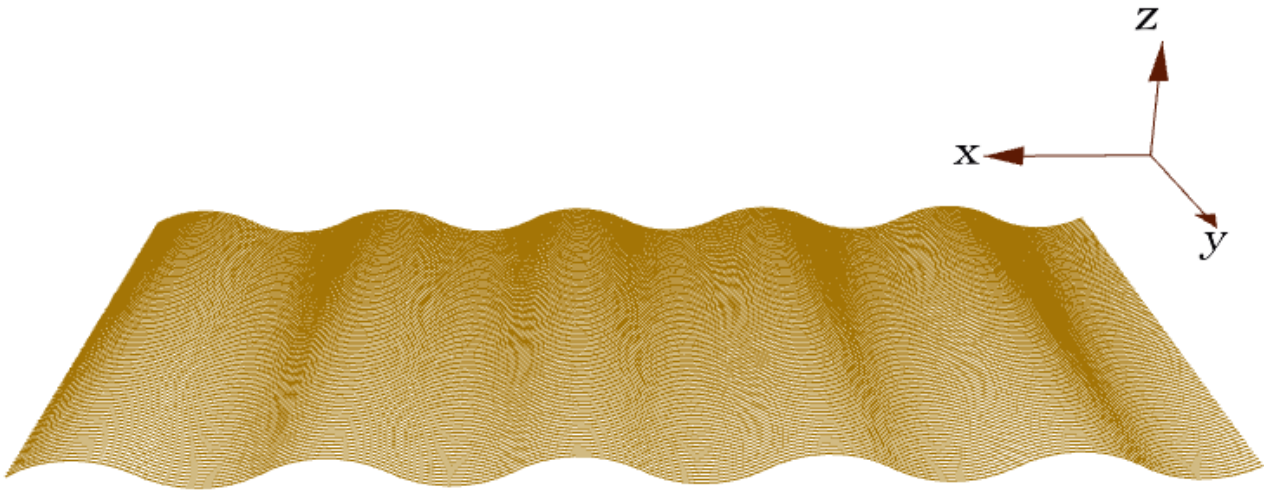

Figure 5.3.1: Deformation of graphene sheet in one dimension. In this case, the displacement is only a function of x. Also $u_y = 0$.

Further, the bending and strain energy can be reduced to

$$\begin{aligned} U_b &= \int \frac{1}{2}\kappa_b \left(\frac{\partial^2 w}{\partial x^2}\right)^2 \\ U_s &= \int \frac{E}{2(1-\nu^2)}\varepsilon_x^2 \\ &= \overline{E}\int \left(\frac{\partial u}{\partial x}\right)^2 + \frac{\partial u_x}{\partial x}\left(\frac{\partial w}{\partial x}\right)^2 + \frac{1}{4}\left(\frac{\partial w}{\partial x}\right)^4, \end{aligned} \tag{5.3.2}$$

where we set $\overline{E} = E/2(1-\nu^2)$[4]. We start with expanding the displacement field in Fourier space as

$$u_x(x) = \sum_{q\in\mathcal{K}_1} \overline{u}(q)\mathbf{e}^{\imath q\cdot x} \tag{5.3.3a}$$

$$w(x) = \sum_{q\in\mathcal{K}_1} \overline{w}(q)\mathbf{e}^{\imath q\cdot x}, \tag{5.3.3b}$$

[4]From now on, we use $\overline{E}$ instead of $E/2(1-\nu^2)$

where $\mathcal{K}_1 := \{q = 2\pi\nu_x/L : \nu_x \in \mathbb{Z}, |q| \geqslant 2\pi/L\}$. The Fourier transform of the above functions can be obtained as[5]

$$\overline{u}(q) = \frac{1}{L}\int_{\mathbb{S}} u_x(x)\mathbf{e}^{-\imath q\cdot x}dx \tag{5.3.6a}$$

$$\overline{w}(q) = \frac{1}{L}\int_{\mathbb{S}} w(x)\mathbf{e}^{-\imath q\cdot x}dx. \tag{5.3.6b}$$

[5]It is worthwhile to mention that the Fourier transformation can be expressed in terms of sinusoidal functions as

$$u_x(x) = \sum_{q\in\mathcal{K}_1} a_q\cos(qx) + b_q\sin(qx). \tag{5.3.4}$$

On the other hand, given that $\overline{u}^{\mathrm{Re}}(q)$ and $\overline{u}^{\mathrm{Im}}(q)$ are the real and imaginary parts of the $\overline{u}(q)$ one can expand the complex Fourier transform as

$$\begin{aligned} u_x(x) &= \sum_{q\in\mathcal{K}_1} \overline{u}(q)\mathbf{e}^{\imath q\cdot x} \\ &= \sum_{q\in\mathcal{K}_1} (\overline{u}^{\mathrm{Re}}(q) + \mathrm{i}\overline{u}^{\mathrm{Im}}(q))(\cos(qx) + \mathrm{i}\sin(qx)) \\ &= \sum_{q\in\mathcal{K}_1} \overline{u}^{\mathrm{Re}}(q)\cos(qx) - \overline{u}^{\mathrm{Im}}(q)\sin(qx) + \mathrm{i}\sum_{q\in\mathcal{K}_1} (\overline{u}^{\mathrm{Im}}(q)\cos(qx) + \overline{u}^{\mathrm{Re}}(q)\sin(qx)), \end{aligned} \tag{5.3.5}$$

But note that for each mode q, there is a conjugate mode $-q$, for which we have: $\overline{u}^{\mathrm{Im}}(-q) = -\overline{u}^{\mathrm{Im}}(q)$, $\overline{u}^{\mathrm{Re}}(-q) = \overline{u}^{\mathrm{Re}}(q)$, $\cos(-qx) = \cos(qx)$, and $\sin(-qx) = -\sin(qx)$ which make the imaginary part of the above summation to vanish. Comparing the above summation with expansion in (5.3.4), one can readily relate the coefficients as: $a_q = \overline{u}^{\mathrm{Re}}(q)$ and $b_q = -\overline{u}^{\mathrm{Im}}(q)$. In this work, for brevity we chose to use the compact complex form as in

Substituting the above expressions into the elastic energy formulation in (5.3.2), results in[6]

$$
\begin{aligned}
U_b &= \int \frac{1}{2}\kappa_b \left(\frac{\partial^2 w}{\partial x^2}\right)^2 = \frac{L^2\kappa_b}{2}\sum_{q\in\mathcal{K}_1} q^4 |\overline{w}(q)|^2 \\
U_s &= \overline{E}\int \left(\frac{\partial u}{\partial x}\right)^2 + \frac{\partial u}{\partial x}\left(\frac{\partial w}{\partial x}\right)^2 + \frac{1}{4}\left(\frac{\partial w}{\partial x}\right)^4 \\
&= L^2\overline{E}\sum_{q\in\mathcal{K}_1} q^2\left(\overline{u}^{\mathrm{Re}}(q)^2 + \overline{u}^{\mathrm{Im}}(q)^2\right) + q\left(\overline{u}^{\mathrm{Re}}(q)\overline{A}^{\mathrm{Im}}(q) - \overline{u}^{\mathrm{Im}}(q)\overline{A}^{\mathrm{Re}}(q)\right) \\
&+ \frac{1}{4}\left(\overline{A}^{\mathrm{Re}}(q)^2 + \overline{A}^{\mathrm{Im}}(q)^2\right) \\
&= L^2\overline{E}\sum_{q\in\mathcal{K}_1}\left(q\overline{u}^{\mathrm{Re}}(q) + \frac{1}{2}\overline{A}^{\mathrm{Im}}(q)\right)^2 + \left(q\overline{u}^{\mathrm{Im}}(q) - \frac{1}{2}\overline{A}^{\mathrm{Re}}(q)\right)^2.
\end{aligned}
\tag{5.3.8}
$$

By definition, the partition function and the free energy are expressed as

$$
Z = \int \mathrm{e}^{-\beta U}\mathcal{D}[u_x, w], \qquad\qquad F = -\beta \log Z. \tag{5.3.9}
$$

The total elastic energy in (5.3.2) is anharmonic with respect to w but quadratic in terms of u_x. Though the partition function integration cannot be easily handled over w, but can

[6]Similarly, the derivatives and their corresponding integrations can be expressed in Fourier expansion as below

$$
\begin{aligned}
&\frac{\partial u_x}{\partial x} = \sum_{q\in\mathcal{K}_1} \mathrm{i}\, q\overline{u}(q)\mathbf{e}^{\imath q\cdot x}, \qquad \int\left(\frac{\partial u_x}{\partial x}\right)^2 = L^2\sum_{q\in\mathcal{K}_1} q^2|\overline{u}(q)|^2, \qquad \int\left(\frac{\partial^2 w}{\partial x^2}\right)^2 = L^2\sum_{q\in\mathcal{K}_1} q^4|\overline{w}(q)|^2 \\
&\left(\frac{\partial w}{\partial x}\right)^2 = \sum_{q\in\mathcal{K}_1}\overline{A}(q)\mathbf{e}^{\imath q\cdot x}, \qquad \int\left(\frac{\partial w}{\partial x}\right)^4 = L^2\sum_{q\in\mathcal{K}_1}|\overline{A}(q)|^2 \\
&\int \frac{\partial u_x}{\partial x}\left(\frac{\partial w}{\partial x}\right)^2 = L^2\sum_{q\in\mathcal{K}_1}\mathrm{i}\, q\overline{u}(q)\overline{A}(-q) = L^2\sum_{q\in\mathcal{K}_1}\mathrm{i}\, q(\overline{u}^{\mathrm{Re}}(q) + \mathrm{i}\,\overline{u}^{\mathrm{Im}}(q))(\overline{A}^{\mathrm{Re}}(-q) + \mathrm{i}\,\overline{A}^{\mathrm{Im}}(-q)) \\
&\quad = L^2\sum_{q\in\mathcal{K}_1}\mathrm{i}\, q(\overline{u}^{\mathrm{Re}}(q) + \mathrm{i}\,\overline{u}^{\mathrm{Im}}(q))(\overline{A}^{\mathrm{Re}}(q) - \mathrm{i}\,\overline{A}^{\mathrm{Im}}(q)) = L^2\sum_{q\in\mathcal{K}_1} q\left(\overline{u}^{\mathrm{Re}}(q)\overline{A}^{\mathrm{Im}}(q) - \overline{u}^{\mathrm{Im}}(q)\overline{A}^{\mathrm{Re}}(q)\right).
\end{aligned}
$$

The superscripts "Re" and "Im" denote the decomposition into real and imaginary parts: $X(q) = X^{\mathrm{Re}}(q) + \mathrm{i}X^{\mathrm{Im}}(q)$, with $\mathrm{i} = \sqrt{-1}$. Also note that we dropped the imaginary part of the above summation, since it vanishes by summing over conjugate modes.

be simply carried out over u_x. Thus, we start with integrating over u_x as below

$$\begin{aligned} Z &= \int \mathrm{e}^{-\beta U} \mathcal{D}[u_x, w] \\ &= \prod_{q \in \mathcal{K}_1} \int_{-\infty}^{\infty} \exp\left(-\beta(U_b + U_s)\right) d\overline{w}(q) d\overline{u}^{\mathrm{Re}}(q) d\overline{u}^{\mathrm{Im}}(q) \\ &= \prod_{q \in \mathcal{K}_1} \int \alpha(q) \exp(-\beta(U_b + U_s^{\mathrm{eff}})) d\overline{w}(q), \end{aligned} \tag{5.3.10}$$

wherein we introduced a so called *effective* strain energy, which includes the remaining term in the exponent after integrating over u_x. Also $\alpha(q)$ is a coefficient, independent of w. Note that U_b is independent of u_x. Therefore we only need to take into account U_s in the integration over u_x. Accordingly, we have

$$\begin{aligned} &\prod_{q \in \mathcal{K}_1} \int_{-\infty}^{\infty} \exp\left(-\beta U_s\right) d\overline{u}^{\mathrm{Re}}(q) d\overline{u}^{\mathrm{Im}}(q) \\ &\quad = \prod_{q \in \mathcal{K}_1} \int_{-\infty}^{\infty} \exp\left(-\beta L^2 \overline{E} \left[q\overline{u}^{\mathrm{Re}}(q) + \frac{1}{2}\overline{A}^{\mathrm{Im}}(q)\right]^2\right) d\overline{u}^{\mathrm{Re}}(q) \\ &\qquad \times \int_{-\infty}^{\infty} \exp\left(-\beta L^2 \overline{E} \left[q\overline{u}^{\mathrm{Im}}(q) - \frac{1}{2}\overline{A}^{\mathrm{Re}}(q)\right]^2\right) d\overline{u}^{\mathrm{Im}}(q). \end{aligned} \tag{5.3.11}$$

Given that $\int_{-\infty}^{\infty} \exp(-a(x+b)^2) dx = \sqrt{\pi/a}$, the integration in (5.3.11), becomes independent of $\overline{A}(q)$

$$\begin{aligned} &\prod_{q \in \mathcal{K}_1} \int_{-\infty}^{\infty} \exp\left(-\beta U_s\right) d\overline{u}^{\mathrm{Re}}(q) d\overline{u}^{\mathrm{Im}}(q) \\ &\quad = \prod_{q \in \mathcal{K}_1} \int_{-\infty}^{\infty} \exp\left(-\beta L^2 \overline{E} \left[q\overline{u}^{\mathrm{Re}}(q) + \frac{1}{2}\overline{A}^{\mathrm{Im}}(q)\right]^2\right) d\overline{u}^{\mathrm{Re}}(q) \\ &\qquad \times \int_{-\infty}^{\infty} \exp\left(-\beta L^2 \overline{E} \left[q\overline{u}^{\mathrm{Im}}(q) - \frac{1}{2}\overline{A}^{\mathrm{Re}}(q)\right]^2\right) d\overline{u}^{\mathrm{Im}}(q) \\ &= \prod_{q \in \mathcal{K}_1} \frac{\pi}{\beta L^2 \overline{E} q^2}. \end{aligned} \tag{5.3.12}$$

Hence, the partition function integration in (5.3.10) will be obtained as

$$
\begin{aligned}
Z &= \prod_{q\in\mathcal{K}_1} \int_{-\infty}^{\infty} \exp\left(-\beta(U_b+U_s)\right) d\overline{w}(q) d\overline{u}^{\mathrm{Re}}(q) d\overline{u}^{\mathrm{Im}}(q) \\
&= \prod_{q\in\mathcal{K}_1} \int \frac{\pi}{\beta L^2 \overline{E} q^2} \exp(-\frac{L^2\beta\kappa_b}{2} q^4 |\overline{w}(q)|^2) d\overline{w}(q) \\
&= \prod_{q\in\mathcal{K}_1} \frac{2\pi^2}{L^4\beta^2\overline{E}\kappa_b q^6},
\end{aligned}
\tag{5.3.13}
$$

which, despite of anharmonic term in the elastic energy formulation (5.3.2) is exactly obtainable. In other word, for the case of one dimensional deformation, the anharmonicity does not add any complexity to the partition function integration and the problem can be easily decoupled to in and out-of-plane deformation modes. In this manner, the fluctuations of the out-of-plane displacement field is exactly the same as described within harmonic approximation

$$
\langle |\overline{w}(q)|^2 \rangle = \frac{k_B T}{L^2 \kappa_b q^4}. \tag{5.3.14}
$$

In the following section, we study this problem in two dimension where the anharmonicity has indeed remarkable effects on the fluctuations.

5.4 Set up of the statistical mechanics problem in two dimensions

In this section, we aim to study the statistical mechanics of graphene, using the fully coupled and nonlinear energy formulation in (5.2.9). To this end, we need to evaluate the partition function and the free energy

$$
Z = \int \mathrm{e}^{-\beta U} \mathcal{D}[u_x, u_y, w], \qquad\qquad F = -\beta \log Z. \tag{5.4.1}
$$

Within harmonic assumption which is quit common for fluid membranes, wherein the in and out-of-plane deformations are not coupled, the partition function is easily obtained as

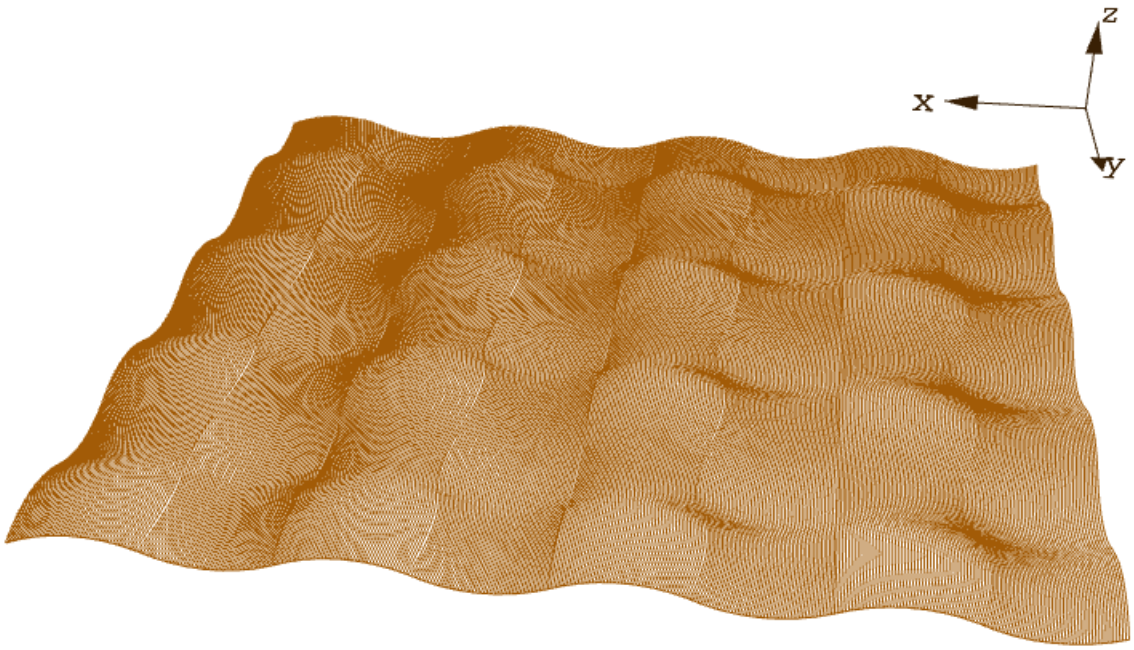

Figure 5.3.2: Deformation of graphene sheet in two dimension. The displacement field is a function of x and y; i.e. $(u_x, u_y, w) = (u_x(x,y), u_y(x,y), w(x,y))$.

a Gaussian integration and hence the fluctuations are evaluated as

$$\langle |\overline{w}(\mathbf{q})|^2 \rangle = \frac{k_B T}{L^2 \kappa_b \mathbf{q}^4}. \tag{5.4.2}$$

However, for the case of a solid membrane, it is impossible to carry out the partition function integration analytically. Our goal is to obtain a reasonable estimate of the free energy and fluctuations. Usually is it easier to analyze the partition function, within Fourier space. Accordingly, we proceed to transform the energy function into Fourier space. We start with expanding the displacement field

$$\mathbf{u}(\mathbf{x}) = \sum_{\mathbf{q}\in\mathcal{K}} \overline{\mathbf{u}}(\mathbf{q}) \mathbf{e}^{\imath \mathbf{q}\cdot\mathbf{x}} \tag{5.4.3a}$$

$$w(\mathbf{x}) = \sum_{\mathbf{q}\in\mathcal{K}} \overline{w}(\mathbf{q}) \mathbf{e}^{\imath \mathbf{q}\cdot\mathbf{x}} \tag{5.4.3b}$$

$$\frac{\partial w(\mathbf{x})}{\partial x_\gamma} \frac{\partial w(\mathbf{x})}{\partial x_\delta} = \sum_{\mathbf{q}\in\mathcal{K}} \overline{A}_{\gamma\delta}(\mathbf{q}) \mathbf{e}^{\imath \mathbf{q}\cdot\mathbf{x}}, \tag{5.4.3c}$$

where $\mathcal{K} := \{\mathbf{q} = 2\pi(\nu_x, \nu_y)/L : \nu_x, \nu_y \in \mathbb{Z}, |\mathbf{q}| \geqslant 2\pi/L\}$ and γ, δ denote x, y. Also, $\mathbf{u}(\mathbf{x}) = (u_x(\mathbf{x}), u_y(\mathbf{x}))$[7]. The Fourier transform of the above functions can be obtained as

$$\overline{\mathbf{u}}(\mathbf{q}) = \frac{1}{L^2}\int_{\mathbb{S}} \mathbf{u}(\mathbf{x})\mathbf{e}^{-\imath\mathbf{q}\cdot\mathbf{x}}d\mathbf{x} \tag{5.4.4a}$$

$$\overline{w}(\mathbf{q}) = \frac{1}{L^2}\int_{\mathbb{S}} w(\mathbf{x})\mathbf{e}^{-\imath\mathbf{q}\cdot\mathbf{x}}d\mathbf{x} \tag{5.4.4b}$$

$$\overline{A}_{\gamma\delta}(\mathbf{q}) = \frac{1}{L^2}\int_{\mathbb{S}} \frac{\partial w(\mathbf{x})}{\partial x_\gamma}\frac{\partial w(\mathbf{x})}{\partial x_\delta}\mathbf{e}^{-\imath\mathbf{q}\cdot\mathbf{x}}d\mathbf{x}. \tag{5.4.4c}$$

It is noted that these Fourier modes have real and imaginary parts; i.e. $\overline{\mathbf{u}}(\mathbf{q}) = \overline{\mathbf{u}}^{\mathrm{Re}}(\mathbf{q}) + \mathbf{i}\,\overline{\mathbf{u}}^{\mathrm{Im}}(\mathbf{q})$, in which the superscripts denote the real and imaginary parts. The corresponding conjugate of each mode is also derived as: $\overline{\mathbf{u}}^*(\mathbf{q}) = \overline{\mathbf{u}}(-\mathbf{q}) = \overline{\mathbf{u}}^{\mathrm{Re}}(\mathbf{q}) - \mathbf{i}\,\overline{\mathbf{u}}^{\mathrm{Im}}(\mathbf{q})$, where $\overline{\mathbf{u}}(\mathbf{q})\overline{\mathbf{u}}^*(\mathbf{q}) = |\overline{\mathbf{u}}(\mathbf{q})|^2$. Further, we remark the orthogonality of Fourier modes

$$\begin{aligned}\int \overline{u}_\gamma(\mathbf{q})\overline{u}_\delta(\mathbf{q}')\mathrm{e}^{i(\mathbf{q}+\mathbf{q}')\cdot\mathbf{x}}d\mathbf{x} &= \delta_{\mathbf{q},-\mathbf{q}'}\overline{u}_\gamma(\mathbf{q})\overline{u}_\delta(\mathbf{q}')L^2 \\ &= \overline{u}_\gamma(\mathbf{q})\overline{u}_\delta(-\mathbf{q})L^2.\end{aligned} \tag{5.4.5}$$

Similar arguments can be made for $\overline{A}_{\gamma\delta}(\mathbf{q})$ and $\overline{w}(\mathbf{q})$. Now we can calculate the integration of each terms in U_{h}, U_{c} and U_{anh} in Fourier space. In the following equations, we

[7]Similarly, $\overline{\mathbf{u}}(\mathbf{q}) = (\overline{u}_x(\mathbf{q}), \overline{u}_y(\mathbf{q}))$

demonstrate the details of the Fourier transformation of these terms

$$\int_{\mathbb{S}} \left(\frac{\partial u_\gamma}{\partial x_\delta}\right)^2 d\mathbf{x} = L^2 \sum_{\mathbf{q}\in\mathcal{K}} q_\delta^2 |\overline{u}_\gamma(\mathbf{q})|^2 = L^2 \sum_{\mathbf{q}\in\mathcal{K}} q_\delta^2 (\overline{u}_\gamma^{\mathrm{Re}}(\mathbf{q})^2 + \overline{u}_\gamma^{\mathrm{Im}}(\mathbf{q})^2) \tag{5.4.6a}$$

$$\int_{\mathbb{S}} \left(\frac{\partial w}{\partial x_\gamma}\frac{\partial w}{\partial x_\delta}\right) d\mathbf{x} = L^2 \sum_{\mathbf{q}\in\mathcal{K}} |\overline{A}_{\gamma\delta}(\mathbf{q})|^2 = L^2 \sum_{\mathbf{q}\in\mathcal{K}} \overline{A}_{\gamma\delta}^{\mathrm{Re}}(\mathbf{q})^2 + \overline{A}_{\gamma\delta}^{\mathrm{Im}}(\mathbf{q})^2 \tag{5.4.6b}$$

$$\begin{aligned}
\int_{\mathbb{S}} \left(\frac{\partial u_\gamma}{\partial x_\delta}\frac{\partial w}{\partial x_k}\frac{\partial w}{\partial x_l}\right) d\mathbf{x} &= L^2 \sum_{\mathbf{q}\in\mathcal{K}} \mathbf{i}\, q_\delta \overline{u}_\gamma(\mathbf{q}) \overline{A}_{kl}(-\mathbf{q}) \\
&= L^2 \sum_{\mathbf{q}\in\mathcal{K}} \mathbf{i}\, q_\delta \left(\overline{u}_\gamma^{\mathrm{Re}}(\mathbf{q}) + \mathbf{i}\, \overline{u}_\gamma^{\mathrm{Im}}(\mathbf{q})\right) \left(\overline{A}_{kl}^{\mathrm{Re}}(\mathbf{q}) - \mathbf{i}\, \overline{A}_{kl}^{\mathrm{Im}}(\mathbf{q})\right) \\
&= L^2 \sum_{\mathbf{q}\in\mathcal{K}} q_\delta \Big\{ \overline{A}_{kl}^{\mathrm{Im}}(\mathbf{q}) \overline{u}_\gamma^{\mathrm{Re}}(\mathbf{q}) - \overline{u}_\gamma^{\mathrm{Im}}(\mathbf{q}) \overline{A}_{kl}^{\mathrm{Re}}(\mathbf{q}) \\
&\qquad + \mathbf{i} \left(\overline{A}_{kl}^{\mathrm{Re}}(\mathbf{q}) \overline{u}_\gamma^{\mathrm{Re}}(\mathbf{q}) + \overline{u}_\gamma^{\mathrm{Im}}(\mathbf{q}) \overline{A}_{kl}^{\mathrm{Im}}(\mathbf{q})\right) \Big\} \\
&= L^2 \sum_{\mathbf{q}\in\mathcal{K}} q_\delta \Big\{ \overline{A}_{kl}^{\mathrm{Im}}(\mathbf{q}) \overline{u}_\gamma^{\mathrm{Re}}(\mathbf{q}) - \overline{u}_\gamma^{\mathrm{Im}}(\mathbf{q}) \overline{A}_{kl}^{\mathrm{Re}}(\mathbf{q}) \Big\}.
\end{aligned} \tag{5.4.6c}$$

Note that for each $\mathbf{q}$ mode in the summation, there is a conjugate of $-\mathbf{q}$, that makes the imaginary part of the summation in (5.4.6c) vanish

$$\begin{aligned}
&q_\delta \left(\overline{A}_{kl}^{\mathrm{Re}}(\mathbf{q}) \overline{u}_\gamma^{\mathrm{Re}}(\mathbf{q}) + \overline{u}_\gamma^{\mathrm{Im}}(\mathbf{q}) \overline{A}_{kl}^{\mathrm{Im}}(\mathbf{q})\right) + (-q_\delta) \left(\overline{A}_{kl}^{\mathrm{Re}}(-\mathbf{q}) \overline{u}_\gamma^{\mathrm{Re}}(-\mathbf{q}) + \overline{u}_\gamma^{\mathrm{Im}}(-\mathbf{q}) \overline{A}_{kl}^{\mathrm{Im}}(-\mathbf{q})\right) \\
&= q_\delta \left(\overline{A}_{kl}^{\mathrm{Re}}(\mathbf{q}) \overline{u}_\gamma^{\mathrm{Re}}(\mathbf{q}) + \overline{u}_\gamma^{\mathrm{Im}}(\mathbf{q}) \overline{A}_{kl}^{\mathrm{Im}}(\mathbf{q})\right) - q_\delta \left(\overline{A}_{kl}^{\mathrm{Re}}(\mathbf{q}) \overline{u}_\gamma^{\mathrm{Re}}(\mathbf{q}) + (-\overline{u}_\gamma^{\mathrm{Im}}(\mathbf{q}))(-\overline{A}_{kl}^{\mathrm{Im}}(\mathbf{q}))\right) \\
&= 0.
\end{aligned} \tag{5.4.7}$$

Since, there will not be any contribution from the imaginary parts of the summations, to the free energy, in the remaining of this paper, we take them out from our calculations.

Substituting the Fourier expansions in the expression for U_{h}, U_{c}, and U_{anh}, results in the following

$$\int U_{\mathrm{h}} d\mathbf{x} = \frac{L^2}{2} \sum_{\mathbf{q}\in\mathcal{K}} \kappa_b \mathbf{q}^4 |\overline{w}(\mathbf{q})|^2 + \frac{E}{1-\nu^2} \left(\mathbf{q}^2 |\overline{\mathbf{u}}(\mathbf{q})|^2 + 2\nu q_x \overline{u}_x(\mathbf{q}) q_y \overline{u}_y(\mathbf{q}) \right)$$
$$+ \frac{E}{1+\nu} \left(q_y^2 |\overline{u}_x(\mathbf{q})|^2 + q_x^2 |\overline{u}_y(\mathbf{q})|^2 - 2 q_x q_y \overline{u}_x(\mathbf{q}) \overline{u}_y(-\mathbf{q}) \right)$$
$$= \frac{L^2}{2} \sum_{\mathbf{q}\in\mathcal{K}} \overline{U}_{\mathrm{h}}(\mathbf{q}), \tag{5.4.8a}$$

$$\int U_{\mathrm{c}} d\mathbf{x} = \frac{L^2}{2} \sum_{\mathbf{q}\in\mathcal{K}} \frac{E}{1-\nu^2} \Big\{ \overline{A}_{xx}^{\mathrm{Re}}(\mathbf{q}) (q_x \overline{u}_x^{\mathrm{Im}}(\mathbf{q}) + \nu q_y \overline{u}_y^{\mathrm{Im}}(\mathbf{q})) + \overline{A}_{yy}^{\mathrm{Re}}(\mathbf{q}) (q_y \overline{u}_y^{\mathrm{Im}}(\mathbf{q}) + \nu q_x \overline{u}_x^{\mathrm{Im}}(\mathbf{q}))$$
$$- \overline{A}_{xx}^{\mathrm{Im}}(\mathbf{q}) (q_x \overline{u}_x^{\mathrm{Re}}(\mathbf{q}) + \nu q_y \overline{u}_y^{\mathrm{Re}}(\mathbf{q})) - \overline{A}_{yy}^{\mathrm{Im}}(\mathbf{q}) (q_y \overline{u}_y^{\mathrm{Re}}(\mathbf{q}) + \nu q_x \overline{u}_x^{\mathrm{Re}}(\mathbf{q})) \Big\}$$
$$+ \frac{E}{1+\nu} \Big\{ \overline{A}_{xy}^{\mathrm{Re}}(\mathbf{q}) (q_y \overline{u}_x^{\mathrm{Im}}(\mathbf{q}) + q_x \overline{u}_y^{\mathrm{Im}}(\mathbf{q})) - \overline{A}_{xy}^{\mathrm{Im}}(\mathbf{q}) (q_y \overline{u}_x^{\mathrm{Re}}(\mathbf{q}) + q_x \overline{u}_y^{\mathrm{Re}}(\mathbf{q})) \Big\}$$
$$= \frac{L^2}{2} \sum_{\mathbf{q}\in\mathcal{K}} \overline{U}_{\mathrm{c}}(\mathbf{q}), \tag{5.4.8b}$$

$$\int U_{\mathrm{anh}} d\mathbf{x} = \frac{L^2}{8} \sum_{\mathbf{q}\in\mathcal{K}} \frac{E}{1-\nu^2} \left(|\overline{A}_{xx}(\mathbf{q})|^2 + |\overline{A}_{yy}(\mathbf{q})|^2 + 2|\overline{A}_{xy}(\mathbf{q})|^2 \right)$$
$$= \frac{L^2}{2} \sum_{\mathbf{q}\in\mathcal{K}} \overline{U}_{\mathrm{anh}}(\mathbf{q}), \tag{5.4.8c}$$

wherein we dropped all the imaginary parts of the summations.

Note that the total elastic energy is harmonic w.r.t the in-plane displacement field. Therefore, using the expression of the total elastic energy in Fourier space, we can proceed to evaluate the partition function integration over the in-plane displacement field

$$
\begin{aligned}
Z &= \int \exp(-\beta U)\mathcal{D}[w,\mathbf{u}] \\
&= \prod_{\mathbf{q}\in\mathcal{K}} \int_{-\infty}^{\infty} \exp\left(-\frac{\beta L^2}{2}\sum_{\mathbf{q}\in\mathcal{K}}(\overline{U}_{\mathrm{h}}(\mathbf{q})+\overline{U}_{\mathrm{c}}(\mathbf{q})+\overline{U}_{\mathrm{anh}}(\mathbf{q}))\right) d\overline{w}(\mathbf{q}) d\overline{u}_x^{\mathrm{Re}}(\mathbf{q}) d\overline{u}_x^{\mathrm{Im}}(\mathbf{q}) d\overline{u}_y^{\mathrm{Re}}(\mathbf{q}) d\overline{u}_y^{\mathrm{Im}}(\mathbf{q}) \\
&= \prod_{\mathbf{q}\in\mathcal{K}} \int \alpha(\mathbf{q}) \exp(-\beta(U_b + U_s^{\mathrm{eff}})) d\overline{w}(\mathbf{q}),
\end{aligned}
\tag{5.4.9}
$$

wherein we integrate out the in-plane displacement fields u_x and u_y. The remaining terms are expressed as the effective strain energy, which is a function of solely out-of-plane displacement. In this manner we have renormalized the partition function, which should be integrated over the out-of-plane field. The effective strain energy, which consists of the remaining terms after integrating out the in-plane fields, can be expressed as

$$
U_s^{\mathrm{eff}} = \frac{1}{8} EL^2 \sum_{\mathbf{q}\in\mathcal{K}} \Psi(\mathbf{q})\Psi^*(\mathbf{q}), \tag{5.4.10}
$$

in which, for ease of notation, we have defined $\Psi(\mathbf{q})$ as

$$
\Psi(\mathbf{q}) = \frac{1}{\mathbf{q}^2}\left\{ q_y^2 \overline{A}_{xx}(\mathbf{q}) + q_x^2 \overline{A}_{yy}(\mathbf{q}) - 2q_x q_y \overline{A}_{xy}(\mathbf{q}) \right\}. \tag{5.4.11}
$$

Furthermore, one can express the strain energy using the transverse projector operator—

which has been widely used in elastic problems by the physics community—as below[8]

$$\Psi(\mathbf{q}) = P_{ij}^T(\mathbf{q})\overline{A}_{ij}(\mathbf{q}), \tag{5.4.12}$$

in which

$$P_{ij}^T(\mathbf{q}) = \delta_{ij} - \frac{q_i q_j}{\mathbf{q}^2}. \tag{5.4.13}$$

Also, the elastic energy due to the pre-existing strain field is a constant and independent of the fluctuations, and hence can be taken out of the calculations. Accordingly, the total effective elastic energy in Fourier space can be written as

$$\begin{aligned} U^{\text{eff}} &= U_b + U_s^{\text{eff}} \\ &= \frac{1}{2}\kappa_b L^2 \sum_{\mathbf{q}\in\mathcal{K}} \mathbf{q}^4 w(\mathbf{q})^2 + \frac{E\varepsilon_0}{2(1-\nu)} L^2 \sum_{\mathbf{q}\in\mathcal{K}} \mathbf{q}^2 |\overline{w}(\mathbf{q})|^2 + \frac{E\varepsilon_0^2}{1-\nu} \\ &\qquad + \frac{1}{2} E L^2 \sum_{\mathbf{q}\in\mathcal{K}} \left\{ |\frac{1}{2} P_{ij}^T(\mathbf{q}) A_{ij}(\mathbf{q})|^2 \right\}. \end{aligned} \tag{5.4.14}$$

The above expression when $\varepsilon_0 = 0$ has been derived earlier by Nelson and Peliti ([132]). The term $E\varepsilon_0^2/(1-\nu)$ is a constant and has no consequences on the fluctuations of the displacement field and hence from now on will be disregarded in the calculations. Up to this point, we have decoupled the problem by integrating the in-plane displacement field. We are now left with a nonlinear energy formulation which is a function of only out-of-plane displacement w. In the following section we use the above energy formulation to study the fluctuations of w.

[8] Note that $\Psi(\mathbf{q})\Psi^*(\mathbf{q}) = \Psi(\mathbf{q})\Psi(-\mathbf{q}) = |\Psi(\mathbf{q})|^2$ and is expanded as below

$$\begin{aligned} \Psi(\mathbf{q})\Psi(-\mathbf{q}) &= |\Psi(\mathbf{q})|^2 \\ &= \frac{1}{(q_x^2+q_y^2)^2} \Big\{ q_x^4 \overline{A}_{yy}^{\text{Re}}(\mathbf{q})^2 + q_x^4 \overline{A}_{yy}^{\text{Im}}(\mathbf{q})^2 + q_y^4 \overline{A}_{xx}^{\text{Re}}(\mathbf{q})^2 + q_y^4 \overline{A}_{xx}^{\text{Im}}(\mathbf{q})^2 - 4q_x q_y^3 \overline{A}_{xx}^{\text{Im}}(\mathbf{q}) \overline{A}_{xy}^{\text{Im}}(\mathbf{q}) \\ &+ 2q_x^2 q_y^2 \overline{A}_{xx}^{\text{Im}}(\mathbf{q}) \overline{A}_{yy}^{\text{Im}}(\mathbf{q}) - 4q_x^3 q_y \overline{A}_{xy}^{\text{Im}}(\mathbf{q}) \overline{A}_{yy}^{\text{Im}}(\mathbf{q}) + 4q_x^2 q_y^2 \overline{A}_{xy}^{\text{Im}}(\mathbf{q})^2 + q_x^4 \overline{A}_{yy}^{\text{Im}}(\mathbf{q})^2 + q_y^4 \overline{A}_{xx}^{\text{Im}}(\mathbf{q})^2 \\ &- 4q_x q_y^3 \overline{A}_{xx}^{\text{Re}}(\mathbf{q}) \overline{A}_{xy}^{\text{Re}}(\mathbf{q}) + 2q_x^2 q_y^2 \overline{A}_{xx}^{\text{Re}}(\mathbf{q}) \overline{A}_{yy}^{\text{Re}}(\mathbf{q}) - 4q_x^3 q_y \overline{A}_{xy}^{\text{Re}}(\mathbf{q}) \overline{A}_{yy}^{\text{Re}}(\mathbf{q}) + 4q_x^2 q_y^2 \overline{A}_{xy}^{\text{Re}}(\mathbf{q})^2 \Big\}. \end{aligned}$$

5.5 Effective Bending Stiffness

In this section, we study the fluctuations of the out-of-plane displacement field, and in particular, the effective stiffness of a solid membrane, using the nonlinear energy formulation (5.4.14). The idea is that one can capture the effects of nonlinearities in a so-called *renormalized* bending stiffness, that can be employed to a quadratic Hamiltonian. Let $H_{\rm q}$ and $H_{\rm nq}$ be the quadratic and non-quadratic parts of the total energy H, respectively. Then

$$H = H_{\rm q} + H_{\rm nq} := \sum_{\mathbf{k}\in\mathcal{K}} \frac{1}{2}\kappa^{\rm eff}(\mathbf{k})\mathbf{k}^4|\overline{w}(\mathbf{k})|^2, \tag{5.5.1}$$

where we introduced a form of $\mathbf{k}$ dependency for the effective rigidity, $\kappa^{\rm eff}(\mathbf{k})$. Note that within linearized formulations, the bending rigidity κ_b, is constant for all fluctuations modes and results in a $1/|\mathbf{k}|^4$ dependence of the out-of-plane undulations. However, in the presence of pre-strain term or the nonlinear in-plane strain, the fluctuations are described in a general form as

$$\langle|\overline{w}(\mathbf{k})|^2\rangle \sim (\sum_i \alpha_i|\mathbf{k}|^{\xi_i})^{-1} = \frac{1}{\alpha_1|\mathbf{k}|^{\xi_1} + \alpha_2|\mathbf{k}|^{\xi_2} + \alpha_3|\mathbf{k}|^{\xi_3} + \alpha_4|\mathbf{k}|^{\xi_4} + \cdots}, \tag{5.5.2}$$

where ξ_i are not necessarily integers. Note that in this case, the dominant modes of the fluctuations are the long wave-length modes, where $\mathbf{k} \to 0$. Therefore, the term with smaller exponents ξ_i in the denominator of (5.5.2) will be the leading term in the summation. Accordingly, one can *approximately* describe the fluctuations in terms of the leading term as: $\langle\overline{w}(\mathbf{k})^2\rangle \sim 1/\mathbf{k}^\zeta$, with ζ being the smallest exponent in the denominator (5.5.2). In this manner, the effective bending stiffness can be defined from the fluctuations as: $\kappa^{\rm eff}(\mathbf{k}) \sim \mathbf{k}^{\zeta-4}$. From now on, we set $\eta = 4 - \zeta \geqslant 0$ and our goal will be to get an estimate of η.

We start with the regular perturbation approach in the following subsection. Afterward, we improve the resulting effective bending stiffness, using a Variational perturbation method in the second part of this section.

5.5.1 Perturbation approximation

Consider a nonlinear Hamiltonian $H = H_0 + H_p$, where H_0 is its quadratic functional and H_p is its nonlinear part. The idea is that the nonlinear part is a small perturbation compared to the quadratic functional H_0. Let F, be the free energy of the system. In the absence of the nonlinear perturbation term H_p, the partition function Z_0 and free energy F_0 can be easily obtained using standard Gaussian integrations. The effect of the nonlinear term on the total free energy of the system, can be then estimated by a perturbation expansion around F_0. We start with expanding the partition function of the system Z

$$Z = \int \exp(-\beta(H_0 + H_p))\mathcal{D}[w] = Z_0\langle \exp(-\beta H_p)\rangle_{H_0}, \tag{5.5.3}$$

wherein the subscript $\langle\cdot\rangle_{H_0}$ denotes average value, with respect to H_0. The exponential term in the above equation can be expanded in a Taylor series as

$$\exp(-\beta H_p) = 1 - \beta H_p + \frac{1}{2}(\beta H_p)^2 + \cdots = \sum_{n=0}^{\infty} \frac{(-\beta H_p)^n}{n!}. \tag{5.5.4}$$

Then the free energy of the system is obtained as

$$F = -\frac{1}{\beta}\log Z = F_0 - \frac{1}{\beta}\log(1 + \sum_{n=1}^{\infty} \frac{\langle(-\beta H_p)^n\rangle_{H_0}}{n!}). \tag{5.5.5}$$

Expanding the logarithm term we have

$$\log\left(\sum_{n=0}^{\infty} \frac{(-\beta)^n\langle H_P^n\rangle_{H_0}}{n!}\right) = \left(\sum_{n=1}^{\infty} \frac{(-\beta)^n\langle H_P^n\rangle_{H_0}}{n!}\right) - \frac{1}{2}\left(\sum_{n=1} \frac{(-\beta)^n\langle H_P^n\rangle_{H_0}}{n!}\right)^2 + \cdots, \tag{5.5.6}$$

and hence, the free energy expansion is derived as

$$F = F_0 - \frac{1}{\beta}\sum_{n=1}^{\infty} \frac{(-\beta)^n}{n!}\langle H_P^n\rangle_{H_0}^c, \tag{5.5.7}$$

where the superscript $\langle\cdot\rangle^c$ denotes the cumulant averages[9]. The infinite series in the above equation, gives us the exact average amount of energy that the nonlinear term is adding to the system. In practice, however, one need to truncate the series to some finite order. If the nonlinear term is small, one can expect to achieve a reasonable estimate by evaluating the first few terms of perturbation expansion (5.5.7). In the following of this section we use this notion to obtain an estimate of the excess energy that is added to the system due to nonlinearity. The excess free energy, can be then captured in terms of the effective bending stiffness. The average energy of the system with nonlinear Hamiltonian in (5.4.14), up to first order is

$$\begin{aligned}\langle H\rangle &= \left\langle \frac{1}{2}\kappa_b L^2 \sum_{\mathbf{k}\in\mathcal{K}} \mathbf{k}^4 |\overline{w}(\mathbf{k})|^2 + \frac{E\varepsilon_0}{2(1-\nu)} L^2 \sum_{\mathbf{k}\in\mathcal{K}} \mathbf{k}^2 |\overline{w}(\mathbf{k})|^2 \right\rangle_{H_0} + \left\langle \frac{1}{2} E L^2 \sum_{\mathbf{q}\in\mathcal{K}} |\frac{1}{2} P^T_{ij}(\mathbf{q}) \overline{A}_{ij}(\mathbf{q})|^2 \right\rangle_{H_0} \\ &:= \frac{L^2}{2} \sum_{\mathbf{k}\in\mathcal{K}} \kappa_{\text{eff}}(\mathbf{k})\ \mathbf{k}^4 \langle |\overline{w}(\mathbf{k})|^2 \rangle_{H_0}. \end{aligned} \tag{5.5.9}$$

To calculate the averages in (5.5.9), we start by expanding the out-of-plane displacement field in Fourier space

$$w(\mathbf{x}) = \sum_{\mathbf{k}\in\mathcal{K}} \overline{w}(\mathbf{k}) \mathrm{e}^{\mathrm{i}\mathbf{k}\cdot\mathbf{x}} \tag{5.5.10a}$$

$$\begin{aligned}\frac{\partial w}{\partial x_i}\frac{\partial w}{\partial x_j} &= \sum_{\mathbf{k},\mathbf{k}'\in\mathcal{K}} -k_i k'_j \overline{w}(\mathbf{k})\overline{w}(\mathbf{k}') \mathrm{e}^{\mathrm{i}(\mathbf{k}+\mathbf{k}')\cdot\mathbf{x}} \\ &= \sum_{\mathbf{k},\mathbf{q}\in\mathcal{K}} -k_i(q_j-k_j)\overline{w}(\mathbf{k})\overline{w}(\mathbf{q}-\mathbf{k}) \mathrm{e}^{\mathrm{i}\mathbf{q}\cdot\mathbf{x}} = \sum_{\mathbf{q}\in\mathcal{K}} \overline{A}_{ij}(\mathbf{q}) \mathrm{e}^{\mathrm{i}\mathbf{q}\cdot\mathbf{x}}, \end{aligned} \tag{5.5.10b}$$

in which

$$\overline{A}_{ij}(\mathbf{q}) = \sum_{\mathbf{k}\in\mathcal{K}} -k_i(q_j-k_j)\overline{w}(\mathbf{k})\overline{w}(\mathbf{q}-\mathbf{k}). \tag{5.5.11}$$

[9]The cumulant averages, up to fourth order are derived as below

$$\begin{aligned}&\langle H_P\rangle^c_{H_0} = \langle H_P\rangle_{H_0} \\ &\langle H_P^2\rangle^c_{H_0} = \langle H_P^2\rangle_{H_0} - \langle H_P\rangle^2_{H_0} \\ &\langle H_P^3\rangle^c_{H_0} = \langle H_P^3\rangle_{H_0} - 3\langle H_P^2\rangle_{H_0}\langle H_P\rangle_{H_0} + 2\langle H_P\rangle^3_{H_0} \\ &\langle H_P^4\rangle^c_{H_0} = \langle H_P^4\rangle_{H_0} - 3\langle H_P^3\rangle_{H_0}\langle H_P\rangle_{H_0} - 3\langle H_P^2\rangle^2_{H_0} + 12\langle H_P^2\rangle_{H_0}\langle H_P\rangle^2_{H_0} - 6\langle H_P\rangle^4_{H_0}. \end{aligned} \tag{5.5.8}$$

In the next step, we combine the above expressions with operator $P_{ij}(\mathbf{q})$

$$P^T_{ij}(\mathbf{q})\overline{A}_{ij}(\mathbf{q}) = \sum_{\mathbf{k}\in\mathcal{K}} \left(-k_i(q_i-k_i) + \frac{k_i q_i q_j (q_j - k_j)}{\mathbf{q}^2}\right) \overline{w}(\mathbf{k})\overline{w}(\mathbf{q}-\mathbf{k})$$
$$= \sum_{\mathbf{k}\in\mathcal{K}} \frac{\mathbf{k}^2\mathbf{q}^2 - (\mathbf{k}\cdot\mathbf{q})^2}{\mathbf{q}^2}\overline{w}(\mathbf{k})\overline{w}(\mathbf{q}-\mathbf{k}) = \sum_{\mathbf{k}\in\mathcal{K}} \Omega(\mathbf{q},\mathbf{k})\overline{w}(\mathbf{k})\overline{w}(\mathbf{q}-\mathbf{k}). \quad (5.5.12)$$

Finally, we calculate the magnitude of the above expressions in each mode

$$|P^T_{ij}(\mathbf{q})\overline{A}_{ij}(\mathbf{q})|^2 = \left(P^T_{ij}(\mathbf{q})\overline{A}_{ij}(\mathbf{q})\right) \times \left(P^T_{ij}(-\mathbf{q})\overline{A}_{ij}(-\mathbf{q})\right)$$
$$= \sum_{\mathbf{k},\mathbf{k}'\in\mathcal{K}} \Omega(\mathbf{q},\mathbf{k})\Omega(-\mathbf{q},\mathbf{k}')\overline{w}(\mathbf{k})\overline{w}(\mathbf{q}-\mathbf{k})\overline{w}(\mathbf{k}')\overline{w}(-\mathbf{q}-\mathbf{k}'). \quad (5.5.13)$$

The first term in the above expression is a constant and does not contribute to the fluctuations of w. Further, the last term is a harmonic term and can be included in the quadratic part of the total elastic energy.

Now, we proceed to calculate the average of the expression in (5.5.13). Note that the averaging is carried out with respect to the quadratic part of the elastic energy that in the presence of a nonzero uniform strain field along x and y directions is

$$H_0 = \frac{L^2}{2}\sum_{\mathbf{k}\in\mathcal{K}} (\kappa_b \mathbf{k}^4 + \frac{E\varepsilon_0}{(1-\nu)}\mathbf{k}^2)|\overline{w}(\mathbf{k})|^2. \quad (5.5.14)$$

Using the above Hamiltonian, we proceed to calculate the following average

$$\sum_{\mathbf{q}\in\mathcal{K}} \langle |P^T_{ij}(\mathbf{q})A_{ij}(\mathbf{q})|^2\rangle_{H_0} = \sum_{\mathbf{q},\mathbf{k},\mathbf{k}'\in\mathcal{K}} \Omega(\mathbf{q},\mathbf{k})\Omega(-\mathbf{q},\mathbf{k}') \left\langle \overline{w}(\mathbf{k})\overline{w}(\mathbf{q}-\mathbf{k})\overline{w}(\mathbf{k}')\overline{w}(-\mathbf{q}-\mathbf{k}')\right\rangle_{H_0}. \quad (5.5.15)$$

From Wick's theorem, the above average —with respect to the *quadratic* Hamiltonian

(5.5.14)— is nonzero only when the modes $\mathbf{k}_i$ are decoupled and that is

$$\begin{aligned}\langle \overline{w}(\mathbf{k}_1)\overline{w}(\mathbf{k}_2)\overline{w}(\mathbf{k}_3)\overline{w}(\mathbf{k}_4)\rangle_{H_0} = \langle|\overline{w}(\mathbf{k}_1)|^2\rangle_{H_0}\langle|\overline{w}(\mathbf{k}_2)|^2\rangle_{H_0}\Big\{&\delta(\mathbf{k}_1,-\mathbf{k}_3)\delta(\mathbf{k}_2,-\mathbf{k}_4)\\ &+\delta(\mathbf{k}_1,-\mathbf{k}_4)\delta(\mathbf{k}_2,-\mathbf{k}_3)\Big\}\\ &+\langle|\overline{w}(\mathbf{k}_1)|^2\rangle_{H_0}\langle|\overline{w}(\mathbf{k}_3)|^2\rangle_{H_0}\delta(\mathbf{k}_1,-\mathbf{k}_2)\delta(\mathbf{k}_3,-\mathbf{k}_4). \qquad (5.5.16)\end{aligned}$$

Note that the case $\mathbf{k} = -\mathbf{q}+\mathbf{k}$ is true only in zeroth mode when $\mathbf{q}\to 0$. The only nonzero case for all modes is when $\mathbf{k} = -\mathbf{k}'$. Hence, the summation in (5.5.15) can be obtained as

$$\sum_{\mathbf{q}\in\mathcal{K}}\langle|P^T_{ij}(\mathbf{q})\overline{A}_{ij}(\mathbf{q})|^2\rangle_{H_0} = \sum_{\mathbf{q},\mathbf{k}\in\mathcal{K}}\Omega(\mathbf{q},\mathbf{k})^2\langle|\overline{w}(\mathbf{k})|^2\rangle_{H_0}\langle|\overline{w}(\mathbf{q}-\mathbf{k})|^2\rangle_{H_0}. \qquad (5.5.17)$$

Now, substituting the averages of quadratic term in (5.5.14), as well as the non-quadratic part in (5.5.17), into the Equation (5.5.9), one can obtain the first order estimate of the effective stiffness as below

$$\begin{aligned}\langle H\rangle &= \frac{L^2}{2}\sum_{\mathbf{k}\in\mathcal{K}}\left(\kappa_b\mathbf{k}^4+\frac{E\varepsilon_0}{(1-\nu)}\mathbf{k}^2+\frac{E}{4}\sum_{\mathbf{q}\in\mathcal{K}}\Omega(\mathbf{q},\mathbf{k})^2\langle|\overline{w}(\mathbf{q}-\mathbf{k})|^2\rangle_{H_0}\right)\langle|\overline{w}(\mathbf{k})|^2\rangle_{H_0}\\ &:= \frac{L^2}{2}\sum_{\mathbf{k}\in\mathcal{K}}\kappa^{\text{eff}}(\mathbf{k})\mathbf{k}^4\langle|\overline{w}(\mathbf{k})|^2\rangle_{H_0}, \qquad (5.5.18)\end{aligned}$$

from which, the effective stiffness, is evaluated as

$$\kappa^{\text{eff}}(\mathbf{k}) = \kappa_b+\frac{E\varepsilon_0}{(1-\nu)\mathbf{k}^2}+\frac{1}{4}k_BTE\sum_{\mathbf{q}\in\mathcal{K}}\frac{\Omega(\mathbf{q},\mathbf{k})^2}{|\mathbf{k}|^4(\kappa_b|\mathbf{q}-\mathbf{k}|^4+E\varepsilon_0|\mathbf{q}-\mathbf{k}|^2/(1-\nu))}. \qquad (5.5.19)$$

In what follows, we analyze the above expression for two cases of zero and non-zero pre-strain field ε_0.

Case I: $\varepsilon_0 \neq 0$

Our goal is to find the dominant factor in (5.5.19). To this end, we seek for the $\mathbf{k}$ dependency of the last term in (5.5.19). In the long wave-length as $\mathbf{k} \to 0$— which is the leading mode in the summation—, the numerator varies as $(\mathbf{k}^2\mathbf{q}^2 - (\mathbf{k}\cdot\mathbf{q})^2)^2 \sim \mathbf{k}^4\mathbf{q}^4$, while the denominator varies as $\left(\kappa_b|\mathbf{q}-\mathbf{k}|^4 + E\varepsilon_0|\mathbf{q}-\mathbf{k}|^2/(1-\nu)\right)|\mathbf{q}|^4|\mathbf{k}|^4 \sim |\mathbf{q}|^4|\mathbf{k}|^4 E\varepsilon_0|\mathbf{q}-\mathbf{k}|^2/(1-\nu)$. Thus, the dominant term of the whole fraction in the summation is proportional to

$$\frac{(\mathbf{k}^2\mathbf{q}^2 - (\mathbf{k}\cdot\mathbf{q})^2)^2}{\left(\kappa_b|\mathbf{q}-\mathbf{k}|^4 + E\varepsilon_0|\mathbf{q}-\mathbf{k}|^2/(1-\nu)\right)|\mathbf{q}|^4|\mathbf{k}|^4} \sim \frac{1}{E\varepsilon_0|\mathbf{q}-\mathbf{k}|^2/(1-\nu)}. \tag{5.5.20}$$

Carrying out the summation of the above expression over $\mathbf{q}$[10], results in a constant that is independent of $\mathbf{k}$. Accordingly, the dominant term in the expression (5.5.19) will be $E\varepsilon_0/\mathbf{k}^2$ and the effective stiffness can be expressed as

$$\kappa^{\text{eff}}(\mathbf{k}) \sim \kappa_b + \frac{E\varepsilon_0}{(1-\nu)\mathbf{k}^2} + \text{Const.}, \tag{5.5.21}$$

from which the fluctuations are obtained as

$$\langle w^2 \rangle \sim \frac{k_B T}{E\varepsilon_0} \log(1 + \frac{E\varepsilon_0 L^2}{2\pi^2(\kappa_b + \alpha)}), \tag{5.5.22}$$

where α is the constant in (5.5.21). It is noted that the above result is *qualitatively* the same as what is obtained using the linearized energy formulation.

[10]The summation can be carried out using a double integration, or alternatively in polar coordinate with varying radius of $q = |\mathbf{q}|$.

Case II: $\varepsilon_0 = 0$

When the in-plane pre-strain term is zero, the expression for the effective bending stiffness in (5.5.19) reduces to

$$\kappa^{\text{eff}}(\mathbf{k}) = \kappa_b + \frac{1}{4} k_B T E \sum_{\mathbf{q}\in\mathcal{K}} \frac{\Omega(\mathbf{q},\mathbf{k})^2}{|\mathbf{k}|^4 \kappa_b |\mathbf{q}-\mathbf{k}|^4}. \tag{5.5.23}$$

Using similar scaling arguments, one can readily show that the fraction in the above summation is proportional to

$$\frac{(\mathbf{k}^2\mathbf{q}^2 - (\mathbf{k}\cdot\mathbf{q})^2)^2}{\kappa_b |\mathbf{q}-\mathbf{k}|^4 |\mathbf{q}|^4 |\mathbf{k}|^4} \sim \frac{1}{\kappa_b |\mathbf{q}-\mathbf{k}|^4}, \tag{5.5.24}$$

and consequently, when the summation is carried out over $\mathbf{k}'$, the resulting leading order is obtained as: $\sum_{\mathbf{q}\in\mathcal{K}} |\mathbf{q}-\mathbf{k}|^{-4} \sim |\mathbf{k}|^{-2}$. Therefore, the effective stiffness for this case can be written as

$$\kappa^{\text{eff}}(\mathbf{k}) = \kappa_b + \frac{\alpha' k_B T E}{\kappa_b |\mathbf{k}|^2}, \tag{5.5.25}$$

in which α' is the correction factor. The fluctuation is then obtained as

$$\langle w^2 \rangle \sim \frac{\kappa_b}{\alpha' E} \log(1 + \frac{\alpha' k_B T E L^2}{4\pi^2 \kappa_b^2}). \tag{5.5.26}$$

The results in (5.5.21) and (5.5.25) are first order estimations from perturbation expansion and might be reasonably accurate for low temperatures. In the following, we will use a variational perturbation approach to improve our predictions on effective stiffness and the out-of-plane fluctuations.

5.5.2 Variational perturbation approximation

We intend to improve our results, obtained in the preceding part, using variational perturbation method. This has not been well-appreciated yet, that with a slight modification of the conventional perturbation method, one can achieve remarkable enhancement of estima-

tions. In the following, as this method is employed, we explain the details of the procedure. We start with adding and subtracting a trial Hamiltonian to the nonlinear energy formulation in (5.4.14). In order to describe the bending mode fluctuations, lets consider the trial Hamiltonian as

$$\mathcal{H}_0 = \frac{1}{2}L^2 \sum_{\mathbf{k}\in\mathcal{K}} \kappa^{\text{eff}}(\mathbf{k})\mathbf{k}^4 |w_{\mathbf{k}}|^2. \tag{5.5.27}$$

Then the total elastic energy can be written as

$$U_b + U_s^{\text{eff}} = \mathcal{H}_0 + (U_b + U_s^{\text{eff}} - \mathcal{H}_0). \tag{5.5.28}$$

Now consider the perturbation expansion of the free energy associated with the above Hamiltonian

$$F_\infty = F_0 - \frac{1}{\beta}\sum_{N=1}^{\infty} \frac{(-\beta)^N}{N!} \langle \Big[U_b + U_s^{\text{eff}} - \mathcal{H}_0\Big]^N \rangle_{\mathcal{H}_0}^c, \tag{5.5.29}$$

wherein F_0 is the free energy corresponding to the trial Hamiltonian $\mathcal{H}_0$, and the superscript c denotes the cumulant averages. Needless to say that the full expansion as $N \to \infty$ is independent of the choice of the trial Hamiltonian. In practice, however, the series is truncated up to a finite order M to obtain an estimate of the free energy. Unlike the infinite series expansion in Equation (5.5.29), the truncated series F_M *does* depend on the choice of the trial Hamiltonian $\mathcal{H}_0$. Accordingly, in order to obtain an optimized estimate, we need to minimize the *sensitivity* of the truncated series to the trial Hamiltonian. To this end, we set ([136])

$$\frac{\partial F_M}{\partial \kappa^{\text{eff}}(\mathbf{k})} := 0. \tag{5.5.30}$$

In a rather good approximation, the result for the truncated series of the variational free energy from this method will converge i.e. $F_M \approx F_{M+1}$ and achieves its minimal sensitivity

to the trial function. We remark that restricting calculations to first order in the truncated series yields just the well-known *Bogoliubov theorem* [8] for the upper bound of the exact free energy

$$F_{\text{var}} \leqslant F_0 + \langle U_b + U_s^{\text{eff}} - \mathcal{H}_0 \rangle_{\mathcal{H}_0}. \tag{5.5.31}$$

In what follows, we will use this approach up to first order to obtain a closed form estimation of the effective stiffness of the system.

We proceed to calculate the expectation values in the right hand side of the equation (5.5.29) up to first order.

$$\begin{aligned}\langle U_b \rangle_{\mathcal{H}_0} + \langle U_s^{\text{eff}} \rangle_{\mathcal{H}_0} = L^2 \sum_{\mathbf{k}\in\mathcal{K}} \Bigg\{ & \frac{\kappa_b}{2\beta\kappa^{\text{eff}}(\mathbf{k})} + \frac{E\varepsilon_0}{2\beta(1-\nu)\kappa^{\text{eff}}(\mathbf{k})|\mathbf{k}|^2} \\ & + E \sum_{\mathbf{q}\in\mathcal{K}} \frac{\Omega(\mathbf{q},\mathbf{k})^2}{8\beta^2|\mathbf{k}|^4|\mathbf{q}-\mathbf{k}|^4\kappa^{\text{eff}}(\mathbf{k})\kappa^{\text{eff}}(\mathbf{q}-\mathbf{k})} \Bigg\}.\end{aligned} \tag{5.5.32}$$

Then substituting all the terms results in the following form for the variational free energy

$$\begin{aligned}F_{\text{var}} = C_{\text{F}} + L^2 \sum_{\mathbf{k}\in\mathcal{K}} \Bigg\{ & \frac{1}{2\beta}\log(\kappa^{\text{eff}}(\mathbf{k})) + \frac{\kappa_b}{2\beta\kappa^{\text{eff}}(\mathbf{k})} + \frac{E\varepsilon_0}{2\beta(1-\nu)\kappa^{\text{eff}}(\mathbf{k})|\mathbf{k}|^2} \\ & + E \sum_{\mathbf{q}\in\mathcal{K}} \frac{\Omega(\mathbf{q},\mathbf{k})^2}{8\beta^2|\mathbf{k}|^4|\mathbf{q}-\mathbf{k}|^4\kappa^{\text{eff}}(\mathbf{k})\kappa^{\text{eff}}(\mathbf{q}-\mathbf{k})} \Bigg\},\end{aligned} \tag{5.5.33}$$

in which C_{F} is a constant of no consequences. In the next step we take the derivatives of the above variational free energy with respect to the variational parameter $\kappa_{\text{eff}}(\mathbf{k})$.

$$\frac{\partial F_{\text{var}}}{\partial \kappa^{\text{eff}}(\mathbf{k})} := 0$$

$$0 := \sum_{\mathbf{k}\in\mathcal{K}} \Bigg\{ \frac{1}{2\beta\kappa^{\text{eff}}(\mathbf{k})} - \frac{\kappa_b}{2\beta\kappa^{\text{eff}}(\mathbf{k})^2} - \frac{E\varepsilon_0}{2\beta(1-\nu)\kappa^{\text{eff}}(\mathbf{k})^2|\mathbf{k}|^2}$$
$$- E\sum_{\mathbf{q}\in\mathcal{K}} \frac{\Omega(\mathbf{q},\mathbf{k})^2}{8\beta^2|\mathbf{k}|^4|\mathbf{q}-\mathbf{k}|^4\kappa^{\text{eff}}(\mathbf{k})\kappa^{\text{eff}}(\mathbf{q}-\mathbf{k})} \left(\frac{1}{\kappa^{\text{eff}}(\mathbf{k})} + \frac{1}{\kappa^{\text{eff}}(\mathbf{q}-\mathbf{k})} \frac{\partial \kappa^{\text{eff}}(\mathbf{q}-\mathbf{k})}{\partial \kappa^{\text{eff}}(\mathbf{k})} \right) \Bigg\}. \tag{5.5.34}$$

Now as we discussed in the beginning of this section, in order to make analytical progress, we focus on the leading term in the expression for the effective stiffness. Assuming that the leading term is described as: $\kappa^{\text{eff}}(\mathbf{k}) \sim |\mathbf{k}|^{-\eta}$ we get,

$$\frac{\partial \kappa^{\text{eff}}(\mathbf{q}-\mathbf{k})}{\partial \kappa^{\text{eff}}(\mathbf{k})} = \frac{\partial \kappa^{\text{eff}}(\mathbf{q}-\mathbf{k})/\partial \mathbf{k}}{\partial \kappa^{\text{eff}}(\mathbf{k})/\partial \mathbf{k}} = \frac{|\mathbf{q}-\mathbf{k}|^{-\eta-1}}{|\mathbf{k}|^{-\eta-1}} = \frac{\kappa^{\text{eff}}(\mathbf{q}-\mathbf{k})}{\kappa^{\text{eff}}(\mathbf{k})} \frac{|\mathbf{k}|}{|\mathbf{q}-\mathbf{k}|}. \tag{5.5.35}$$

Substituting the above expression into the derivation of F_s^{eff} results in

$$\frac{\partial U_s^{\text{eff}}}{\partial \kappa^{\text{eff}}(\mathbf{k})} = \sum_{\mathbf{k}\in\mathcal{K}} \Bigg\{ \frac{1}{2\beta\kappa^{\text{eff}}(\mathbf{k})} - \frac{\kappa_b}{2\beta\kappa^{\text{eff}}(\mathbf{k})^2} - \frac{E\varepsilon_0}{2\beta(1-\nu)\kappa^{\text{eff}}(\mathbf{k})^2|\mathbf{k}|^2}$$
$$- E\sum_{\mathbf{q}\in\mathcal{K}} \frac{\Omega(\mathbf{q},\mathbf{k})^2}{8\beta^2|\mathbf{k}|^4|\mathbf{q}-\mathbf{k}|^4\kappa^{\text{eff}}(\mathbf{k})^2\kappa^{\text{eff}}(\mathbf{q}-\mathbf{k})} \left(1 + \frac{|\mathbf{k}|}{|\mathbf{q}-\mathbf{k}|} \right) \Bigg\}. \tag{5.5.36}$$

Now summing all the terms result in the following implicit equation for the effective bending stiffness

$$\kappa^{\text{eff}}(\mathbf{k}) = \kappa_b + \frac{E\varepsilon_0}{(1-\nu)|\mathbf{k}|^2} + \frac{k_B T E}{4} \sum_{\mathbf{q}\in\mathcal{K}} \frac{\Omega(\mathbf{q},\mathbf{k})^2}{|\mathbf{k}|^4|\mathbf{q}-\mathbf{k}|^4\kappa^{\text{eff}}(\mathbf{q}-\mathbf{k})} \left(1 + \frac{|\mathbf{k}|}{|\mathbf{q}-\mathbf{k}|} \right). \tag{5.5.37}$$

In what follows, we analyze the above expression for two cases of zero and non-zero pre-strain field ε^0.

Case I: $\varepsilon^0 \neq 0$

We proceed to analyze the equation (5.5.37) based on scaling argument, similar to what we presented in the preceding subsection. Starting with the last term in (5.5.37), we have

$$\begin{aligned}\frac{\Omega(\mathbf{q},\mathbf{k})^2}{|\mathbf{k}|^4|\mathbf{q}-\mathbf{k}|^4\kappa^{\text{eff}}(\mathbf{q}-\mathbf{k})}\left(1+\frac{|\mathbf{k}|}{|\mathbf{q}-\mathbf{k}|}\right) &= \frac{(\mathbf{k}^2\mathbf{q}^2-(\mathbf{k}\cdot\mathbf{q})^2)^2}{|\mathbf{q}-\mathbf{k}|^4|\mathbf{k}|^4|\mathbf{q}|^4\kappa^{\text{eff}}(\mathbf{q}-\mathbf{k})}\left(1+\frac{|\mathbf{k}|}{|\mathbf{q}-\mathbf{k}|}\right)\\ &\sim \frac{1}{|\mathbf{q}-\mathbf{k}|^4\kappa^{\text{eff}}(\mathbf{q}-\mathbf{k})}\left(1+\frac{|\mathbf{k}|}{|\mathbf{q}-\mathbf{k}|}\right). \qquad (5.5.38)\end{aligned}$$

Summing the above expression over $\mathbf{q}$ results in

$$\sum_{\mathbf{q}} \sim \frac{1}{|\mathbf{q}-\mathbf{k}|^{4-\eta}}\left(1+\frac{|\mathbf{k}|}{|\mathbf{q}-\mathbf{k}|}\right) \sim \frac{1}{|\mathbf{k}|^{2-\eta}}. \qquad (5.5.39)$$

Finally the effective modulus can be expressed as

$$\kappa^{\text{eff}}(\mathbf{k}) = \kappa_b + \frac{E\varepsilon_0}{(1-\nu^2)|\mathbf{k}|^2} + \frac{\gamma}{|\mathbf{k}|^{2-\eta}}, \qquad (5.5.40)$$

wherein γ —the correction factor—, is a constant of no consequence. Given that $\eta > 0$, the dominant factor, in the long wave-length fluctuations is obviously the second term, which is proportional to $1/|\mathbf{k}|^2$ and consequently, $\eta \approx 2$. Note that this is the same result as what is obtained using regular perturbation method.

Case II: $\varepsilon^0 = 0$

We now consider the results of the variational perturbation method for this case. The effective stiffness in (5.5.37) for this case reduces to

$$\kappa^{\text{eff}}(\mathbf{k}) = \kappa_b + \frac{k_B T E}{4}\sum_{\mathbf{q}\in\mathcal{K}} \frac{\Omega(\mathbf{q},\mathbf{k})^2}{|\mathbf{k}|^4|\mathbf{q}-\mathbf{k}|^4\kappa^{\text{eff}}(\mathbf{q}-\mathbf{k})}\left(1+\frac{|\mathbf{k}|}{|\mathbf{q}-\mathbf{k}|}\right). \qquad (5.5.41)$$

Again, let the $\kappa^{\text{eff}}(\mathbf{q}-\mathbf{k}) \sim \Theta|\mathbf{q}-\mathbf{k}|^{-\eta}$, where Θ is an unknown constant. Then the above summation is proportional to $1/|\mathbf{k}|^{2-\eta}$. One can solve the resulting implicit equation

for η and Θ as

$$\kappa^{\text{eff}}(\mathbf{k}) := \Theta|\mathbf{k}|^{-\eta} \sim \frac{k_B T E}{\Theta|\mathbf{k}|^{2-\eta}}, \tag{5.5.42}$$

from which we obtain the effective bending stiffness as

$$\kappa^{\text{eff}}(\mathbf{k}) \sim \sqrt{E k_B T}|\mathbf{k}|^{-1}. \tag{5.5.43}$$

Using this result one can explore the dependence of the out of plane fluctuations on the length scale and temperature

$$\begin{aligned} \langle |w(\mathbf{k})|^2 \rangle &\sim \frac{k_B T}{\kappa^{\text{eff}}(\mathbf{k})\mathbf{k}^4} \\ &\sim \frac{1}{|\mathbf{k}|^3}\sqrt{\frac{k_B T}{E}}. \end{aligned} \tag{5.5.44}$$

The fluctuations of the out plane field $\langle w^2 \rangle$ is obtained by summing over all possible modes

$$\begin{aligned} \langle w^2 \rangle &\sim \sum_{\mathbf{k}} \frac{1}{|\mathbf{k}|^3}\sqrt{\frac{k_B T}{E}} \\ &\sim \int \frac{2\pi k dk}{k^3}\sqrt{\frac{k_B T}{E}} \\ &\sim \frac{1}{k_{\min}}\sqrt{\frac{k_B T}{E}} \sim L\sqrt{\frac{k_B T}{E}}. \end{aligned} \tag{5.5.45}$$

Unlike the case where $\varepsilon^0 \neq 0$, in this case the result from Variational perturbation method is different from what is obtained using conventional perturbation expansion. In the following section we study the fluctuations of graphene, using molecular dynamic simulation, to further examine the accuracy of our theoretical estimations.

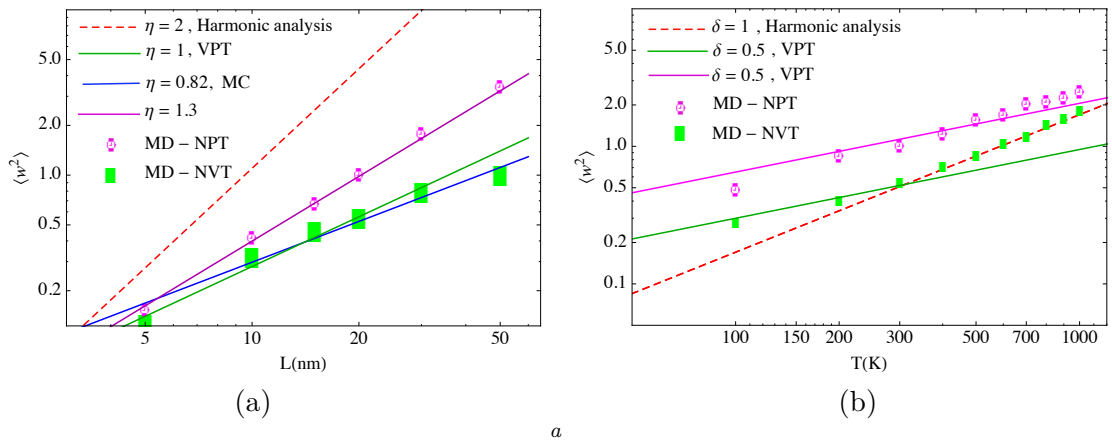

Figure 5.6.1: (a) Fluctuation amplitude as a function of a graphene membrane size at $T =$ 300 K, (b) fluctuations amplitude as a function of temperature .

[a](a) Fluctuation amplitude as a function of a graphene membrane size at $T = 300$ K, fitted by the scaling law, $\langle w^2 \rangle \propto L_0^{\eta}$, with different exponents obtained from harmonic analysis, VPT, Monte Carlo and MD for NPT and NVT ensembles.(b) Fluctuations amplitude as a function of temperature, $\langle w^2 \rangle \propto T^{\delta}$, with $L_0 = 20nm$.

5.6 Molecular Dynamic Simulation

We perform MD simulations of monolayer graphene using LAMMPS, an open source code [137]. The second-generation reactive empirical bond-order (REBO) potential [138] is used for the multibody C-C interactions in graphene. Square-shaped graphene membranes of different linear dimensions are simulated at finite temperatures with periodic boundary conditions. The temperature is controlled by a Nose-Hoover thermostat. Each simulation runs up to 40 ns (time step: 1 fs), with the first 10 ns for the system to equilibrate and the subsequent 30 ns for calculations of the time-averaged quantities. The time integration scheme closely follows the time-reversible measure-preserving Verlet and rRESPA integrators derived by Tuckerman et al.[139]. To simulate monolayer graphene without interlayer interactions, relatively thick simulation boxes are used (thickness $>$ 20 nm). MD simulations with both constant pressure (NPT) and constant volume (NVT) ensembles are performed. In NPT simulations, the dimensions of the simulation box are allowed to change to maintain a constant pressure (or stress). On the other hand, the NVT ensemble is used to simulate graphene subjected to a pre-strain (ε^0). In such simulations, the dimensions of the simulation box are fixed as $L = L_0(1 + \varepsilon^0)$, where L_0 is the linear dimension of the

graphene membrane in the ground state (T = 0 K). The in-plane reaction stress is evaluated as a function of the pre-strain and temperature by time-averaged virial stress [140]

$$\sigma = -\langle \frac{1}{L^2} \sum_{\substack{i,j \\ i \neq j}} \mathbf{F}_{ij} \otimes (\mathbf{r}_i - \mathbf{r}_j) + \frac{1}{L^2} \sum_i m_i \mathbf{v}_i \otimes \mathbf{v}_j \rangle_t, \tag{5.6.1}$$

where $\mathbf{F}_{ij}$ is the interatomic force between two atoms (i and j), $\mathbf{r}_i$ is the position vector of i-th atom, $\mathbf{v}_i$ is the velocity vector, m_i is the atomic mass, and $\langle \cdot \rangle_t$ denotes time average of the enclosed quantity. The virial formula is modified to yield the 2D stress for graphene.

In both NPT and NVT simulations, the mean amplitude of the out-of-plane thermal fluctuation is calculated by a time averaged RMS, namely

$$\overline{h} = \sqrt{\left\langle \sum_{i=1}^{N} \frac{w_i^2}{N} \right\rangle_t} \tag{5.6.2}$$

where N is the total number of atoms and w_i is the out-of-plane displacement of i-th atom. Based on the ergodic hypothesis (Weiner, 2002), the time average (over a sufficiently long period) from MD simulation is equivalent to the ensemble average in statistical mechanics. Consequently, the numerical results from MD simulations can be compared directly with the predictions based on statistical mechanics.

5.7 Discussion

In this work, we have revisited the statistical mechanics of solid membranes. Unlike fluid membrane, the in-plane and out of plane deformations are coupled in solid membranes. This coupling is a result of a strong geometric nonlinearity in the energy formulation. The nonlinear energy formulation does not allow us to employ the conventional equipartition theorem for the fluctuations of displacement field. Accordingly we have used some advanced methods to obtain analytical approximate solution for the fluctuations and the effective bending stiffness. We started with regular perturbation expansion. The first order perturbation ap-

proximation results in a $1/k^2$ dependance of effective bending stiffness. We further improved our estimation by employing a variational approach. Up to first order we have obtained $1/k$ dependance of bending stiffness. This result is obtained earlier by Nelson and Peliti [132] using a self consistent approach.

We also note that dependance of the out plane fluctuations in general can be stated as:

$$\langle w^2 \rangle \sim L^{\eta} T^{\delta} \tag{5.7.1}$$

Comparing Equation (5.7.1) with MD simulations under NPT and NVT ensembles, a few points are highlighted as follow:

- Within linear framework as is used for fluid membranes, $\eta = 2$ and $\delta = 1$. However, in this work, for graphene monolayers, we have obtained $\eta = 1$ and $\delta = 0.5$. These exponents appeared to be in fairly reasonable agreement with molecular dynamic simulation data. Note that under NVT ensemble the total area of the sheet is conserved and hence the kinematics of the deformation is close to that of von-Karman plate theory. The simulations are performed for a limited range of sheet size of graphene (5-50)nm. Within this range, our prediction is consistent with the data from MD shown in Figure 5.6(a). The results are demonstrated in log-log scale, where the slopes of the straight lines represent the exponent η. For larger sizes of the graphene sheets that are not shown in this figure, we speculate that the green line— corresponding to $\eta = 1$— diverges from the MD data. In the long-wave length limit, better predictions can be obtained by proceeding to higher order of VPT and numerical calculations.

- The results for simulations under NPT ensemble are slightly different. This is due to the fact that the NPT simulations are performed such that the in-plane stress field is relaxed. In this manner, the effects of nonlinearities arising from the coupling of in and out-of-plane deformations are softened. Typically, fluctuations under NVT

ensemble result in non-zero entropic in-plane stress field. In NPT simulations, the in-plane forces are relaxed with artificially external compressive forces such that the total stress field becomes zero [71]. As a result of these external compressive forces, the fluctuations are slightly augmented, when compared to NVT ensemble.

- We also compared our results on temperature dependency of the fluctuations to MD simulations for a broad range of temperature, (100-1000)K, in Figure 5.6(b). Our prediction is consistent with data for NVT simulations up to 400 K. However, for higher temperature, the MD results appear to converge to linear elasticity limit, where $\delta = 1$. This can be explained by recognizing the fact that at high temperatures, graphene sheet undergoes thermal expansions, while the in-plane area is maintained fixed. In this case, the extra area of the graphene sheet, resulting from thermal expansions is ceased by external compressive forces to conserve the total in-plane area. Accordingly, the nonlinearities are softened by thermal expansions and the compressive forces at high temperature.

- The results on NPT ensemble in contrast, is in reasonable agreement with the theoretical predictions even at high temperatures. This is due to the fact that unlike NVT simulations, the area can freely expand at high temperature and hence, the in-plane stress field does not change with the temperature.

Chapter 6

The Quest for the Determination of the Gaussian Modulus—Exploiting Membrane Edge Fluctuations; Implications for Lipid Bilayers and Graphene

The Gaussian modulus of a biological membrane, in addition to the bending rigidity, sets the energy scale for various important biological processes such as cell fission and generally, any event accompanied by a topological change. Unlike the bending rigidity, the Gaussian modulus is notoriously difficult to evaluate via either experiments or atomistic simulations. Measured thermal fluctuation spectrum provides a facile route to estimate the bending modulus of a membrane from either experiments or molecular dynamics simulations. Unfortunately, the Gaussian modulus is decoupled from the thermal fluctuation behavior of a membrane and thus precludes an easy estimation. In this work, recognizing that the Gaussian modulus plays a non-trivial role in the fluctuations of a membrane edge, we derive closed-form expressions for edge fluctuations. Combined with atomistic simula-

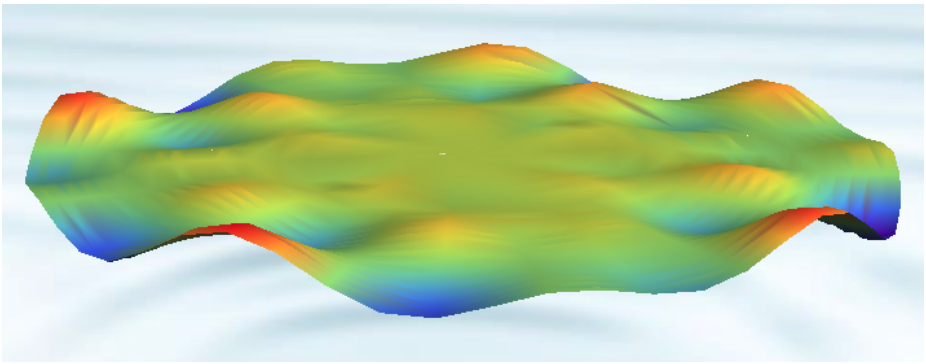

[a]

Figure 6.1.1: Schematic of a finite size 2D elastic sheet under edge forces.

[a]Due to the non-vanishing boundary conditions on the edge, the equilibrium state is no longer flat. Studying the mechanics of 2D materials, within finite size, where the effects of edge forces are significant, can be a potential route to discover their edge properties as well as Gaussian modulus.

tions, we use the developed approach to extract Gaussian modulus of graphene. Our results possibly provide the first reliable estimate of this elusive property.

6.1 Introduction

2D materials, both fluid(soft) and solid(hard) membranes are best known for their unusual flexibility and the ability to sustain large deformations that make them suitable for a number of fascinating applications in areas such as electronics, energy harvesting, biological systems among many others. They are mechanically described as elastic sheets that are resilient to areal change (in-plane deformations), but are quite flexible to undergo large curvatures. Specifically, the well-known Helfrich-Canham [1, 2, 79, 80, 81] theoretical framework parametrizes the energy cost of the deformation of a tensionless patch of a membrane by a quadratic function of curvature

$$F_b = \int \frac{1}{2}\kappa_b(H - H_0)^2 + \kappa_G(K - K_0). \tag{6.1.1}$$

Here κ_b and $\bar{\kappa}$ are the bending moduli that, respectively, correspond the energy change due to changes in the mean (H) and Gaussian (K) curvatures. The corresponding spontaneous curvatures are denoted by H_o and K_o.

Equation. (6.1.1) has been extensively used to described the mechanics of fluid membranes (biological membranes). Typical bending modulus (κ_b) of most lipid-bilayers is between 5 and $25k_BT$—-small enough compared to the thermal energy scale that membranes undulate or fluctuate noticeably at physiological temperatures [4, 5, 6, 7, 8]. The study of these experimentally observed and widely studied thermal fluctuations has been one of the cornerstones of biophysical research on membranes [6, 7, 8, 82, 83]. Statistical mechanics of membranes without edge—within periodic boundary conditions— is well-developed for both flat and curved geometries [28, 29, 30, 31, 32]. Such a simplified geometry, has been used to study the so-called entropic (steric) repulsive force between membranes [84, 33, 34], entropic effects on biological phenomena such as self-assembly, adhesion, binding-unbinding transitions, membrane fusion and many others [6, 85, 86, 87]. In particular, the experimentally measured fluctuation spectra or calculated via microscopic methods such as molecular dynamics, has provided a facile route to estimate mechanical and other related properties of membranes [13, 14, 15, 16]. For a membrane with periodic boundary condition, the following result for the fluctuations of the out of plane displacement field h, can be easily derived based on the linearized version of the quadratic Hamiltonian described in Equation (6.1.1) : $\langle h^2 \rangle \propto k_BT/\kappa_b$[5]. This basic result has been extended to numerous other physically relevant contexts providing an avenue to extract useful information e.g. incorporation of electromechanical coupling, tilt of lipids, presence of proteins or inclusions, proximity to substrates or other vesicles among others [17, 18, 19, 20, 21, 22, 23, 24].

With bending modulus of biological membranes, calculated and studied from both experiments and molecular dynamic simulations for decades, we are left with controversial values in the literature for Gaussian modulus. It is still a striking challenge to (computationally) compute or (experimentally)measure the Gaussian modulus. Due to the Gauss-Bonnet theorem [3], the contribution of Gaussian curvature in the change of energy of a membrane without any edge is zero, unless the membrane undergoes topological transformations. Nevertheless, the membrane is neither always closed nor subjected to isometric transformations. Pore formation during electroporation, vesicle formation, cellular uptake of macromolecules are examples of cases where the contributions of Gaussian curvature become influential.

Apart from investigations of Gaussian modulus, motivated by these implications, several works appeared to augment Helfrich model, to account for edge properties under various topological and boundary conditions [141, 142, 143, 144, 145, 146, 94]. In the simplest model, the edge energy is considered to be a line energy proportional to the length of the membrane [141]:[1]

$$F_{\mathcal{C}} = \int_{\partial\Omega} \phi_0. \tag{6.1.2}$$

In analogous to membrane surface tension, ϕ_0 is recognized as edge tension and has been measured both experimentally and theoretically [147, 148, 149, 150, 151, 152] and a quite notable variation exist among the reported data. The experimentally measured values of the edge tension appeared to significantly depend on the applied methods. Nevertheless, typical values of the edge tension are in the range of (3-40) pN [147, 148, 149, 150, 151, 152]. Depending on the length of the free edge as well as the boundary conditions and external stimuli (such as electric field, osmotic pressure or chemical gradients), the edge tension is likely to play a dominant role along with the Gaussian curvature that can possibly leads to transformations that cannot be predictable within solely Helfrich theory [94].

Current molecular dynamics techniques to estimate the Gaussian modulus require simulation of a finite membrane patch [153, 154]. Then based on the probability of the patch to close and form a vesicle, the Gaussian modulus can be extracted. While this technique does produce good results, it requires some special attention when creating the starting structure, namely that the membrane patch must be pre-curved and axis-symmetric; simulation of a finite patch also requires a sufficient simulation volume such that the patch will not be influenced by its periodic image, if using periodic boundary conditions, or any constraints placed at the boundaries. In the context of statistical mechanics, however, the effects of the Gaussian modulus and in particular an open edge, characterized by edge tension, on the thermal fluctuations and its entropic consequences, remain as open questions in the literature.

[1] In a general form, Biria et al.[94] formulate the edge-energy density that depends on the geometry of the boundary of the lipid bilayer through the normal and geodesic curvatures and the geodesic torsion.

Apart from biological membranes, 2D crystalline graphene—as an example of solid membrane— also has been acknowledged for its flexibility to undergo large out-of-plane deformations. Bending stiffness for graphene has been computed using both DFT and MD [9, 10, 11]. Unlike biological membranes, the fluctuations spectra cannot be used to determine the bending modulus of graphene. Elasticity of solid membranes, is somewhat more complicated compared to their fluid counterparts. While the bending energy is parametrized by Equation (6.1.1), the elastic energy cost for their in-plane deformations should be also accounted for. This is mainly because their in and out-of plane displacement fields are coupled. The kinematic of the deformation is similar to von-Karman nonlinear plate theory. Due to nonlinearities arising from the coupling between the in and out-of-plane deformations, thermal fluctuations cannot be analytically expressed to extract the mechanical properties. Nevertheless, reported values for graphene bending rigidity at zero Kelvin, range (1.2-1.6)eV—just a few times larger than the bending rigidity of biological membranes (at room temperature) [9, 10, 11]. At the same time, there is not much data in the literature on the Gaussian modulus of graphene monolayers [11, 155].

To utilize the exceptional electromechanical properties of graphene monolayers in electronics and energy harvesting systems, graphene nano ribbons (GNRs) with nanoscale width (w<20nm) appeared to be likely the most practical geometry. Depending on direction of the surface termination, the edge of these ribbons can be armchair, zigzag or a mixture of them. Surface terminations, appeared to cause permanent deformations on graphene sheets. The edge energy, in this case, can be relaxed by either elongation of the edge or out of plane deformations. Existing values of edge force for graphene are mostly obtained at very low temperature [11, 156, 157, 158, 159], where the effects of thermal fluctuations can be neglected. Note that the edge deformations will be involved with in-plane *nonlinear* stretching energy, bending energy—including both mean and Gaussian curvatures— as well as the edge energy. Among these, the contributions of Gaussian modulus and edge energy on thermal rippling of graphene monolayes have been less understood and require further attentions from both theoretical and atomistic point of views.

In this work, a new approach is presented to extract the Gaussian modulus and edge properties from the fluctuations spectra at a free edge. While this method can be used directly for fluid membranes, the results for solid membranes, require some careful physical interpretations as the geometric nonlinearities renormalize the effective mechanical properties at finite temperature. Central idea of the statistical mechanics and fluctuations of membranes influenced by boundary conditions is presented in Section 6.2. Our approach is employed to an example geometry to derive the correlation function at a free edge of an elastic membrane in Section 6.3. We perform molecular dynamic simulations of lipid bilayer and graphene with free edges in Section 6.4. Finally, a detailed discussion about our results is given in Section 6.6.

6.2 Central idea and formulation

Consider an open elastic membrane, having a smooth and orientable surface Ω, enclosed by a space curve $\partial\Omega$ that represents the edge of the surface. The bending energy density associated with the deformation of the surface Ω can be expressed as a function of the mean and Gaussian curvatures, being the only invariants of the curvature tensor: $\psi = \overline{\psi}(H, K)$. [2].

Up to quadratic order—and in the absence of the spontaneous mean and Gaussian

[2]Let $\mathbf{n}$ be the normal vector field on Ω. Then the curvature tensor $\mathbf{L}$ and mean and Gaussian curvatures (H, K) can be obtained as

$$\begin{aligned} &\mathbf{L} = -\nabla_S \mathbf{n}, \\ &H = -\frac{1}{2}\mathrm{div}_S\, \mathbf{n}, \quad K = \frac{1}{2}\left((\mathrm{tr}\,\mathbf{L})^2 - \mathrm{tr}(\mathbf{L}^2)\right), \end{aligned} \tag{6.2.1}$$

where ∇_S and div_S correspond to surface gradient and surface divergence operators. To explain the surface operators, let surface projection tensor be defined as

$$\mathbf{P} = \mathbf{I} - \mathbf{n} \otimes \mathbf{n},$$

where $\mathbf{I}$ is the identity tensor. The surface gradient, surface Laplacian and surface divergence of a scalar field f and a vector field $\mathbf{g}$ can then be defined in terms of $\mathbf{P}$ and their smooth extensions f^e and $\mathbf{g}^e$ as[94]

$$\begin{aligned} &\nabla_S f = \mathbf{P}\nabla f^e, \qquad \nabla_S \mathbf{g} = (\nabla \mathbf{g}^e)\mathbf{P}, \\ &\mathrm{div}_S \mathbf{g} = \mathbf{P} \cdot \nabla \mathbf{g}^e, \qquad \Delta_S f = \mathrm{div}_S(\nabla_S f). \end{aligned}$$

Finally, the curvature tensor takes the following form: $\mathbf{L} = -\nabla_S \mathbf{n}$.

curvatures— the bending energy density is given by

$$\overline{\psi} = \frac{1}{2}\kappa_b H^2 + \kappa_G K. \tag{6.2.2}$$

Further, the edge energy— as proposed by Biria et al.[94]—is geometric dependent. In the absence of the edge torsion, the edge energy density is expressed as [94]

$$\phi = \phi_0 + \bar{\phi}(\kappa_n, \kappa_g), \tag{6.2.3}$$

where ϕ_0 is a constant and is known as edge(line) tension. Also, κ_n, κ_g are the normal and geodesic curvatures, respectively[3]. Up to quadratic order, ϕ can be expressed [144]

$$\phi = \phi_0 + \frac{1}{2}\kappa_e(\kappa_n^2 + \kappa_g^2) + \cdots, \tag{6.2.4}$$

where κ_e is defined as the bending stiffness associated with the edge.

Now lets assume that all possible deformations are along the normal of the surface: $\mathbf{u} = U\mathbf{n}$. Minimization of the total elastic energy, in the absence of external forces and moments[94], then leads to the following Euler-Lagrange equations

$$\begin{aligned}&\overline{\psi}_H(2H^2 - K) + \frac{1}{2}\triangle_S\overline{\psi}_H + 2\overline{\psi}_K HK + 2\triangle_S(\overline{\psi}_K H)\\ &- \mathrm{div}_S(\mathbf{L}\nabla_{\mathbf{S}}\overline{\psi}_{\mathbf{K}}) - 2(\nabla_S H)\cdot(\nabla_S\overline{\psi}_K) - 2\overline{\psi}_K\triangle_S H - 2\psi H = 0,\end{aligned} \tag{6.2.5}$$

where the subscript H(and K) denotes derivative with respect to H(and K). The corre-

[3]Let $\mathbf{e}$ be the tangent unit vector of the edge curve $\partial\Omega$. Then $\nu = \mathbf{e}\times\mathbf{n}$ would be tangent to the surface Ω and normal the edge curve. The total curvature vector of the edge curve is obtained by taking the derivative of $\mathbf{e}$ with respect to the edge's arc length

$$\kappa = \mathbf{e}' = \kappa_n\mathbf{n} - \kappa_g\nu,$$

where κ_n and κ_g are the component of the curvature along the normal vectors of the surface and the edge, respectively.

sponding boundary conditions on the edge are also given by

$$(\mathbf{L}\nabla_S\overline{\psi}_K - \frac{1}{2}\nabla_S\overline{\psi}_H - 2H\nabla_S\overline{\psi}_K)\cdot\nu + \bar{\phi}_{\kappa_n}\kappa_n^2 + \bar{\phi}_{\kappa_g}\kappa_n\kappa_g - \phi\kappa_n - \overline{\phi}'_{\kappa_n} = 0 \tag{6.2.6a}$$

$$\frac{1}{2}\overline{\psi}_H + \overline{\psi}_K\kappa_n + \bar{\phi}_{\kappa_n}\kappa_g - \bar{\phi}_{\kappa_g}\kappa_n = 0, \tag{6.2.6b}$$

for free edges and

$$U = 0, \qquad \nabla_S U\cdot\mathbf{n} = 0, \tag{6.2.7}$$

for constrained edges, depending on the boundary conditions. Now let Ω be on the x-y plane occupying an area of A. Within linearized approximations the mean and Gaussian curvatures are expressed as

$$H = -\frac{1}{2}\nabla^2 U, \qquad K = U_{xx}U_{yy} - (U_{xy})^2. \tag{6.2.8}$$

Further, under the assumption of zero tangential deformations, the curvatures of the edge can be obtained as

$$\kappa_n = \frac{\partial^2 U}{\partial s^2}, \qquad \kappa_g = 0, \tag{6.2.9}$$

where s is the arc-length of the edge curve.

[4]

The above equations are the general form of the boundary conditions of a membrane, with arbitrary geometry. We note that so far, we considered linear approximations for the mean and Gaussian curvatures. Also, we neglect the in-plane deformations. This is a fairly reasonable assumption for fluid membranes, since the in and out-of-plane deformations are decoupled. However, for solid membranes, such as graphene, it is best to start with the nonlinear von-Karman plate theory, in which the in and out-of-plane deformations are in-

[4]Let θ (as shown in Figure. 6.2.1) be the angle between the normal of the edge and the x axis.

deed coupled. Nevertheless, when the in-plane strains are small and negligible, for the sake of analytical progress, one can approximately use the above linearized equations. In the remaining of this paper, we use the linearized approximation of the elastic energy, to obtain closed form solutions for the fluctuations of membrane, in the presence of boundary conditions.

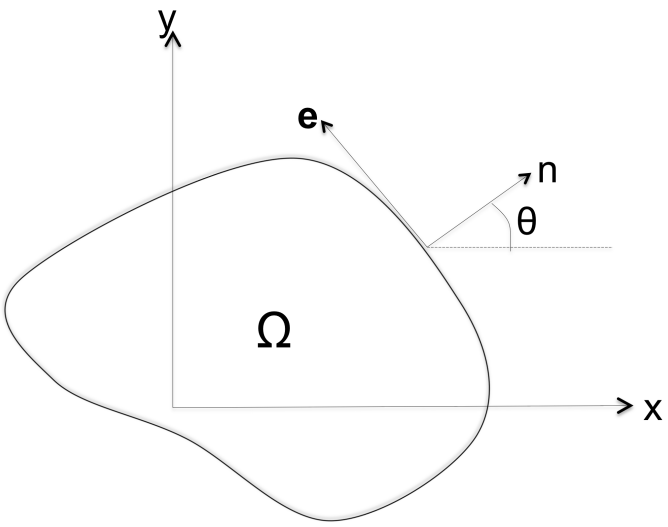

Figure 6.2.1: Schematic of a planar surface embedded in domain Ω, having a closed edge $\partial\Omega$. The unit tangent and normal vectors of the edge curve are shown. Also θ is defined as the angle between the normal vector to the edge and the x axis.

Depending on clamped or free edges, one can specify different set of boundary conditions. For clamped edge, one need to set

$$\begin{aligned} h(\mathbf{x}) &:= 0, \qquad \mathbf{x} \in \partial\Omega \\ \frac{\partial h(\mathbf{x})}{\partial n} &:= 0, \qquad \mathbf{x} \in \partial\Omega, \end{aligned} \tag{6.2.10}$$

while for free edges, we obtain

$$\begin{aligned} &\kappa_b \frac{\partial(\nabla^2 h)}{\partial n} + \bar{\kappa}\frac{\partial}{\partial s}\Big\{ \sin\theta\cos\theta(\frac{\partial^2 h}{\partial y^2} - \frac{\partial^2 h}{\partial x^2})\Big\} \\ &+ \bar{\kappa}\frac{\partial}{\partial s}\Big\{(\sin^2\theta - \cos^2\theta)\frac{\partial^2 h}{\partial y \partial x}\Big\} + \sigma\frac{\partial^2 h}{\partial s^2} - \kappa_s\frac{\partial^4 h}{\partial s^4} := 0, \\ &\qquad\qquad \mathbf{x} \in \partial\Omega \\ &\kappa_b\nabla^2 h - \bar{\kappa}\left(2\sin\theta\cos\theta\frac{\partial^2 h}{\partial x \partial y} - \sin^2\theta\frac{\partial^2 h}{\partial x^2}\right. \\ &\qquad\qquad \left. - \cos^2\theta\frac{\partial^2 h}{\partial y^2}\right) := 0, \\ &\qquad\qquad \mathbf{x} \in \partial\Omega. \end{aligned} \tag{6.2.11}$$

Statistical mechanics of elastic membranes is extensively studied in the literature. In the majority of these work, the membrane—occupying a domain of $\Omega^{\mathrm{P}} = (0, L)^2$ in the xy plane— is assumed to be large enough that the effects of boundary conditions are negligible; i.e. the energy at the boundary in is hence neglected. Accordingly, a periodic boundary condition is assumed in all the directions. In this manner, due to Gauss-Bonnet theorem, the integration of the Gaussian curvature of a membrane, without edge is constant. Hence, the elastic energy is described solely in terms of the mean curvature. For periodic boundary conditions the out-of-plane deformation of the membrane can be easily described in Fourier space as

$$h(\mathbf{x}) = \sum_{\mathbf{q}\in\mathbb{K}} \bar{h}_{\mathbf{q}} \mathrm{e}^{\imath \mathbf{q}\cdot\mathbf{x}}, \tag{6.2.12}$$

in which to avoid divergencies, we introduce cut-off lengths for wave vectors as: $q := |\mathbf{q}| \in [q_{\min}, q_{\max}]$, i.e.

$$\mathbb{K} = \{\mathbf{q} : \mathbf{q} = \frac{2\pi}{L}(\nu_x, \nu_y), \nu_x, \nu_y \in \mathbb{Z}, |\mathbf{q}| \in [q_{\min}, q_{\max}]\}.$$

Substituting the expansion (6.2.12) in the *linearized* elastic energy gives us

$$\begin{aligned} U_{\Omega^{\mathrm{P}}} &= \frac{L^2}{2} \sum_{\mathbf{q},\mathbf{q}'\in\mathbb{K}} \kappa_b |\mathbf{q}|^2 |\mathbf{q}'|^2 \bar{h}_{\mathbf{q}} \bar{h}_{\mathbf{q}'} \int_{\Omega^{\mathrm{P}}} \mathrm{e}^{\imath(\mathbf{q}+\mathbf{q}')\cdot\mathbf{x}} \\ &= \frac{L^2}{2} \sum_{\mathbf{q},\mathbf{q}'\in\mathbb{K}} \kappa_b |\mathbf{q}|^2 |\mathbf{q}'|^2 \bar{h}_{\mathbf{q}} \bar{h}_{\mathbf{q}'} \delta(\mathbf{q}, -\mathbf{q}') \\ &= \frac{L^2}{2} \sum_{\mathbf{q}\in\mathbb{K}} \kappa_b |\mathbf{q}|^4 \bar{h}_{\mathbf{q}} \bar{h}_{-\mathbf{q}} \\ &= \frac{L^2}{2} \sum_{\mathbf{q}\in\mathbb{K}} \kappa_b |\mathbf{q}|^4 |\bar{h}_{\mathbf{q}}|^2, \end{aligned} \tag{6.2.13}$$

in which we used the orthogonality property of the Fourier transformations. Equipartition theorem states that the ensemble average of elastic energy for each mode of fluctuations is equal to $\frac{1}{2}k_B T$. Therefore, the ensemble average of the self correlation function in each

mode is obtained as[5]

$$\langle|\bar{h}_{\mathbf{q}}|^2\rangle = \frac{k_B T}{L^2 \kappa_b |\mathbf{q}|^4}. \tag{6.2.14}$$

Further, for a periodic geometry, since the two-point correlation function is translationally and rotationally invariant, it only depends on the distance between the two points, $r = |\mathbf{r}| = |\mathbf{x} - \mathbf{x}'|$, rather than their positions $(\mathbf{x}, \mathbf{x}')$

$$\begin{aligned}
\langle h(\mathbf{x}) h(\mathbf{x}')\rangle &= \sum_{\mathbf{q},\mathbf{q}'\in\mathbb{K}} \langle \bar{h}_{\mathbf{q}} \bar{h}_{\mathbf{q}'} \mathrm{e}^{\imath(\mathbf{q}\cdot\mathbf{x}+\mathbf{q}'\cdot\mathbf{x}')}\rangle \\
&= \sum_{\mathbf{q},\mathbf{q}'\in\mathbb{K}} \mathrm{e}^{\imath(\mathbf{q}\cdot\mathbf{x}+\mathbf{q}'\cdot\mathbf{x}')} \langle \bar{h}_{\mathbf{q}} \bar{h}_{\mathbf{q}'}\rangle \\
&= \sum_{\mathbf{q}\in\mathbb{K}} \mathrm{e}^{\imath\mathbf{q}\cdot(\mathbf{x}-\mathbf{x}')} \langle|\bar{h}_{\mathbf{q}}|^2\rangle \delta(\mathbf{q}, -\mathbf{q}') \\
&= \frac{k_B T}{L^2 \kappa_b} \sum_{\mathbf{q}\in\mathbb{K}} \frac{\mathrm{e}^{\imath\mathbf{q}\cdot\mathbf{r}}}{|\mathbf{q}|^4},
\end{aligned} \tag{6.2.15}$$

which is clearly independent of the position of the two points. Similarly, the self correlation function $\langle h^2(\mathbf{x})\rangle$ is independent of the position and is the phase *and* spatial average of $h^2(\mathbf{x})$

$$\begin{aligned}
\langle h^2\rangle &= \langle h^2(\mathbf{x}_1)\rangle = \langle h^2(\mathbf{x}_2)\rangle \\
&= \frac{1}{L^2}\int_{\Omega^{\mathrm{P}}} \langle h^2(\mathbf{x})\rangle = \frac{k_B T}{L^2 \kappa_b} \sum_{\mathbf{q}\in\mathbb{K}} \frac{1}{|\mathbf{q}|^4}.
\end{aligned} \tag{6.2.16}$$

As it can be seen the periodic boundary conditions, dramatically simplify our calculations, and give us closed form expressions for the fluctuations which only depends on the bending modulus. The expression in (6.2.14) has been used to extract the bending stiffness of fluid membranes from molecular dynamic simulations. In real cases, however, the fluctuations can be affected by different geometry and boundary conditions. Further, the periodic boundary conditions, automatically remove the contributions from Gaussian modulus and edge properties, (κ_s, ϕ_0), since these parameters enters the equations only

[5] Also note that the modes are decoupled, i.e.

$$\langle h_{\mathbf{q}} h_{\mathbf{q}'}\rangle = \langle|h_{\mathbf{q}}|^2\rangle \delta(\mathbf{q}, -\mathbf{q}').$$

through boundary conditions. The statistical mechanics of a system, influenced by a set of boundary conditions, is hard to handle within conventional approaches. Generally, the partition function Z—from which one can obtain the ensemble averages $\langle \mathbb{X} \rangle$ and the free energy F— is defined as

$$\begin{aligned} Z &= \int \exp\left(-\frac{1}{k_B T}\int \frac{1}{2}\kappa_b h \nabla^4 h\right) \mathcal{D}[h], \quad F = -k_B T \log Z, \\ \langle \mathbb{X} \rangle &= \frac{1}{Z}\int \mathbb{X} \exp\left(-\frac{1}{k_B T}\int \frac{1}{2}\kappa_b h \nabla^4 h\right) \mathcal{D}[h], \end{aligned} \tag{6.2.17}$$

in which $\mathcal{D}[h]$ denotes integration over all *possible* functions of $h(\mathbf{x})$, that *do satisfy* the boundary conditions. To ensure this, one need to look for the eigenvalues of the associated differential operator ∇^4 for the given geometry and the boundary conditions in (6.2.11). Expanding the displacement field in a set of orthogonal eigenfunctions, $u_{m,n}(\mathbf{x})$, one can express the eigenvalue as

$$\nabla^4 h(\mathbf{x}) = \sum_{m,n} \lambda_{m,n}^4 h_{m,n} u_{m,n}(\mathbf{x}), \tag{6.2.18}$$

where $\lambda_{m,n}$ is the eigenvalue associated with the biharmonic operator for the given geometry and boundary conditions. Further, $h_{m,n}$ is the amplitude of $h(\mathbf{x})$, corresponding to mode (m, n) and is obtained as

$$h_{m,n} = \frac{1}{A}\int_\Omega h(\mathbf{x}) u_{m,n}^*(\mathbf{x}), \tag{6.2.19}$$

where A is

$$A = \int_\Omega u_{m,n}(\mathbf{x}) u_{m,n}^*(\mathbf{x}). \tag{6.2.20}$$

Consequently, the integration in the exponent of the partition function can be written as

$$\int \frac{1}{2}\kappa_b \left(h\nabla^4 h\right) d\mathbf{x} = \frac{1}{2}\kappa_b A \sum_{m,n} h_{m,n}\lambda_{m,n}^4 h_{m,n}^*. \tag{6.2.21}$$

Using the equipartition theorem, the correlation function then, can be expressed as

$$\langle h(\mathbf{x})h(\mathbf{x}')\rangle = \frac{k_B T}{\kappa_b A}\sum_{m,n}\frac{u_{m,n}(\mathbf{x})u_{m,n}^*(\mathbf{x}')}{\lambda_{m,n}^4}. \tag{6.2.22}$$

It is not always, easy and straightforward to obtain a closed-form expression for the eigenvalues and eigenfunctions. In the case of an infinite sheet, for which a periodic boundary conditions is assumed, one can easily obtain the eigenvalues and eigenfunctions, in Fourier space as $\mathbf{q}$ and $\mathrm{e}^{i\mathbf{q}\cdot\mathbf{x}}$, respectively. However, when the set of admissible functions for h is restricted in the path integration of the partition function, the eigenvalues and eigenfunctions should be solved for the given set of boundary conditions. Alternatively, one can solve for the Green's function in terms of the same eigenvalue and eigenfunctions

$$G(\mathbf{x},\mathbf{x}') = \sum_{m,n} G_{m,n}(\mathbf{x}')u_{m,n}(\mathbf{x}) \tag{6.2.23}$$

$$\begin{aligned}\kappa_b\nabla^4 G(\mathbf{x},\mathbf{x}') &= \sum_{m,n}\lambda_{m,n}^4 G_{m,n}(\mathbf{x}')u_{m,n}(\mathbf{x}) \\ &= \delta(\mathbf{x},\mathbf{x}') = \sum_{m,n} u_{m,n}(\mathbf{x})u_{m,n}^*(\mathbf{x}'),\end{aligned} \tag{6.2.24}$$

from which we obtain

$$G_{m,n}(\mathbf{x}') = \frac{u_{m,n}^*(\mathbf{x}')}{\kappa_b\lambda_{m,n}^4} \tag{6.2.25}$$

$$\begin{aligned}G(\mathbf{x},\mathbf{x}') &= \sum_{m,n} G_{m,n}(\mathbf{x}')u_{m,n}(\mathbf{x}) \\ &= \sum_{m,n}\frac{u_{m,n}(\mathbf{x})u_{m,n}^*(\mathbf{x}')}{\kappa_b\lambda_{m,n}^4},\end{aligned} \tag{6.2.26}$$

which is exactly what we have in the summation of (6.2.22). Therefore, the correlation

functions can be easily written in terms of the Green's function as

$$\langle h(\mathbf{x})h(\mathbf{x}')\rangle = \frac{k_B T}{A} G(\mathbf{x},\mathbf{x}'). \tag{6.2.27}$$

In order to study the statistical mechanics of a system, influenced by a set of boundary conditions, one may choose to *either* evaluate the eigenvalues and eigenfunctions or derive the Green's function in its closed form, rather than the series form in (6.2.25). In this work we aim to study an example of fluctuations of membranes that are affected by non-vanishing boundary conditions. We will use the resulting expression for the fluctuations to extract the Gaussian modulus and edge properties from MD simulations.

6.3 Fluctuations of a free edge

In this part we use the derivation in the preceding section to derive the correlations function for a free edge. We fit our analytical results to the data from MD simulations to extract the edge properties as well as the Gaussian modulus for both lipid membrane and graphene.

Consider a membrane of size L^2, with a free edge and a clamped (opposite) edge. Our goal is to study the fluctuations of the membrane at (and near) the free edge (and far enough from the other three edges), where the contributions of the edge parameters and Gaussian modulus are important. In order to make analytical progress, we model this case with a semi-infinite sheet, with one free edge, to make sure that the fluctuations of the free edge is not affected by the other edges' conditions. Now, consider a semi-infinite sheet embedded in the domain $\Omega^1 := [\mathbf{x} = (x, y); -\infty < x < 0, -\infty < y < \infty]$, having a free edge at $\partial\Omega^1 := [\mathbf{x} = (0, y); -\infty < y < \infty]$. Therefore, we have periodic boundary conditions only in y direction. For this case the boundary conditions in (6.2.11) reduce to

$$\kappa_b \nabla^2 h + \bar{\kappa}\frac{\partial^2 h}{\partial y^2} = 0, \quad \mathbf{x} \in \partial\Omega^1 \tag{6.3.1}$$

$$\frac{\partial}{\partial x}\left(\kappa_b \nabla^2 h - \bar{\kappa}\frac{\partial^2 h}{\partial y^2}\right) + \phi_0 \frac{\partial^2 h}{\partial y^2} - \kappa_s \frac{\partial^4 h}{\partial y^4} = 0, \quad \mathbf{x} \in \partial\Omega^1 \tag{6.3.2}$$

The Green's function for the given geometry and the above set of boundary conditions is given by the solution of

$$\kappa_b \nabla^4 G(\mathbf{x}, \mathbf{x}') = \delta(\mathbf{x}, \mathbf{x}'). \tag{6.3.3}$$

Again, due to the translational invariance in the y-direction, $y - y'$ may be substituted for r and derivatives with respect to y and y' may be combined to be considered as derivatives with respect to r. Therefore, the Green's function and its boundary conditions (6.3.1), and (6.3.2) can be written as

$$\kappa_b \nabla^4 G(x, x', r) = \delta(x - x')\delta(r), \tag{6.3.4}$$

$$\kappa_b \nabla^2 G(x, x', r) + \bar{\kappa} \frac{\partial^2 G(x, x', r)}{\partial r^2} = 0, \quad \mathbf{x} \text{ (or } \mathbf{x}') \in \partial\Omega^1, \tag{6.3.5}$$

$$\begin{aligned} &\frac{\partial}{\partial x}\left(\kappa_b \nabla^2 G(x, x', r) - \bar{\kappa} \frac{\partial^2 G(x, x', r)}{\partial r^2}\right) \\ &\quad + \phi_0 \frac{\partial^2 G(x, x', r)}{\partial r^2} - \kappa_s \frac{\partial^4 G(x, x', r)}{\partial r^4} = 0, \quad \mathbf{x} \text{ (or } \mathbf{x}') \in \partial\Omega^1. \end{aligned} \tag{6.3.6}$$

The preceding boundary condition equations, (6.3.5) and (6.3.6), are actually a set of four equations. Two equations when $x = 0$ and $x' \neq 0$ and two equations for when $x' = 0$ and $x \neq 0$[6]. Now, the full set of equations, (6.3.4),(6.3.5), and (6.3.6), will need to be solved[7].

The first step to solving this set of differential equations is to find a particular solution which satisfies the equation and boundary conditions. This can be done by finding a solution to the infinite system by first taking the Fourier transform of (6.3.4) to go from $r \to q$ and

[6]These are almost the exact same equations as derived by Gompper and Kroll up to this point. The solution to these equations is found by Gompper and Kroll[160] under different assumptions; either the gaussian modulus is set to zero or the edge modulus and edge tension are set to zero. In these cases, solutions have already been presented [160]; however, no solution is given without making any assumptions. Since the gaussian modulus is such a difficult property to measure, it is best not to make any assumptions about the impact of any terms in the energy equations.

[7]A methodolgy similar to that of Gompper and Kroll will be used, but described in much more detail and with no assumptions made in order to arrive at a full solution for the Green's function.

$x \to k$ which leads to

$$\kappa_b(k^2+q^2)^2 G(q,k,x') = \mathrm{e}^{-ikx'}. \tag{6.3.7}$$

In this context the current definitions of the Fourier and inverse Fourier transforms are given by

$$G(q,x,x') = \frac{1}{L}\int \mathrm{e}^{-iqr} G(r,x,x')\,dr, \tag{6.3.8}$$

$$G(r,x,x') = \frac{1}{2\pi}\int \mathrm{e}^{iqr} G(q,x,x')\,dq, \tag{6.3.9}$$

where L is the length of the edge. Taking the inverse Fourier transform as defined in (6.3.9) to return from $k \to x$ gives

$$G_P(q,x,x') = \frac{1}{2\pi}\int \frac{\mathrm{e}^{ik(x-x')}}{\kappa_b(k^2+q^2)^2}\,dk. \tag{6.3.10}$$

This equation can now be solved simply using residue theorem to obtain the particular solution

$$G_P(q,x,x') = \frac{1}{4\kappa_b q^3}\mathrm{e}^{-q|x-x'|}(1+q|x-x'|). \tag{6.3.11}$$

This solution was derived to satisfy (6.3.4) but also must satisfy the boundary conditions. To check that (6.3.5) and (6.3.6) are satisfied, both must undergo multiple Fourier transforms to go from $r \to q$. In fact, it is useful to apply the Fourier transform from $r \to q$ to reduce the entire problem to a fourth order ordinary differential equation where only derivatives with respect to x (or x') occur. After transformation the boundary conditions can be written as

$$\frac{\partial^2 G}{\partial x^2} - q^2(1+\alpha)G = 0 \quad \mathbf{x}\ (\text{or } \mathbf{x}') \in \partial\Omega^1, \tag{6.3.12}$$

$$\frac{\partial^3 G}{\partial x^3} + q^2(\alpha-1)\frac{\partial G}{\partial x} - f(q)G = 0 \quad \mathbf{x}\ (\text{or } \mathbf{x}') \in \partial\Omega^1, \tag{6.3.13}$$

where α is $\bar{\kappa}/\kappa_b$ and

$$f(q) = \frac{\kappa_s}{\kappa_b}q^4 + \frac{\sigma}{\kappa_b}q^2$$

and all primes denote a derivative with respect to x (or x'). From here, by taking the proper

derivatives of (6.3.11) and substituting them into the transformed boundary conditions, it is clear that the particular solution does not satisfy the boundary conditions.

Now that a particular solution to the problem has been found, it is necessary to find the homogeneous solution to the problem. To do so, equation (6.3.4) will also need to be transformed and set equal to zero, leading to

$$\frac{\partial^4 G}{\partial x^4} - 2q^2 \frac{\partial^2 G}{\partial x^2} + q^4 G = 0. \tag{6.3.14}$$

The characteristic equation of (6.3.14) shows that the differential equation has two two-fold real roots at $\pm q$. Therefore the solution will be some linear combination of

$$\mathrm{e}^{qx},\ x\mathrm{e}^{qx},\ \mathrm{e}^{-qx},\ x\mathrm{e}^{-qx}. \tag{6.3.15}$$

Since the out-of-plane fluctuations of the membrane cannot go to infinity as x goes to negative infinity (recall that the domain of x is from $-\infty \to 0$), any solution from (6.3.15) that does so may be eliminated. This removes any possible solution with a negative exponent since x is always negative. The solution must also satisfy the boundary equations for both x and x', therefore the homogeneous solution to the problem may be written as

$$G_H = (A\mathrm{e}^{qx} + Bx\mathrm{e}^{qx})(C\mathrm{e}^{qx'} + Dx'\mathrm{e}^{qx'}). \tag{6.3.16}$$

Taking the total solution, given by $G = G_P + G_H$, the coefficients A, B, C, and D can be found by substituting into the boundary conditions (6.3.12) and (6.3.13) and solving the set of four equations simultaneously. Recall That each boundary condition may be used as two equations: once when $x = 0$ and derivatives are taken with respect to x, and once when $x' = 0$ and derivatives are taken with respect to x'. Before solving for these coefficients, it is useful to rewrite the full solution in a new form by expanding the homogeneous solution

and grouping like terms. The full solution can then be written as

$$G(x,x',q) = \frac{1}{4\kappa_b q^3}\mathrm{e}^{-q|x-x'|}(1+q|x-x'|) + \left(A+Bx+Cx'+Dxx'\right)\mathrm{e}^{q(x+x')}, \tag{6.3.17}$$

where A, B, C, and D are regrouped coefficients which differ slightly from those in (6.3.16), but still remain constant with respect to x. Taking the proper derivatives of (6.3.17) with respect to x and substituting into equations (6.3.12) and (6.3.13) and simplifying gives the following set of equations

$$\frac{-2-\alpha}{4\kappa_b q} + \frac{\alpha x'}{4\kappa_b} + 2q[B+Dx'] - q^2\alpha[A+Cx'] = 0 \qquad \mathbf{x} \in \partial\Omega^1, \tag{6.3.18}$$

$$\frac{-2-\alpha}{4\kappa_b q} + \frac{\alpha x}{4\kappa_b} + 2q[C+Dx] - q^2\alpha[A+Bx] = 0 \qquad \mathbf{x}' \in \partial\Omega^1, \tag{6.3.19}$$

$$\frac{2+q\alpha x'}{4\kappa_b} + (2+\alpha)q^2(B+Dx') + (q^3\alpha - f(q))[A+Cx'] - \frac{f(q)}{4\kappa_b q^3}(1-qx') = 0, \qquad \mathbf{x} \in \partial\Omega^1, \tag{6.3.20}$$

$$\frac{2+q\alpha x}{4\kappa_b} + (2+\alpha)q^2(C+Dx) + (q^3\alpha - f(q))(A+Bx) - \frac{f(q)}{4\kappa_b q^3}(1-qx) = 0, \qquad \mathbf{x}' \in \partial\Omega^1. \tag{6.3.21}$$

Solving this set of equations simultaneously for the unknown coefficients gives

$$A = \frac{1}{4\kappa_b q^3}\frac{2f(q) - q^3(8+4\alpha+\alpha^2)}{M}, \tag{6.3.22}$$

$$B = C = \frac{1}{4\kappa_b q^3}\frac{q(\alpha^2 q^3 - 2f(q))}{M}, \tag{6.3.23}$$

$$D = \frac{1}{4\kappa_b q^3}\frac{-q^2(2\alpha^2 q^3)}{M}, \tag{6.3.24}$$

where

$$M = \alpha(4+\alpha)q^3 - 2f(q). \tag{6.3.25}$$

The final solution with all coefficients in place can now be written as

$$\begin{aligned} G(x,x',q) = &\frac{1}{4\kappa_b q^3}\mathrm{e}^{-q|x-x'|}(1+q|x-x'|) \\ &+ \frac{1}{4\kappa_b q^3}\mathrm{e}^{q(x+x')}\left[U + Vq(x+x') - Wq^2 xx'\right], \end{aligned} \tag{6.3.26}$$

where

$$U = \frac{1}{M}(2f(q) - q^3(8+4\alpha+\alpha^2)), \tag{6.3.27}$$

$$V = \frac{1}{M}(\alpha^2 q^3 - 2f(q)), \tag{6.3.28}$$

$$W = \frac{1}{M}(2\alpha^2 q^3), \tag{6.3.29}$$

Finally, taking the values along edges $\mathbf{x} = \mathbf{x}' = (0, y)$, gives us the self correlation of the edge in Fourier space as

$$\langle |h(q)|^2 \rangle = \frac{k_B T}{L} G(0,0,q). \tag{6.3.30}$$

6.4 Molecular dynamics of a free edge

In this section we process MD simulations for lipid membranes and graphene monolayer sheets. The geometry is the same as discussed in the preceding section. We assume periodic boundary condition along the the free edge. We also set the clamped opposite edge far enough from the free edge such that the fluctuations on the free edge are not affected by the boundary condition on the opposite edge.

Graphene monolayer has been recognized as a solid membrane, where the in and out-of-plane deformations are coupled. The kinematic of the deformation in solid membranes is analogous to von-Karman plate theory. Let $\mathbf{u}$ and h be the in and out-of-plane displacement

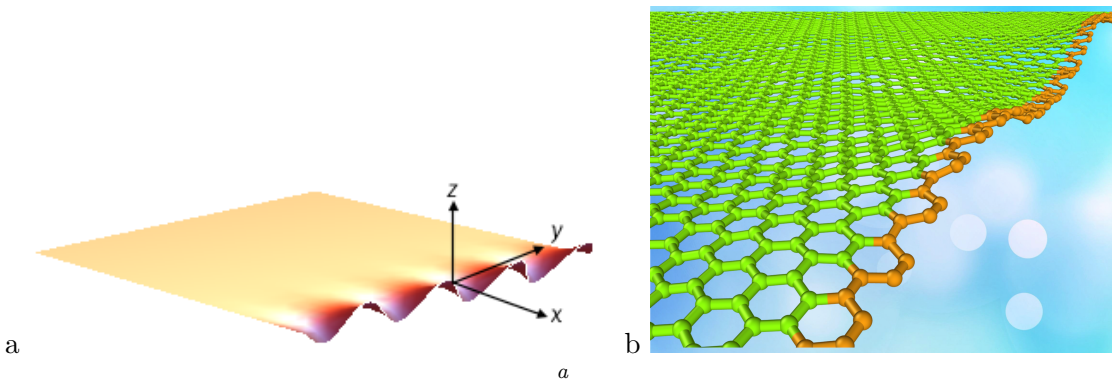

Figure 6.4.1: Details on the geometry of the simulation. (a) Schematic of a sheet with one free edge. (b) Snapshots from MD simulations of graphene, with free edges.

[a](a)While the opposite edge is clamped, the other two perpendicular edges are simply-supported. We have used this boundary conditions in MD simulations of graphene to stabilize the free edge. (b) The dimensions of the sheet is shown, with $L_0 = 8.5nm$. We have used periodic boundary conditions in z-directions. The distance between the two sheets is $d = 24nm$. This will ensure that the sheets are not interacting with each other.

fields, respectively. Then the in-plane strain field is defined as

$$\varepsilon_{\gamma\delta} = \frac{1}{2}\left(\frac{\partial u_\gamma}{\partial x_\delta} + \frac{\partial u_\delta}{\partial x_\gamma} + \frac{\partial h}{\partial x_\gamma}\frac{\partial h}{\partial x_\delta}\right). \tag{6.4.1}$$

Having the strain field in (6.4.1), the resulting stress tensor can be written as

$$\sigma_{\gamma\delta} = \frac{E}{1-\nu^2}\left(\varepsilon_{\gamma\delta} + \frac{\nu}{1-\nu}\varepsilon_{kk}\delta_{\gamma\delta}\right), \tag{6.4.2}$$

where E and ν are the elastic Young modulus and poisson ratio of the graphene sheet, respectively. Then, using the above stress field and the strain field in (6.4.1), the in-plane strain energy can be written as

$$U_s = \int \frac{1}{2}\sigma_{\gamma\delta}\varepsilon_{\gamma\delta}, \tag{6.4.3}$$

which implies that even in the absence of the in-plane motions—where $\mathbf{u} = 0$—the out-of-plane deformations results in a *quartic* stretching energy. The total energy is the summation of the bending energy and the stretching energy in (6.4.3). Due to the nonlinear contribution of the stretching energy, the thermal fluctuations of graphene monolayers are not analytically obtainable even for an infinite sheet, with no boundaries. MD simulations of

graphene monolayers, with periodic boundary conditions in all directions, show that the apparent bending stiffness of graphene at finite temperature is much larger than its bare value—at zero kelvin. This can be physically explained by the fact that graphene's in-plane Young's modulus is relatively high that at finite temperature, suppresses the fluctuations—due to nonlinearities. Consequently, the bare value of graphene monolayers are all reported at zero kelvin. At finite temperature, depending on the size of the sheet and the temperature, graphene monolayers exhibit stiffening with various intensities.

In this work, the linear elasticity gives us an estimate of the mechanical properties. To minimize the effects arising from nonlinearities, we perform MD simulations under NPT ensemble to relax the in-plane stress field as much as possible.

We perform MD simulations of monolayer graphene using LAMMPS, an open source code [137]. The second- generation reactive empirical bond-order (REBO) potential [138] is used for the multibody C–C interactions in graphene. The temperature is controlled by a Nose-Hoover thermostat. Each simulation runs up to 20 ns (time step: 1 fs), with the first 10 ns for the system to equilibrate and the subsequent 10 ns for calculations of the time-averaged quantities. The time integration scheme closely follows the time-reversible measure-preserving Verlet and rRESPA integrators derived by Tuckerman et al. [139]. In order to avoid interlayer interactions, relatively thick simulation boxes are used (thickness 24.5 nm). The free edge studied in this work is armchair, however, same procedure can be applied to zigzag edge or any mixture of these two. Graphene monolayer, with a free edge undergoes relatively large fluctuations. Beyond a certain size scale the free edge becomes unstable and undergoes folding and rotating around the clamped edge. In order to stabilize the free edge a slightly different boundary condition is used for graphene, compared to lipid bilayers. The schematic is shown in Figure 6.4.1 where three edges are fixed and one edge is allowed to freely fluctuate. To model the simply supported edges, only one row of the atoms on the edge is fixed. For the clamped edge, more than one row of atoms should be fixed to satisfy the boundary conditions on both displacement field (h) as well as the gradient of the displacement field (∇h). While this geometry stabilizes the free edge, it doesn't add much complexity to our theoretical calculations. For further details, the reader is referred

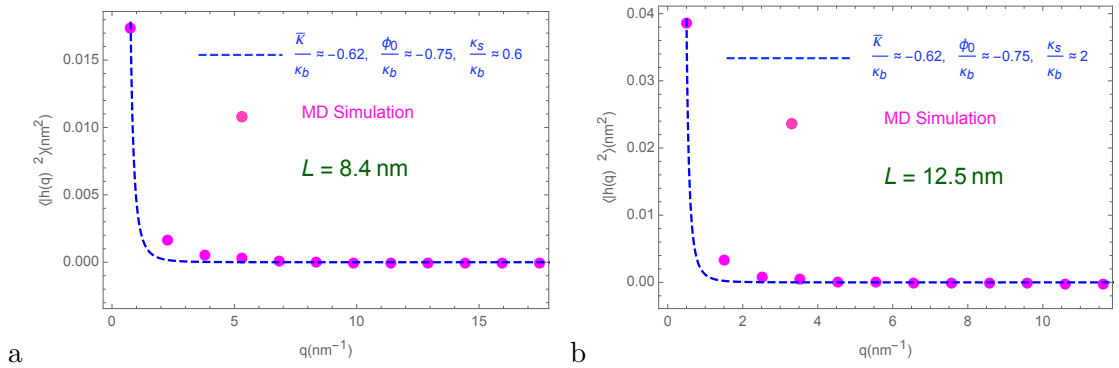

Figure 6.4.2: Fluctuations of the free edge of graphene monolayer for two sizes of $L = 8.4nm$ and $L = 12.5nm$.

to the supplementary materials.

6.5 Results

With the simulations complete, the data along the edge must undergo a discrete Fourier transform defined by

$$h(q) = \frac{1}{N}\sum_{k=1}^{N} z(0, y_k)e^{-iqy_k}\,, \tag{6.5.1}$$

where N is the number of data points along the edge, $z(0, y_k)$ is the height fluctuation, and q is given by $q = 2\pi m L^{-1}$ with $m = 0, 1, 2, ...$ The transformed fluctuation spectrum can then be related to the Green's function by (6.3.30).

With the Fourier transformed data, the solution $G(0, 0, q)$ is fit to the data using a least squares fit to find the optimized values for the Gaussian modulus, edge modulus, and edge tension.

For graphene monolayer, since we have used a different boundary conditions, the Fourier transform of the data is not the same as (6.5.1). In fact, in each mode, we can have either $\sin(qy)$ *or* $\cos(qy)$ and *not both* of them. Let the length of the free edge be $2L$ expanded in the domain $-L < y < L$ and $q = \pi m/L$. Then the deformation modes have to satisfy $h(L) = h(-L) = 0$. Hence, we cannot have eigenfunctions such as $\cos(2\pi ny/2L)$ or $\sin((2n-1)\pi x/2L)$. Accordingly, for odd (even) values of m, we only used $\sin(m\pi y/L)$

$(\sin(m\pi y/L))$. The results are shown in Figure 6.4.2 for two different sizes $L = 8.4nm$ and $L = 12.5nm$.

6.6 Discussion and Conclusion

I this work, a new method is presented to estimate the Gaussian modulus and edge properties by studying the thermal fluctuations of an open edge. In the following we discuss the results on Gaussian modulus and edge properties of graphene monolayer.

The results on fluctuations of a graphene edge is demonstrated in Figure 6.4.2. Existing values for graphene mechanical properties in the literature are mostly reported at zero Kelvin. Even the bare value of the bending modulus κ_b cannot be extracted at finite temperature, using fluctuations spectra. This is due to the coupling between the in- and out-of-plane deformations that stiffens the graphene sheet against out-of-plane fluctuations. Accordingly, the fluctuations data for graphene sheet, within periodic boundary conditions at finite temperature, do not follow the $1/q^4$ trend. The theoretical model used in this work, is however based on linearized elasticity and assumes uncoupled in- and out-of-plane deformations. In this manner, using the *effective* bending modulus, instead of its *bare* value gives us better fit of the data from MD simulations. The effective bending stiffness of graphene appeared to be size-dependent. For larger size, given that the long wave-length fluctuations are larger, the nonlinear in-plane energy cost has stronger stiffening effects. For further details on the variations of effective bending stiffness with respect to membrane size and temperature, the reader is referred to[71]. Here, we simply used $\kappa^{\text{eff}} \sim 160 k_B T$, while typical bare values for graphene at zero Kelvin is reported in the range of $\kappa_b \sim (50 - 70) k_B T$[8]. Our estimation is based on comparison of some of the data on fluctuations of graphene sheet at room temperature[71] with the harmonic approximation; $\langle h^2 \rangle \propto L^2/\kappa^{\text{eff}}$.

Similarly, the Gaussian modulus and edge properties are likely to get renormalized at finite temperature. In this case, one may either use the corresponding bare values of these

[8] $k_B T$ is the energy scale at room temperature, $T = 300$K.

properties —that are reported at zero Kelvin— within fully nonlinear elasticity, or use the corresponding renormalized values within linear approximation. Note that a free edge undergoes larger thermal fluctuations than the rest of the membrane. In fact, a free edge, influenced by edge forces, sustains ground-state non-zero deformations, that arise from the competition between in-plane stretching energy and the compressive edge force. At finite temperature, if the effective stiffness of the graphene is κ_1 and the effective stiffness of the edge is κ_2, one can observe stiffening at the edge; i.e. $\kappa_2 > \kappa_1$, by comparing their fluctuations spectra. This effect can be captured by the edge modulus κ_s. Our results show that for larger sizes of the edge, this value should be larger to fit the MD data. This is due to the fact that for longer wave-length fluctuations the stiffening effects of the nonlinear in-plane energy become stronger.

In molecular dynamic simulations of graphene, we observed that the free edge within periodic boundary condition, is unstable and undergoes folding and rotating around that clamped edge. To stabilize the edge, we slightly modify the other two perpendicular edges to simply-supported, where the displacement field is zero. To stimulate the simply supported boundary condition, we set the displacement of all the atoms at these edges to be zero. In this way, Fourier transform of the deformation function of the free edge, does not include all the modes as in periodic boundary condition. Only those modes that satisfy the simply-supported boundary conditions will be present. Let the free edge of length $2L$ extend in domain $-L < y < L$. Then the deformation modes have to satisfy $h(L) = h(-L) = 0$. Hence, we cannot have eigenfunctions such as $\cos(2\pi ny/L)$ or $\sin((2n-1)\pi x/L)$. Accordingly, we have removed these modes when transforming the MD data into Fourier space. While this boundary condition, stabilize the free edge, it appeared not to add much complexity into our calculations.

Finally, we highlight that while the edge properties and Gaussian modulus can be calculated for both fluid and solid membranes using the present method, the results for solid membranes require some physical interpretations as the properties get renormalized by the temperature. Our work is likely to provide a new route— for the first time— to extract

these properties from fluctuations spectra.

Chapter 7

Renormalization of Flexoelectricity in Lipid Bilayer Membranes due to External Charge and Dipolar Distributions

In this communication we show that the interplay between the deformation geometric-nonlinearity and distributions of external charges and dipoles lead to the renormalization of the the membrane's native flexoelectric response. Our work provides a framework for a mesoscopic interpretation of flexoelectricity and if necessary, artificially "design" tailored flexoelectricity in membranes. Comparison with experiments indicate reasonable quantitative agreement.

7.1 Introduction

There is growing evidence that flexoelectricity provides one of the key mechanisms that permits biological membranes to couple mechanical deformation to electrical stimuli. Specifically, flexoelectricity refers to the development of polarization upon change in membrane

curvature. Mathematically

$$\mathbf{P}^S = \gamma\kappa\mathbf{n}, \tag{7.1.1}$$

where $\mathbf{P}^S$ is the area density of the electric polarization, γ is defined as flexoelectric coefficient, κ is the mean curvature, and $\mathbf{n}$ is the unit normal vector on the surface. While this effect was first appreciated in liquid crystals [161], parallel developments have occurred in crystalline materials also cf. [162] and references therein. In the context of biological membranes, the pioneering work is that due to Petrov who has also authored two review articles on this topic [163, 164] that summarize a fair amount of the literature on this topic.

Recent attention to this phenomenon has primarily been spurred via the postulated ramifications of flexoelectricity in various biological functions e.g. outer hair cell electromotility and its role in cochlear amplification and sharp frequency discrimination [76, 165, 166], tether formation [47, 167] and ion transport[168]. It is also worthwhile to point out a recent work by Brownell et. al. [47] that provides the most compelling experimental evidence to date of the converse flexoelectric effect.

In this work we examine the effect of external charges or dipolar distributions on the apparent flexoelectricity of a lipid bilayer membrane. In a naively linearized setting, external charges do not change the apparent flexoelectricity. We show, however, that carefully accounting for geometric nonlinearity and the associated change in the electrical quantity permits the observation of some non-trivial coupling effects. Insightful works in this direction have appeared earlier. For example, Ref. [169] developed a simple model to understand the contribution of electric double layers on the flexoelectric coefficient. The focus of the present work is to (i) provide a rigorous framework to link external charges and dipoles to flexoelectricity which can be then easily be generalized to complex situations, (ii) show that the external charges and dipoles renormalize the flexoelectric coefficient *because* of the interaction of geometric nonlinearity of deformation and electrostatics, and (iii) make some simple predictions to interpret existing experiments showing low and high values of flexoelectricty for different types of membranes.

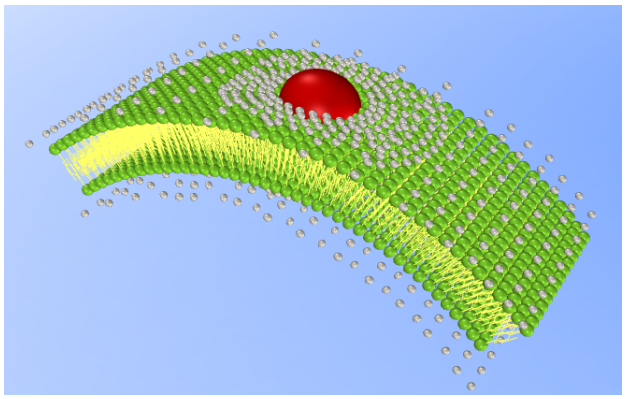

Figure 7.1.1: Lipid bilayer inside an electrolyte bath.

[a]The head molecules are charged and due to curvature there will ensue a net polarization inside the membrane, $P(r)$. Also the ionized water molecules are attracted by the negative head molecules of the membrane and make an external dipole layer, $P^e(r)$.

7.2 Theoretical Framework

We begin with the three dimensional theory of flexoelectric materials and derive the theory for membrane by making some kinematic assumptions. Let $\mathbb{U} \subset \mathbb{R}^2$ be an open bounded domain in XY-plane. Consider a thin dielectric membrane occupying $\Omega_R = \mathbb{U} \times (-h/2, h/2) \subset \mathbb{R}^3$, where h is the thickness of the membrane and the subscript R indicates the *reference configuration*. Let $(\boldsymbol{\chi}, \mathbf{P}) : \Omega_R \to \mathbb{R}^3 \times \mathbb{R}^3$ be the deformation and polarization describing the thermodynamic state of the membrane, $\mathbf{X} = (X, Y, Z)$ (resp. $\boldsymbol{\chi} = (x, y, z)$) be the Lagrangian (resp. Euler) coordinates, $\mathbf{F} = \mathrm{Grad}\boldsymbol{\chi}$ be the deformation gradient, $\mathbf{C} = \mathbf{F}^T\mathbf{F}$ is the Cauchy-Green strain tensor, and $J = \det \mathbf{F}$ be the Jacobian. Also, assume that there exist external polarization $\mathbf{P}_0^e : \Omega_R \to \mathbb{R}^3$ and charge density $\rho_0^e : \Omega_R \to \mathbb{R}$ attached to the material points of the membrane, and the top and bottom surfaces of the membrane are short-circuited. In the *reference configuration* the Maxwell equation can be written as

$$\mathrm{Div}\mathbf{D} = \rho_0^e, \tag{7.2.1}$$

where $\mathbf{D} = -\epsilon_0 J\mathbf{C}^{-1}\mathrm{Grad}\xi + \mathbf{F}^{-1}(\mathbf{P} + \mathbf{P}_0^e)$ is the electric displacement defined in Ω_R, and the potential $\xi = 0$ on the top & bottom surface. Since the membrane is thin, bending

is presumably the dominating mode of deformation and hence the Kirchhoff hypothesis is enforced ($\boldsymbol{\chi} = (x, y, z)$)

$$x = X - Z\frac{\partial w(X,Y)}{\partial X}, \qquad y = Y - Z\frac{\partial w(X,Y)}{\partial Y},$$
$$z = Z + w(X,Y), \tag{7.2.2}$$

where $w(X, Y)$ is the out-of-plane displacement of the mid-plane ($Z = 0$). Further, we introduce polarization per unit area as

$$\mathbf{P}^S = (P_X^S, P_Y^S, P_Z^S) = \int_{-h/2}^{h/2} \mathbf{P}(X, Y, Z)dZ.$$

To model the flexoelectric effect, we postulate that the internal/stored energy of the membrane is given by

$$U[\boldsymbol{\chi}, \mathbf{P}] = \int_{\mathbb{U}} \Big[\frac{1}{2}k_b(\Delta w)^2 + fP_Z^S\Delta w + \frac{1}{2}a|\mathbf{P}^S|^2\Big], \tag{7.2.3}$$

where $\Delta(\cdot) = \frac{\partial^2(\cdot)}{\partial X^2} + \frac{\partial^2(\cdot)}{\partial Y^2}$ is the in-plane Laplace operator with respect to the Lagrangian coordinates, and k_b, f and a are material constants. In particular, the first term is the classical Helfrich-Canham bending energy, the second gives rise to flexoelectric coupling and the last term describes the dielectric property of the membrane. By the principle of minimum free energy we claim that the equilibrium state of the membrane is determined by the minimization problem

$$\min_{(\boldsymbol{\chi},\mathbf{P})}\{F[\boldsymbol{\chi}, \mathbf{P}] := U[\boldsymbol{\chi}, \mathbf{P}] + \mathcal{E}^{\text{elect}}[\boldsymbol{\chi}, \mathbf{P}]\}, \tag{7.2.4}$$

where $\mathcal{E}^{\text{elect}}$ is the electric energy associated with the electric field and boundary devices [17]

$$\mathcal{E}^{\text{elect}}[\boldsymbol{\chi}, \mathbf{P}] = \frac{\epsilon_0}{2}\int_{\Omega_R} J|\mathbf{F}^{-T}\text{Grad}\xi|^2.$$

To find the Euler-Lagrange equations associated with (7.2.4), we now consider the variations of displacement and polarization

$$w \to w_\delta = w + \delta\tilde{w}, \qquad \mathbf{P} \to \mathbf{P}_\delta = \mathbf{P} + \delta\tilde{\mathbf{P}}.$$

Then the first variation of the total free energy shall vanish for any $(\tilde{w}, \tilde{\mathbf{P}})$

$$\frac{d}{d\delta} F[\boldsymbol{\chi}_\delta, \mathbf{P}_\delta]\Big|_{\delta=0} = 0.$$

By tedious yet standard calculation and keeping only the leading order terms [170], we obtain the following Euler-Lagrange equations on the mid-plane $\mathbb{U}$

$$\begin{cases} aP_X^S + h\xi_{,X} = 0, \\ aP_Y^S + h\xi_{,X} = 0, \\ f\Delta w + aP_Z^S + h\xi_{,Z} = 0, \\ \Delta(k_b\Delta w + fP_Z^S) - f_Z^{\text{elect}} = 0, \end{cases} \tag{7.2.5}$$

where

$$f_Z^{\text{elect}} = \int_{-h/2}^{h/2} [\Sigma_{31}^{\text{MW}} - \Sigma_{13}^{\text{MW}}]_{,X} + [\Sigma_{32}^{\text{MW}} - \Sigma_{23}^{\text{MW}}]_{,Y}\, dZ$$

is the Z component of the electrostatic force and

$$\boldsymbol{\Sigma}_{\text{MW}} = -\frac{\epsilon_0}{2} J|\text{grad}\xi|^2 \mathbf{F}^{-T} - \text{grad}\xi \otimes \mathbf{D} \tag{7.2.6}$$

is the *Piola-Maxwell* stress. We remark that equations (7.2.5)-(7.2.6), together with the Maxwell equation (7.2.1) for electrostatics form a a closed system with five equations and five unknowns $\xi, w, P_X^S, P_Y^S, P_Z^S$. Analytical solutions to the above nonlinear differential equations will be interesting but difficult and not addressed here.

In this paper we will study a simple problem to asses the role of external charges and dipoles on the "apparent flexoelectricity" of a membrane. To this end, we conduct a thought

experiment and re-define the flexoelectric coupling coefficient f in terms of change of electric displacement. Consider a flat membrane with zero curvature which is referred to as the initial state whereas the final state of our experiment is a bent membrane having a net polarization. We denote by $\mathbf{D}^i$ and $\mathbf{D}^f$ the electric displacement for the initial and final states in the reference configuration, respectively. For simplicity, suppose that the in-plane components of the polarization are negligible and the membrane is under one dimensional uniform bending — fairly reasonable assumptions for small curvatures. Since the potential difference across the thickness of the membrane is zero and the polarization density is constant along the thickness of the membrane, then from the third equation of (7.2.5) we obtain: $P_Z^S = -\frac{f\kappa}{a}$, where $\kappa = \Delta w = const.$ We further assume that the polarization density is constant along the thickness and obtain the polarization (per unit volume) $\mathbf{P} = \frac{\mathbf{P}^S}{h}$.

The measurable quantity is the electric current in this process. Recall that the electric displacement in the reference configuration is given by $\mathbf{D} = -\epsilon_0 J\mathbf{C}^{-1}\text{Grad}\xi + \mathbf{F}^{-1}(\mathbf{P} + \mathbf{P}^e)$ and denote by D_Z^f and D_Z^i be the final and initial out-of-plane components of the electric displacement, respectively. By an ammeter we can measure the change in the electric displacement in two stages as below

$$Q = \int_0^\infty I(t)dt = (D_Z^f - D_Z^i)\Big|_{Z=0} A,$$

where A is the area of the membrane. Now, in the absence of external charges and polarization $\mathbf{P}_0^e = \rho_0^e = 0$, the solution to the electrostatic problem (7.2.1) is clearly given by $\xi = 0$ in Ω_R, and therefore, $D_Z^f - D_Z^i = \frac{P_Z^S}{h}$, and hence

$$f = -\frac{Q}{\kappa A}ah = -\frac{D_Z^f - D_Z^i}{\kappa}ah. \tag{7.2.7}$$

Since the current (or charge Q) is the quantity that is measured in experiments, we now *define* the "apparent" or effective fleoxelectric constant, pristine or with external charges and dipoles, by the above equation. Before proceeding further, it is instructive to examine the relation between the flexoelectric constant in our model f to the one often found in the literature and cited in the introduction (7.1.1): γ. In our theoretical framework, for a

homogenous membrane and in the absence of an external electric field, the third equation of (7.2.5) implies that: $P = -\frac{f}{a}\kappa$. In view of (7.1.1), we obtain that: $\gamma = -\frac{f}{a}$.

7.3 Flexoelectric coefficient in the presence of external charges and dipoles

The primary constituent of any biomembrane is a molecule with two different subdomains; one is hydrophilic and tends to attract the positive charges inside the electrolyte, while the other part is hydrophobic. When these molecules are exposed to water, they arrange themselves into two sheets in a way that the hydrophobic tails group point in toward the center of the bilayer, while the hydrophilic head molecules tends to be in contact with the ionized water molecules. During deformation, the density of charges and dipoles inside and on the surfaces of the membrane alters and results in a nonzero net polarization. For simplicity, here we consider a small part of a cylindrically deformed lipid membrane inside an electrolyte bath, Fig. 7.3.1. Lipid molecules may carry dipoles or charges either along the thickness of the membrane or on the surfaces. These dipoles and charges might be "external" or the intrinsic properties of the lipid molecules. The former may be due to proteins and ion channels, for instance. In the following section, we consider the simplest possible case, in which the distributions of the charges and dipoles are radial neglecting any angular variation. The simplifying assumption is useful for illustration however the framework described earlier can be used for more general cases also. Consider a cylindrically deformed membrane of radius R, as shown in Fig. 7.3.1. Let ρ_0^e, P_0^e be the external charge density and the out-of-plane polarization in the reference configuration that are independent of in-plane positions. Assume that the induced out-of-plane polarization P is also independent of in-plane positions. Then in the current configuration the external and induced polarization p^e, p in the current configuration, to the leading order, orient radially, together with the

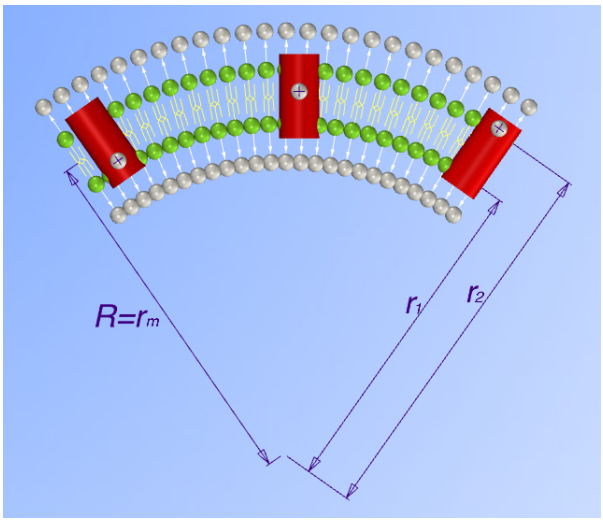

Figure 7.3.1: Lipid bilayer under external charges and dipoles.

external charge density ρ^e, can only be a function of r, and for $r \in (r_1, r_2)$,

$$\begin{cases} p(r) = P(r - r_m)/J, \\ p^e(r) = P_0^e(r - r_m)/J, \\ \rho^e(r) = \rho_0^e(r - r_m)/J, \end{cases} \tag{7.3.1}$$

where r_1, r_2 and r_m are the radiuses of the inner, outer and middle surfaces, respectively, and $r_2 - r_1 = h$ is the thickness of the membrane. Based on the symmetry assume that the electric potential $\xi = \xi(r)$. Then in the current polar coordinates equation (7.2.1) can be written as

$$\frac{1}{r}\frac{d}{dr}\{r[-\epsilon_0 \frac{d}{dr}\xi + p(r) + p^e(r)]\} = \rho^e(r). \tag{7.3.2}$$

Let $d(r) = -\epsilon_0 \frac{d}{dr}\xi + p(r) + p^e(r)$ be the radial electric displacement in the current configuration. Imposing the short circuit condition, we obtain

$$d(r_1) = \frac{1}{h}\int_{r_1}^{r_2} \left(p + p^e - \frac{1}{r}\int_{r_1}^{r} r'\rho(r')dr'\right) dr. \tag{7.3.3}$$

To assess the change in dielectric displacement, we subtract the electric displacement at zero curvature. Based on the small curvature assumption, we have $J(r) = \frac{r}{r_m}$. We denote by d^i and d^f the initial and final electric displacements in the current configuration, respectively. Let $\varepsilon = \kappa(r - r_m)$. Then the change in the out-of-plane electric displacement is

$$\begin{aligned} d^f(r_1) - d^i(r_1) &= \frac{1}{h}\int_{r_1}^{r_2}\Big(\frac{P_0(r) - \varepsilon P_0^e(r)}{J} \\ &\quad + \frac{1}{r}\int_{r_1}^{r} r'\frac{\varepsilon\rho_0^e(r')}{J}dr'\Big)dr \\ &= -\kappa\Big\{\frac{r_m f}{r_1 ah} + \frac{1}{h}\int_{r_1}^{r_2}\Big(\frac{r_m(r - r_m)}{r}P_0^e(r) \\ &\quad - \frac{1}{r}\int_{r_1}^{r} r_m(r' - r_m)\rho_0^e(r')dr'\Big)dr\Big\}. \end{aligned}$$

As before, we need to evaluate the change of electric displacement in the reference configuration. Noticing that $\mathbf{D} = J\mathbf{F}^{-1}\mathbf{d}$ and neglecting the higher orders of small terms we obtain:

$$D^f(r_1) - D^i(r_1) = \frac{r_1}{r_m}\left(d^f(r_1) - d^i(r_1)\right). \tag{7.3.4}$$

Again, we assess the apparent flexoelectric coefficient by Eq. (7.2.7), and obtain

$$\begin{aligned} f_{\text{eff}} &= -\frac{D^f(r_1) - D^i(r_1)}{\kappa}ah \\ &=: f + f_P^e + f_C^e, \end{aligned}$$

where f_P^e and f_C^e, given by

$$f_P^e = a\int_{r_1}^{r_2}\frac{r_1(r - r_m)}{r}P_0^e(r)dr, \tag{7.3.5}$$

$$f_C^e = -a\int_{r_1}^{r_2}\frac{1}{r}\int_{r_1}^{r} r_1(r' - r_m)\rho_0^e(r')dr'dr, \tag{7.3.6}$$

are the flexoelectric coefficients due to external polarization and charge, respectively. We now consider, in turn, as also discussed in Petrov[163], the dipolar and monopole charge contributions to the effective flexoelectricity.

7.4 Results and Discussion

7.4.1 Contribution of External Charges to the Effective Flexoelectricity

In this part we estimate $-\frac{f_C^e}{a}$. The charges may be either due to the negative head of the lipid molecules or positive ions of electrolyte which are attracted by the fully hydrated head groups or the ion pump channels along the thickness of the membrane, as shown in Fig. 2. For simplicity, we only focus on the first case—-the charges are distributed over the inner and outer surfaces of the membrane. After deformation, the charge densities on both sides differ in an opposite sense. The outer surface charge density will be smaller due to stretching of the surface, while the converse is true for the inner surface due to compression. Also we can estimate the ion per head lipid to be a few unit of the electron charge, $-1.6 \times 10^{-19} C$. Assuming that the thickness of the membrane is about $5nm$, we evaluate the Eq. (7.3.6) and obtain: $-\frac{f_C^e}{a} = 2.85 \times 10^{-18} C$. This value is of the same order of magnitude of the experimental results.

7.4.2 Contribution of External Dipoles and Integral Proteins to the Effective Flexoeelctricity

In this case, we refer to Fig. 2, in which a membrane is under uniform external dipole layers on the inner and outer surfaces. First we estimate the external polarization density (per area). According to [171]the thickness of the fully hydrated region is about $0.5nm$ and the area per lipid head is about $70\mathring{A}$. Based on these values, one may obtain the polarization density (per area) as: $P^S = 1.14 \times 10^{-10} C \cdot m^{-1}$. Integrating Eq. (7.3.5)over the thickness of the membrane results in: $-\frac{f_P^e}{a} = 5.7 \times 10^{-19} C$. Here we note that experimentally the value of $-\frac{f_P^e}{a}$ has been measured to be a few times of $10^{-18} C$, [163]. The results obtained above depend on the magnitude of the dipoles on the surface. The thickness of the dipole layers is between $0.3 - 1nm$. Therefore, the resultant flexoelectric coefficient can be larger by a factor of 2. Our model allows us to approximately assess the effect of dipole carrying proteins on the effective flexoelectricity. Proteins often carry very large dipole moments e.g. the following have been measured: $480D$ for chymotrypsin, $637D$ for carboxypeptidase A [172]. A detailed boundary value solution for an embedded protein is left for future work,

however, a simple approximation that the protein dipole moment is uniformly smeared across the membrane can readily yield analytical results. While this approximation will ignore a geometrical effect, our model can be however then used trivially to obtain an estimate via the expression for f_P^e. To this end we need to estimate the dipole density due to the integral proteins along the thickness of the membrane. The diameter of the protein's structure is also a few nanometers.

Using $P^p = 500D = 1667.8 \times 10^{-30}\ C \cdot m$ for the dipole moment of the protein, $A^p = \pi \times 10^{-18} m^2$ for the area of the protein and $h = 5 \times 10^{-9} m$, we obtain $1.3 \times 10^{-18} C$ for the flexoelectric coefficient.

As it can be seen from the above calculation, the effect of the dipole carrying integral proteins is fairly substantial and explains the large values experimentally observed.

7.5 Conclusions

The key conclusion of the present work is that it is the interplay between the geometrically nonlinear deformation and electrostatics that lead to the renormalization of flexoelectricity in the presence of external charges and dipoles—-this effect will not be seen in a purely linearized setting where careful distinction is not made between reference and deformed configurations. Our framework is general and can be used to examine the flexoelectric response for membranes with complex electrostatic environment (albeit the calculations may have to proceed numerically). Using simple approximations, we are however, able to provide illustrative and transparent analytical solutions to several cases and make reasonable estimates of the flexoelectric response of different types of membranes. Interestingly, our results point also to the prospects of artificially designing high or low flexoelectricity in model membrane systems.

Chapter 8

Concluding Remarks

In this dissertation, we have addressed several issues in statistical mechanics of 2D materials. Geometrical and constitutive nonlinearities are addressed for both fluid and solid membranes in chapters 2, 3 and 5. Further, constrained fluctuations and effects of boundary conditions are implemented in chapters 4 and 6. Specifically, the following results are obtained in these contexts:

- We have pointed out the rather large discrepancy that exists between the (experimentally estimated) minimum electric field that an ideal fluid membrane can detect and what the existing theoretical models predict. A consistent accounting for the influence of the nonlinear dielectric behavior of membranes on the thermal fluctuations of the membrane electric field appears, in large part, to address this issue. Our mathematical framework yields analytical solution for the thermal electrical noise of membranes. The predictions of our theoretical framework provide noise estimates that are of the same order of magnitude as experiments. In particular, our work provides both a benchmark estimate for model fluid membranes and reasonable predictions for biological membranes.

- A closed-form expression for the spectra of the thermal fluctuations of spherical vesicles duly incorporating nonlinear curvature elasticity terms is presented in Section 3. In conjunction with our results, either molecular dynamics simulations or experimen-

tal flicker spectroscopy may now be used to extract nonlinear elasticity properties. The renormalized bending rigidity due to thermal fluctuations is found to be size-dependent and a dramatic stiffening is predicted to occur for small sub-20 nm vesicle sizes.

- Using a variational perturbation method, we presented a "mechanics-oriented" novel treatment of the thermal fluctuations of graphene, fully accounting for deformation nonlinearities, and evaluated their effect on the effective bending stiffness. We compared the results from our approach to both molecular dynamics simulations as well as other analytical methods in the literature. Our prediction is in a fairly good agreement with the data from molecular dynamic simulations.

- A new approach is presented in chapter 6 to extract the Gaussian modulus and edge properties from the fluctuations spectra at a free edge. Recognizing that the Gaussian modulus plays a non-trivial role in the fluctuations of a membrane edge, we derived closed-form expressions for edge fluctuations. Combined with atomistic simulations, we use the developed approach to extract Gaussian modulus of graphene. While this method can be used directly for fluid membranes, the results for solid membranes, require some careful physical interpretations as the geometric nonlinearities renormalize the effective mechanical properties at finite temperature.

Finally, we studied flexoelectricity as a distinct form of electromechanical coupling in 2D nano-materials, specifically for biological membranes. The interplay between the geometrically nonlinear deformation and electrostatics leads to the renormalization of flexoelectricity in the presence of external charges and dipoles—-this effect will not be seen in a purely linearized setting where careful distinction is not made between reference and deformed configurations. Our framework is general and can be used to examine the flexoelectric response for membranes with complex electrostatic environment.

Bibliography

[1] P. B. Canham, "The minimum energy of bending as a possible explanation of the biconcave shape of the human red blood cell," *Journal of theoretical biology*, vol. 26, no. 1, pp. 61–81, 1970.

[2] W. Helfrich, "Elastic properties of lipid bilayers: theory and possible experiments," *Zeitschrift für Naturforschung C*, vol. 28, no. 11-12, pp. 693–703, 1973.

[3] E. Abbena, S. Salamon, and A. Gray, *Modern differential geometry of curves and surfaces with Mathematica*. CRC press, 2006.

[4] P. C. Nelson, *Biological physics*. Worth, 2007.

[5] R. Phillips, J. Kondev, J. Theriot, and H. Garcia, *Physical biology of the cell*. Garland Science, 2012.

[6] R. Lipowsky, "The conformation of membranes," *Nature*, vol. 349, no. 6309, pp. 475–481, 1991.

[7] U. Seifert, "Configurations of fluid membranes and vesicles," *Advances in physics*, vol. 46, no. 1, pp. 13–137, 1997.

[8] S. A. Safran, *Statistical thermodynamics of surfaces, interfaces, and membranes*, vol. 90. Perseus Books, 1994.

[9] K. N. Kudin, G. E. Scuseria, and B. I. Yakobson, "C 2 f, bn, and c nanoshell elasticity from ab initio computations," *Physical Review B*, vol. 64, no. 23, p. 235406, 2001.

[10] Q. Lu, M. Arroyo, and R. Huang, "Elastic bending modulus of monolayer graphene," *Journal of Physics D: Applied Physics*, vol. 42, no. 10, p. 102002, 2009.

[11] P. Koskinen and O. O. Kit, "Approximate modeling of spherical membranes," *Physical Review B*, vol. 82, no. 23, p. 235420, 2010.

[12] I. Aleksandr and A. Khinchin, *Mathematical foundations of statistical mechanics*. Courier Corporation, 1949.

[13] R. Dimova, "Recent developments in the field of bending rigidity measurements on membranes," *Advances in colloid and interface science*, vol. 208, pp. 225–234, 2014.

[14] H. Engelhardt, H. Duwe, and E. Sackmann, "Bilayer bending elasticity measured by fourier analysis of thermally excited surface undulations of flaccid vesicles," *Journal de Physique Lettres*, vol. 46, no. 8, pp. 395–400, 1985.

[15] J. Faucon, M. Mitov, P. Méléard, I. Bivas, and P. Bothorel, "Bending elasticity and thermal fluctuations of lipid membranes. theoretical and experimental requirements," *Journal de physique*, vol. 50, no. 17, pp. 2389–2414, 1989.

[16] J. Pécréaux, H.-G. Döbereiner, J. Prost, J.-F. Joanny, and P. Bassereau, "Refined contour analysis of giant unilamellar vesicles," *The European Physical Journal E*, vol. 13, no. 3, pp. 277–290, 2004.

[17] L. Liu and P. Sharma, "Flexoelectricity and thermal fluctuations of lipid bilayer membranes: Renormalization of flexoelectric, dielectric, and elastic properties," *Physical Review E*, vol. 87, no. 3, p. 032715, 2013.

[18] P. Nelson and T. Powers, "Renormalization of chiral couplings in titled bilayer membranes," *Journal de Physique II*, vol. 3, no. 10, pp. 1535–1569, 1993.

[19] T. Powers and P. Nelson, "Fluctuating membranes with tilt order," *Journal de Physique II*, vol. 5, no. 11, pp. 1671–1678, 1995.

[20] R. Golestanian, M. Goulian, and M. Kardar, "Fluctuation-induced interactions between rods on a membrane," *Physical Review E*, vol. 54, no. 6, p. 6725, 1996.

[21] H.-K. Lin, R. Zandi, U. Mohideen, and L. P. Pryadko, "Fluctuation-induced forces between inclusions in a fluid membrane under tension," *Physical review letters*, vol. 107, no. 22, p. 228104, 2011.

[22] C. Yolcu and M. Deserno, "Membrane-mediated interactions between rigid inclusions: an effective field theory," *Physical Review E*, vol. 86, no. 3, p. 031906, 2012.

[23] T. Salditt, "Thermal fluctuations and stability of solid-supported lipid membranes," *Journal of Physics: Condensed Matter*, vol. 17, no. 6, p. R287, 2005.

[24] T. Auth, S. Safran, and N. S. Gov, "Fluctuations of coupled fluid and solid membranes with application to red blood cells," *Physical Review E*, vol. 76, no. 5, p. 051910, 2007.

[25] A. Fasolino, J. Los, and M. I. Katsnelson, "Intrinsic ripples in graphene," *Nature materials*, vol. 6, no. 11, pp. 858–861, 2007.

[26] O. Kit, T. Tallinen, L. Mahadevan, J. Timonen, and P. Koskinen, "Twisting graphene nanoribbons into carbon nanotubes," *Physical Review B*, vol. 85, no. 8, p. 085428, 2012.

[27] Z. Xu and M. J. Buehler, "Geometry controls conformation of graphene sheets: membranes, ribbons, and scrolls," *Acs Nano*, vol. 4, no. 7, pp. 3869–3876, 2010.

[28] M. Schneider, J. Jenkins, and W. Webb, "Thermal fluctuations of large quasi-spherical bimolecular phospholipid vesicles," *Journal de Physique*, vol. 45, no. 9, pp. 1457–1472, 1984.

[29] D. Morse and S. Milner, "Fluctuations and phase behavior of fluid membrane vesicles," *EPL (Europhysics Letters)*, vol. 26, no. 8, p. 565, 1994.

[30] D. C. Morse and S. T. Milner, "Statistical mechanics of closed fluid membranes," *Physical Review E*, vol. 52, no. 6, p. 5918, 1995.

[31] X. Michalet, D. Bensimon, and B. Fourcade, "Fluctuating vesicles of nonspherical topology," *Physical review letters*, vol. 72, no. 1, p. 168, 1994.

[32] U. Seifert, "The concept of effective tension for fluctuating vesicles," *Zeitschrift für Physik B Condensed Matter*, vol. 97, no. 2, pp. 299–309, 1995.

[33] L. Freund, "Entropic pressure between biomembranes in a periodic stack due to thermal fluctuations," *Proceedings of the National Academy of Sciences*, vol. 110, no. 6, pp. 2047–2051, 2013.

[34] P. Sharma, "Entropic force between membranes reexamined," *Proceedings of the National Academy of Sciences*, vol. 110, no. 6, pp. 1976–1977, 2013.

[35] T. Kuila, S. Bose, P. Khanra, A. K. Mishra, N. H. Kim, and J. H. Lee, "Recent advances in graphene-based biosensors," *Biosensors and Bioelectronics*, vol. 26, no. 12, pp. 4637–4648, 2011.

[36] M. Kalbacova, A. Broz, J. Kong, and M. Kalbac, "Graphene substrates promote adherence of human osteoblasts and mesenchymal stromal cells," *Carbon*, vol. 48, no. 15, pp. 4323–4329, 2010.

[37] T. R. Nayak, H. Andersen, V. S. Makam, C. Khaw, S. Bae, X. Xu, P.-L. R. Ee, J.-H. Ahn, B. H. Hong, and G. Pastorin, "Graphene for controlled and accelerated osteogenic differentiation of human mesenchymal stem cells," *ACS nano*, vol. 5, no. 6, pp. 4670–4678, 2011.

[38] X. Sun, Z. Liu, K. Welsher, J. T. Robinson, A. Goodwin, S. Zaric, and H. Dai, "Nano-graphene oxide for cellular imaging and drug delivery," *Nano research*, vol. 1, no. 3, pp. 203–212, 2008.

[39] X. Yang, Y. Wang, X. Huang, Y. Ma, Y. Huang, R. Yang, H. Duan, and Y. Chen, "Multi-functionalized graphene oxide based anticancer drug-carrier with dual-targeting function and ph-sensitivity," *Journal of materials chemistry*, vol. 21, no. 10, pp. 3448–3454, 2011.

[40] L. Feng, S. Zhang, and Z. Liu, "Graphene based gene transfection," *Nanoscale*, vol. 3, no. 3, pp. 1252–1257, 2011.

[41] Y. Li, H. Yuan, A. von dem Bussche, M. Creighton, R. H. Hurt, A. B. Kane, and H. Gao, "Graphene microsheets enter cells through spontaneous membrane penetration at edge asperities and corner sites," *Proceedings of the National Academy of Sciences*, vol. 110, no. 30, pp. 12295–12300, 2013.

[42] H. Gao, "Probing mechanical principles of cell–nanomaterial interactions," *Journal of the Mechanics and Physics of Solids*, vol. 62, pp. 312–339, 2014.

[43] R. Joshi, Q. Hu, K. Schoenbach, and H. Hjalmarson, "Improved energy model for membrane electroporation in biological cells subjected to electrical pulses," *Physical review E*, vol. 65, no. 4, p. 041920, 2002.

[44] R. Joshi, Q. Hu, R. Aly, K. Schoenbach, and H. Hjalmarson, "Self-consistent simulations of electroporation dynamics in biological cells subjected to ultrashort electrical pulses," *Physical Review E*, vol. 64, no. 1, p. 011913, 2001.

[45] J. C. Weaver, "Electroporation of cells and tissues," *IEEE Transactions on Plasma Science*, vol. 28, no. 1, pp. 24–33, 2000.

[46] S. W. Jones, "Overview of voltage-dependent calcium channels," *Journal of bioenergetics and biomembranes*, vol. 30, no. 4, pp. 299–312, 1998.

[47] W. E. Brownell, F. Qian, and B. Anvari, "Cell membrane tethers generate mechanical force in response to electrical stimulation," *Biophysical journal*, vol. 99, no. 3, pp. 845–852, 2010.

[48] R. D. Astumian, R. Adair, and J. C. Weaver, "Stochastic resonance at the single-cell level," *Nature*, vol. 388, no. 6643, pp. 632–633, 1997.

[49] S. M. Bezrukov and I. Vodyanoy, "Reply: Stochastic resonance at the single-cell level," *Nature*, vol. 388, no. 6643, pp. 633–633, 1997.

[50] M. H. Repacholi and B. Greenebaum, "Interaction of static and extremely low frequency electric and magnetic fields with living systems: health effects and research needs," *Bioelectromagnetics*, vol. 20, no. 3, pp. 133–160, 1999.

[51] P. Valberg, R. Kavet, and C. Rafferty, "Can low-level 50/60 hz electric and magnetic fields cause biological effects?," *Radiation Research*, vol. 148, no. 1, pp. 2–21, 1997.

[52] M. Simkó and M.-O. Mattsson, "Extremely low frequency electromagnetic fields as effectors of cellular responses in vitro: possible immune cell activation," *Journal of Cellular Biochemistry*, vol. 93, no. 1, pp. 83–92, 2004.

[53] E. Litvak, K. Foster, and M. Repacholi, "Health and safety implications of exposure to electromagnetic fields in the frequency range 300 hz to 10 mhz," *Bioelectromagnetics*, vol. 23, no. 1, pp. 68–82, 2002.

[54] F. Oosawa, "Field fluctuation in ionic solutions and its biological significance," *Journal of theoretical biology*, vol. 39, no. 2, pp. 373–386, 1973.

[55] J. Fay, "Thermal fluctuations of electric field and solute density in biological cells," *Physical Review E*, vol. 56, no. 3, p. 3460, 1997.

[56] J. C. Weaver, T. E. Vaughan, R. K. Adair, and R. D. Astumian, "Theoretical limits on the threshold for the response of long cells to weak extremely low frequency electric fields due to ionic and molecular flux rectification," *Biophysical journal*, vol. 75, no. 5, pp. 2251–2254, 1998.

[57] T. E. Vaughan and J. C. Weaver, "Molecular change signal-to-noise criteria for interpreting experiments involving exposure of biological systems to weakly interacting electromagnetic fields," *Bioelectromagnetics*, vol. 26, no. 4, pp. 305–322, 2005.

[58] K. J. McLeod, R. C. Lee, and H. P. Ehrlich, "Frequency dependence of electric field modulation of fibroblast protein synthesis," *Science*, vol. 236, no. 4807, pp. 1465–1469, 1987.

[59] S. F. Cleary, L.-M. Liu, R. Graham, and R. F. Diegelmann, "Modulation of tendon fibroplasia by exogenous electric currents," *Bioelectromagnetics*, vol. 9, no. 2, pp. 183–194, 1988.

[60] R. Goodman, C. Bassett, and A. S. Henderson, "Pulsing electromagnetic fields induce cellular transcription," *Science*, vol. 220, no. 4603, pp. 1283–1285, 1983.

[61] R. K. Adair, "Static and low-frequency magnetic field effects: health risks and therapies," *Reports on progress in Physics*, vol. 63, no. 3, p. 415, 2000.

[62] R. K. Adair, R. D. Astumian, and J. C. Weaver, "Detection of weak electric fields by sharks, rays, and skates," *Chaos: An Interdisciplinary Journal of Nonlinear Science*, vol. 8, no. 3, pp. 576–587, 1998.

[63] J. WEAVER and R. ASTUMIAN, "The response of living cells to very weak electric fields- the thermal noise limit," *Science*, vol. 247, no. 4941, pp. 459–462, 1990.

[64] R. K. Adair, "Constraints on biological effects of weak extremely-low-frequency electromagnetic fields," *Physical Review A*, vol. 43, no. 2, p. 1039, 1991.

[65] H. Kleinert, *Gauge fields in condensed matter*, vol. 2. World Scientific Singapore, 1989.

[66] M. Bachmann, H. Kleinert, and A. Pelster, "Fluctuation pressure of a stack of membranes," *Physical Review E*, vol. 63, no. 5, p. 051709, 2001.

[67] Y. Hanlumyuang, L. Liu, and P. Sharma, "Revisiting the entropic force between fluctuating biological membranes," *Journal of the Mechanics and Physics of Solids*, vol. 63, pp. 179–186, 2014.

[68] W. Helfrich, "Size distributions of vesicles: the role of the effective rigidity of membranes," *Journal de Physique*, vol. 47, no. 2, pp. 321–329, 1986.

[69] E. Guitter and M. Kardar, "Tethering, crumpling, and melting transitions in hexatic membranes," *EPL (Europhysics Letters)*, vol. 13, no. 5, p. 441, 1990.

[70] M. Bowick and A. Travesset, "Tubular phase of self-avoiding anisotropic crystalline membranes," *Physical Review E*, vol. 59, no. 5, p. 5659, 1999.

[71] W. Gao and R. Huang, "Thermomechanics of monolayer graphene: Rippling, thermal expansion and elasticity," *Journal of the Mechanics and Physics of Solids*, vol. 66, pp. 42–58, 2014.

[72] T. Su and P. K. Purohit, "Thermomechanics of a heterogeneous fluctuating chain," *Journal of the Mechanics and Physics of Solids*, vol. 58, no. 2, pp. 164–186, 2010.

[73] D. Chen and Y. Kulkarni, "Entropic interaction between fluctuating twin boundaries," *Journal of the Mechanics and Physics of Solids*, vol. 84, pp. 59–71, 2015.

[74] C. Kittel, *Elementary statistical physics*. Courier Corporation, 2004.

[75] P. Wiggins and R. Phillips, "Membrane-protein interactions in mechanosensitive channels," *Biophysical journal*, vol. 88, no. 2, pp. 880–902, 2005.

[76] R. M. Raphael, A. S. Popel, and W. E. Brownell, "A membrane bending model of outer hair cell electromotility," *Biophysical journal*, vol. 78, no. 6, pp. 2844–2862, 2000.

[77] S. Singer and G. L. Nicolson, "The fluid mosaic model of the structure of cell membranes," *Membranes and Viruses in Immunopathology; Day, SB, Good, RA, Eds*, pp. 7–47, 1972.

[78] J. N. Israelachvili, D. J. Mitchell, and B. W. Ninham, "Theory of self-assembly of lipid bilayers and vesicles," *Biochimica et Biophysica Acta (BBA)-Biomembranes*, vol. 470, no. 2, pp. 185–201, 1977.

[79] D. Steigmann, "Fluid films with curvature elasticity," *Archive for Rational Mechanics and Analysis*, vol. 150, no. 2, pp. 127–152, 1999.

[80] M. Maleki, B. Seguin, and E. Fried, "Kinematics, material symmetry, and energy densities for lipid bilayers with spontaneous curvature," *Biomechanics and modeling in mechanobiology*, vol. 12, no. 5, pp. 997–1017, 2013.

[81] M. Deserno, "Fluid lipid membranes: From differential geometry to curvature stresses," *Chemistry and physics of lipids*, vol. 185, pp. 11–45, 2015.

[82] D. Nelson, T. Piran, and S. Weinberg, *Statistical mechanics of membranes and surfaces*. World Scientific, 2004.

[83] R. Podgornik and V. A. Parsegian, "Thermal-mechanical fluctuations of fluid membranes in confined geometries: the case of soft confinement," *Langmuir*, vol. 8, no. 2, pp. 557–562, 1992.

[84] W. Helfrich and R.-M. Servuss, "Undulations, steric interaction and cohesion of fluid membranes," *Il Nuovo Cimento D*, vol. 3, no. 1, pp. 137–151, 1984.

[85] E. Evans, "Entropy-driven tension in vesicle membranes and unbinding of adherent vesicles," *Langmuir*, vol. 7, no. 9, pp. 1900–1908, 1991.

[86] M. Rao, "Active fusion and fission processes on a fluid membrane," *Physical review letters*, vol. 87, no. 12, p. 128101, 2001.

[87] J. C. Shillcock and R. Lipowsky, "The computational route from bilayer membranes to vesicle fusion," *Journal of Physics: Condensed Matter*, vol. 18, no. 28, p. S1191, 2006.

[88] W. Xu, X. Wang, Z. Zhong, A. Song, and J. Hao, "Influence of counterions on lauric acid vesicles and theoretical consideration of vesicle stability," *The Journal of Physical Chemistry B*, vol. 117, no. 1, pp. 242–251, 2012.

[89] O.-Y. Zhong-Can and W. Helfrich, "Bending energy of vesicle membranes: General expressions for the first, second, and third variation of the shape energy and applications to spheres and cylinders," *Physical Review A*, vol. 39, no. 10, p. 5280, 1989.

[90] A. Agrawal and D. J. Steigmann, "Boundary-value problems in the theory of lipid membranes," *Continuum Mechanics and Thermodynamics*, vol. 21, no. 1, pp. 57–82, 2009.

[91] D. J. Steigmann, "A concise derivation of membrane theory from three-dimensional nonlinear elasticity," *Journal of Elasticity*, vol. 97, no. 1, pp. 97–101, 2009.

[92] S. Givli, H. Giang, and K. Bhattacharya, "Stability of multicomponent biological membranes," *SIAM Journal on Applied Mathematics*, vol. 72, no. 2, pp. 489–511, 2012.

[93] N. Walani, J. Torres, and A. Agrawal, "Anisotropic spontaneous curvatures in lipid membranes," *Physical Review E*, vol. 89, no. 6, p. 062715, 2014.

[94] A. Biria, M. Maleki, and E. Fried, "Continuum theory for the edge of an open lipid bilayer," *Adv. Appl. Mech*, vol. 21, pp. 1–78, 2013.

[95] J. Fournier and P. Galatola, "Tubular vesicles and effective fourth-order membrane elastic theories," *EPL (Europhysics Letters)*, vol. 39, no. 2, p. 225, 1997.

[96] O. Manyuhina, J. Hetzel, M. Katsnelson, and A. Fasolino, "Non-spherical shapes of capsules within a fourth-order curvature model," *The European Physical Journal E*, vol. 32, no. 3, pp. 223–228, 2010.

[97] D. P. Siegel, "Fourth-order curvature energy model for the stability of bicontinuous inverted cubic phases in amphiphile- water systems," *Langmuir*, vol. 26, no. 11, pp. 8673–8683, 2010.

[98] J. Guven and M. M. Müller, "How paper folds: bending with local constraints," *Journal of Physics A: Mathematical and Theoretical*, vol. 41, no. 5, p. 055203, 2008.

[99] J. Guven, "Membrane geometry with auxiliary variables and quadratic constraints," *Journal of Physics A: Mathematical and General*, vol. 37, no. 28, p. L313, 2004.

[100] H. Kleinert, "Size distribution of spherical vesicles," *Physics Letters A*, vol. 116, no. 2, pp. 57–62, 1986.

[101] D. Föster, "On the scale dependence, due to thermal fluctuations, of the elastic properties of membranes," *Physics Letters A*, vol. 114, no. 3, pp. 115–120, 1986.

[102] L. Peliti and S. Leibler, "Effects of thermal fluctuations on systems with small surface tension," *Physical review letters*, vol. 54, no. 15, p. 1690, 1985.

[103] E. R. May, A. Narang, and D. I. Kopelevich, "Role of molecular tilt in thermal fluctuations of lipid membranes," *Physical Review E*, vol. 76, no. 2, p. 021913, 2007.

[104] H. Kleinert, Z. Narzikulov, and A. Rakhimov, "Quantum phase transitions in optical lattices beyond the bogoliubov approximation," *Physical Review A*, vol. 85, no. 6, p. 063602, 2012.

[105] J. Dreger, A. Pelster, and B. Hamprecht, "Variational perturbation theory for fokker-planck equation with nonlinear drift," *The European Physical Journal B-Condensed Matter and Complex Systems*, vol. 45, no. 3, pp. 355–368, 2005.

[106] H. Kleinert, "Fluctuation pressure of membrane between walls," *Physics Letters A*, vol. 257, no. 5, pp. 269–274, 1999.

[107] P. M. Stevenson, "Optimized perturbation theory," *Physical Review D*, vol. 23, no. 12, p. 2916, 1981.

[108] M. Düttmann, *Variational Methods in Disorder Problems*. PhD thesis, Doctoral dissertation, Diploma Thesis), Department of Physics Freie Universitat Berlin, Berlin, Germany, 2009.

[109] W. D. McComb, *Renormalization methods: a guide for beginners*. Oxford University Press, 2004.

[110] B. Palmieri and S. A. Safran, "Hybrid lipids increase the probability of fluctuating nanodomains in mixed membranes," *Langmuir*, vol. 29, no. 17, pp. 5246–5261, 2013.

[111] R. Brewster, P. A. Pincus, and S. A. Safran, "Hybrid lipids as a biological surface-active component," *Biophysical journal*, vol. 97, no. 4, pp. 1087–1094, 2009.

[112] F. Ahmadpoor, L. Liu, and P. Sharma, "Thermal fluctuations and the minimum electrical field that can be detected by a biological membrane," *Journal of the Mechanics and Physics of Solids*, vol. 78, pp. 110–122, 2015.

[113] E. M. Stein and G. Weiss, *Introduction to Fourier analysis on Euclidean spaces (PMS-32)*, vol. 32. Princeton university press, 2016.

[114] M. Kardar, *Statistical physics of fields*. Cambridge University Press, 2007.

[115] W. Helfrich, "Effect of thermal undulations on the rigidity of fluid membranes and interfaces," *Journal de Physique*, vol. 46, no. 7, pp. 1263–1268, 1985.

[116] W. Helfrich, "Stiffening of fluid membranes and entropy loss of membrane closure: Two effects of thermal undulations," *The European Physical Journal B-Condensed Matter and Complex Systems*, vol. 1, no. 4, pp. 481–489, 1998.

[117] M. Winterhalter and D. Lasic, "Liposome stability and formation: experimental parameters and theories on the size distribution," *Chemistry and physics of lipids*, vol. 64, no. 1, pp. 35–43, 1993.

[118] B. A. Korgel, J. H. van Zanten, and H. G. Monbouquette, "Vesicle size distributions measured by flow field-flow fractionation coupled with multiangle light scattering," *Biophysical journal*, vol. 74, no. 6, pp. 3264–3272, 1998.

[119] B. Coldren, R. Van Zanten, M. Mackel, J. Zasadzinski, and H.-T. Jung, "From vesicle size distributions to bilayer elasticity via cryo-transmission and freeze-fracture electron microscopy," *Langmuir*, vol. 19, no. 14, pp. 5632–5639, 2003.

[120] S. Egelhaaf, M. Müller, and P. Schurtenberger, "Size determination of polymer-like micelles using cryo-electron microscopy," *Langmuir*, vol. 14, no. 16, pp. 4345–4349, 1998.

[121] H. Jung, B. Coldren, J. Zasadzinski, D. Iampietro, and E. Kaler, "The origins of stability of spontaneous vesicles," *Proceedings of the National Academy of Sciences*, vol. 98, no. 4, pp. 1353–1357, 2001.

[122] R. Van Zanten and J. A. Zasadzinski, "Using cryo-electron microscopy to determine thermodynamic and elastic properties of membranes," *Current opinion in colloid & interface science*, vol. 10, no. 5, pp. 261–268, 2005.

[123] V. A. Harmandaris and M. Deserno, "A novel method for measuring the bending rigidity of model lipid membranes by simulating tethers," *The Journal of chemical physics*, vol. 125, no. 20, p. 204905, 2006.

[124] L. Bo and R. E. Waugh, "Determination of bilayer membrane bending stiffness by tether formation from giant, thin-walled vesicles," *Biophysical journal*, vol. 55, no. 3, pp. 509–517, 1989.

[125] D. Cuvelier, I. Derényi, P. Bassereau, and P. Nassoy, "Coalescence of membrane tethers: experiments, theory, and applications," *Biophysical journal*, vol. 88, no. 4, pp. 2714–2726, 2005.

[126] R. Bar-Ziv, T. Frisch, and E. Moses, "Entropic expulsion in vesicles," *Physical review letters*, vol. 75, no. 19, p. 3481, 1995.

[127] J. Li, K. A. Pastor, A.-C. Shi, F. Schmid, and J. Zhou, "Elastic properties and line tension of self-assembled bilayer membranes," *Physical Review E*, vol. 88, no. 1, p. 012718, 2013.

[128] M. Kozlov and W. Helfrich, "Effects of a cosurfactant on the stretching and bending elasticities of a surfactant monolayer," *Langmuir*, vol. 8, no. 11, pp. 2792–2797, 1992.

[129] H. J. Risselada, S. J. Marrink, and M. Müller, "Curvature-dependent elastic properties of liquid-ordered domains result in inverted domain sorting on uniaxially compressed vesicles," *Physical review letters*, vol. 106, no. 14, p. 148102, 2011.

[130] J. D. Moroz, P. Nelson, R. Bar-Ziv, and E. Moses, "Spontaneous expulsion of giant lipid vesicles induced by laser tweezers," *Physical review letters*, vol. 78, no. 2, p. 386, 1997.

[131] L. D. Landau and E. M. Lifshitz, "Course of theoretical physics, theory of elasticity," 1986.

[132] D. Nelson and L. Peliti, "Fluctuations in membranes with crystalline and hexatic order," *Journal de physique*, vol. 48, no. 7, pp. 1085–1092, 1987.

[133] J. A. Aronovitz and T. C. Lubensky, "Fluctuations of solid membranes," *Physical review letters*, vol. 60, no. 25, p. 2634, 1988.

[134] P. Le Doussal and L. Radzihovsky, "Self-consistent theory of polymerized membranes," *Physical review letters*, vol. 69, no. 8, p. 1209, 1992.

[135] M. Paczuski, M. Kardar, and D. R. Nelson, "Landau theory of the crumpling transition," *Physical review letters*, vol. 60, no. 25, p. 2638, 1988.

[136] H. Kleinert, *Path integrals in quantum mechanics, statistics, polymer physics, and financial markets*. World Scientific, 2009.

[137] S. Plimpton, "Fast parallel algorithms for short-range molecular dynamics," *Journal of computational physics*, vol. 117, no. 1, pp. 1–19, 1995.

[138] D. W. Brenner, O. A. Shenderova, J. A. Harrison, S. J. Stuart, B. Ni, and S. B. Sinnott, "A second-generation reactive empirical bond order (rebo) potential energy expression for hydrocarbons," *Journal of Physics: Condensed Matter*, vol. 14, no. 4, p. 783, 2002.

[139] M. Tuckerman, B. J. Berne, and G. J. Martyna, "Reversible multiple time scale molecular dynamics," *The Journal of chemical physics*, vol. 97, no. 3, pp. 1990–2001, 1992.

[140] N. C. Admal and E. B. Tadmor, "A unified interpretation of stress in molecular systems," *Journal of elasticity*, vol. 100, no. 1-2, pp. 63–143, 2010.

[141] D. H. Boal and M. Rao, "Topology changes in fluid membranes," *Physical Review A*, vol. 46, no. 6, p. 3037, 1992.

[142] R. Capovilla, J. Guven, and J. Santiago, "Lipid membranes with an edge," *Physical Review E*, vol. 66, no. 2, p. 021607, 2002.

[143] Z. Tu and Z. Ou-Yang, "Lipid membranes with free edges," *Physical Review E*, vol. 68, no. 6, p. 061915, 2003.

[144] Z. Tu and Z. Ou-Yang, "A geometric theory on the elasticity of bio-membranes," *Journal of Physics A: Mathematical and General*, vol. 37, no. 47, p. 11407, 2004.

[145] Z. Tu, "Compatibility between shape equation and boundary conditions of lipid membranes with free edges," *The Journal of chemical physics*, vol. 132, no. 8, p. 084111, 2010.

[146] Z. Tu, "Geometry of membranes," *arXiv preprint arXiv:1106.2370*, 2011.

[147] P.-H. Puech, N. Borghi, E. Karatekin, and F. Brochard-Wyart, "Line thermodynamics: adsorption at a membrane edge," *Physical review letters*, vol. 90, no. 12, p. 128304, 2003.

[148] G. Melikyan, N. Matinyan, and V. Arakelian, "The influence of gangliosides on the hydrophilic pore edge line tension and monolayer fusion of lipid membranes," *Biochimica et Biophysica Acta (BBA)-Biomembranes*, vol. 1030, no. 1, pp. 11–15, 1990.

[149] S. May, "A molecular model for the line tension of lipid membranes," *The European Physical Journal E*, vol. 3, no. 1, pp. 37–44, 2000.

[150] A. J. García-Sáez, S. Chiantia, J. Salgado, and P. Schwille, "Pore formation by a bax-derived peptide: effect on the line tension of the membrane probed by afm," *Biophysical journal*, vol. 93, no. 1, pp. 103–112, 2007.

[151] E. Karatekin, O. Sandre, H. Guitouni, N. Borghi, P.-H. Puech, and F. Brochard-Wyart, "Cascades of transient pores in giant vesicles: line tension and transport," *Biophysical journal*, vol. 84, no. 3, pp. 1734–1749, 2003.

[152] A. Tian, C. Johnson, W. Wang, and T. Baumgart, "Line tension at fluid membrane domain boundaries measured by micropipette aspiration," *Physical review letters*, vol. 98, no. 20, p. 208102, 2007.

[153] M. Hu, J. J. Briguglio, and M. Deserno, "Determining the gaussian curvature modulus of lipid membranes in simulations," *Biophysical journal*, vol. 102, no. 6, pp. 1403–1410, 2012.

[154] M. Hu, D. H. de Jong, S. J. Marrink, and M. Deserno, "Gaussian curvature elasticity determined from global shape transformations and local stress distributions: a com-

parative study using the martini model," *Faraday discussions*, vol. 161, pp. 365–382, 2013.

[155] Y. Wei, B. Wang, J. Wu, R. Yang, and M. L. Dunn, "Bending rigidity and gaussian bending stiffness of single-layered graphene," *Nano letters*, vol. 13, no. 1, pp. 26–30, 2012.

[156] B. Huang, M. Liu, N. Su, J. Wu, W. Duan, B.-l. Gu, and F. Liu, "Quantum manifestations of graphene edge stress and edge instability: A first-principles study," *Physical review letters*, vol. 102, no. 16, p. 166404, 2009.

[157] V. Shenoy, C. Reddy, A. Ramasubramaniam, and Y. Zhang, "Edge-stress-induced warping of graphene sheets and nanoribbons," *Physical review letters*, vol. 101, no. 24, p. 245501, 2008.

[158] K. V. Bets and B. I. Yakobson, "Spontaneous twist and intrinsic instabilities of pristine graphene nanoribbons," *Nano Research*, vol. 2, no. 2, pp. 161–166, 2009.

[159] Q. Lu and R. Huang, "Excess energy and deformation along free edges of graphene nanoribbons," *Physical Review B*, vol. 81, no. 15, p. 155410, 2010.

[160] G. Gompper and D. Kroll, "Edge correlations of fluid and tethered membranes," *Journal de Physique I*, vol. 2, no. 5, pp. 663–676, 1992.

[161] R. B. Meyer, "Piezoelectric effects in liquid crystals," *Physical Review Letters*, vol. 22, no. 18, p. 918, 1969.

[162] P. Zubko, G. Catalan, and A. K. Tagantsev, "Flexoelectric effect in solids," *Annual Review of Materials Research*, vol. 43, pp. 387–421, 2013.

[163] A. G. Petrov, "Flexoelectricity of model and living membranes," *Biochimica et Biophysica Acta (BBA)-Biomembranes*, vol. 1561, no. 1, pp. 1–25, 2002.

[164] A. G. Petrov, "Electricity and mechanics of biomembrane systems: flexoelectricity in living membranes," *Analytica chimica acta*, vol. 568, no. 1, pp. 70–83, 2006.

[165] A. Spector, N. Deo, K. Grosh, J. Ratnanather, and R. Raphael, "Electromechanical models of the outer hair cell composite membrane," *The Journal of membrane biology*, vol. 209, no. 2-3, pp. 135–152, 2006.

[166] W. Brownell, A. Spector, R. Raphael, and A. Popel, "Micro-and nanomechanics of the cochlear outer hair cell," *Annual review of biomedical engineering*, vol. 3, no. 1, pp. 169–194, 2001.

[167] E. Glassinger, A. Lee, and R. Raphael, "Electromechanical effects on tether formation from lipid membranes: a theoretical analysis," *Physical Review E*, vol. 72, no. 4, p. 041926, 2005.

[168] A. G. Petrov, B. A. Miller, K. Hristova, and P. N. Usherwood, "Flexoelectric effects in model and native membranes containing ion channels," *European biophysics journal*, vol. 22, no. 4, pp. 289–300, 1993.

[169] K. Hristova, I. Bivas, A. Petrov, and A. Derzhanski, "Influence of the electric double layers of the membrane on the value of its flexoelectric coefficient," *Molecular Crystals and Liquid Crystals*, vol. 200, no. 1, pp. 71–77, 1991.

[170] L. Liu, "On energy formulations of electrostatics for continuum media," *Journal of the Mechanics and Physics of Solids*, vol. 61, no. 4, pp. 968–990, 2013.

[171] V. Kumaran, "Effect of surface charges on the curvature moduli of a membrane," *Physical Review E*, vol. 64, no. 5, p. 051922, 2001.

[172] J. Antosiewicz, "Computation of the dipole moments of proteins.," *Biophysical journal*, vol. 69, no. 4, p. 1344, 1995.